Evaluation of Carbon Reduction Options for Industrial Combined Heat and Power Plants

R.R. Kapoor

Master of Science Thesis

TU Delft Delft University of Technology

Energy, Flow and Process Technology

Evaluation of Carbon Reduction Options for Industrial Combined Heat and Power Plants

Master of Science Thesis

For the degree of Master of Science in Energy, Flow and Process Technology at Delft University of Technology

R.R. Kapoor

August 13, 2021

Faculty of Mechanical, Maritime and Materials Engineering (3mE) · Delft University of Technology

Delft University of Technology
Department of
Process and Energy

The undersigned hereby certify that they have read and recommend to the Faculty of Mechanical, Maritime and Materials Engineering (3mE) for acceptance of the thesis entitled

Evaluation of Carbon Reduction Options for Industrial Combined Heat and Power Plants

by

R.R. Kapoor

in partial fulfillment of the requirements for the degree of

Master of Science Energy, Flow and Process Technology

Dated: August 13, 2021

Supervisor(s):

Prof.dr.ir. Sikke Klein

Reader(s):

Prof.dr.ir. W. de Jong

Dr. A. Gangoli Rao

Ir. Kees Biesheuvel (Dow Benelux)

Abstract

Industry is a major contributor to the rise in global CO_2 emissions, constituting one fifth of the global energy consumption, of which significant amount is provided by fossil fuel combustion. Following the Paris agreement, emphasis has been made on decarbonization of the industrial sector. This thesis focuses on industrial decarbonization by employing Carbon Capture and Storage for Combined Heat and Power (CHP) gas turbine plants.

The scope of this thesis includes conceptual modelling and thermodynamic analysis of potential decarbonization options for zero carbon CHP plants. The studied options include post-combustion capture, exhaust gas recirculation, pre-combustion capture and oxyfuel combustion. As conventional air Brayton cycles are not applicable for oxy-fuel combustion in gas turbines, different working fluids and cycle configurations are proposed and thermodynamic performance is evaluated. Selected cycles were then compared based on thermodynamics, economics and off-Design performance at a typical constant power to heat ratio of 0.78.

It was observed that oxyfuel CHP cycle with CO_2 working fluid is a promising solution for zero carbon CHP with 100% CO_2 reduction. However, this solution requires new turbomachinery design. In view of this, a retrofit analysis is also performed in this thesis which evaluates if an existing air designed gas turbine can be used for CO_2 operation. It was concluded from this analysis that it is possible to operate an air gas turbine on CO_2 by incorporating proposed modifications of higher compressor inlet temperature (473K) and a turbine inlet nozzle area 20% larger than design. These modifications, however also lead to serious performance deterioration.

Table of Contents

List of Figures

List of Tables

Acknowledgements

First of all, I would like to express my deep gratitude towards my supervisor, Prof.dr.ir. Sikke Klein. His knowledge and expertise in this field have made me set professional goals for myself. He has always encouraged my amateur ideas, yet gotten me on track when I would get lost. He has taught me to always look at the bigger picture along with the small details. I would sincerely like to thank him for supporting and guiding me throughout my thesis.

I would like to thank Mr. Kees Biesheuvel and Mr. Steven Prins, for providing me the opportunity to do my Master thesis at Dow Benelux, for arranging an extremely insightful visit to the plant, and for their regular feedback during the entire thesis. I would also like to thank Institute of Sustainable Process Technology (ISPT) for making all the necessary arrangements for this research.

I would like to thank Prof. Wolfgang Sanz, Dr. Matteo Romano, Dr. Matteo Pini, and Dr. Anthony Jackson for taking out their time and arranging online meetings that got converted into enlightening discussions. I also express my gratitude to Prof.dr.ir. W. de Jong and Dr. A. Gangoli Rao for being a part of my thesis committee.

I would like to thank my parents, Mr. Ravi Kapoor and Mrs. Nilaxy Kapoor. I have always looked up to them as my role models. They have always been a constant source of support and care. Their belief in me strengthens my belief in myself. They were my inspiration to pursue my Masters degree, it would not have been possible without them.

I would finally like to thank my friends, both from India and Delft. I thank Asif Hasan for always patiently answering my very basic technical questions.

Delft, University of Technology — R.R. Kapoor
August 13, 2021

Chapter 1

Introduction

1-1 Existing Energy scenario

The global CO_2 emissions from the energy sector are on the rise since the industrial revolution. CO_2 being a greenhouse gas (GHG), traps heat in the earth's atmosphere and it's increasing concentration by human activities is responsible for global warming. As a result of the Paris agreement, the aim is to reduce the net GHG emissions in the EU by 55% until 2030 of the value in 1990 and to achieve net zero emissions by 2050. Major contribution to the total GHG emissions is from the power, transport and the industrial process heating sector as shown in figure 1-1.

1-1-1 Industrial process heating overview

According to the International Energy Agency (IEA), industrial heat makes up two-thirds of industrial energy demand and almost one-fifth of global energy consumption [IEA (2018)]. Figure 1-2 clearly supports the statement and shows the contribution of industrial heat to the total energy consumption. Common manufacturing industrial processes that require process heating are metal and non metal melting, metal heat treating, coking, drying, etc. Apart from these, petroleum refining, pulp and paper and chemical sectors are leading industrial markets for process heat. Steam heating accounts for a significant amount of energy used in low and medium grade (200 to 650° C) industrial process heating. For example the fuel used to generate steam accounts for 89% of the total fuel used in the pulp and paper industry, 60% of the total fuel used in the chemical manufacturing industry, and 30% of the total fuel used in the petroleum refining industry [Industrial Process Heating]. Figure 1-3 shows the share of various industrial sub-sectors to the global CO_2 emissions from industry.

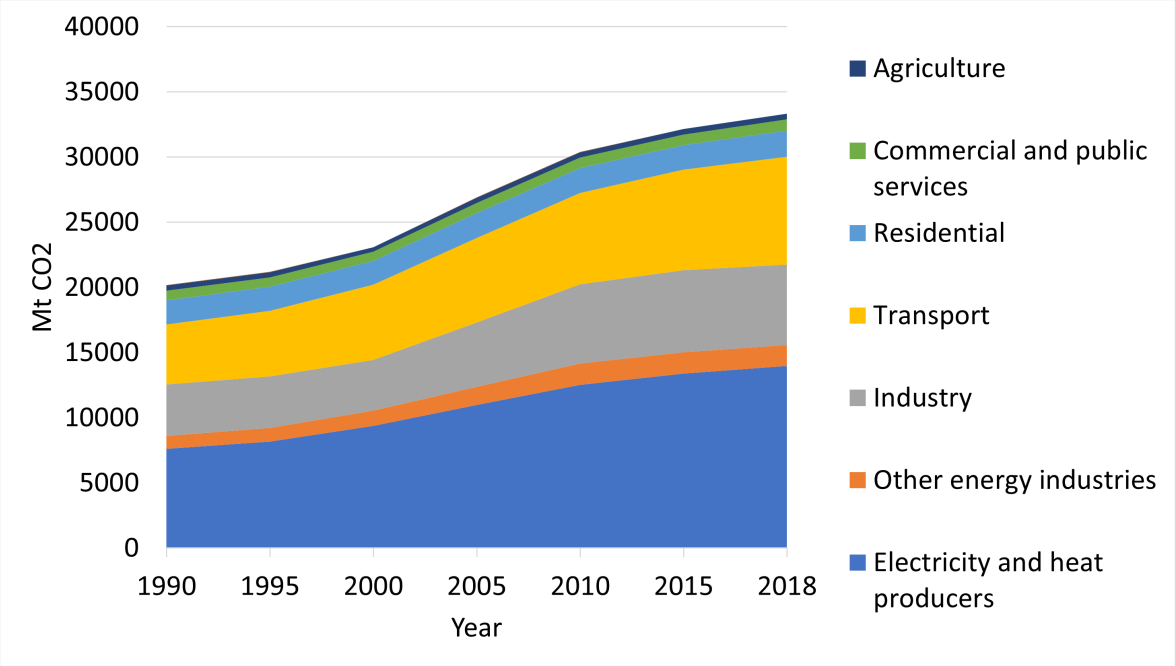

Figure 1-1: CO_2 emissions by year taken from IEA (2020)

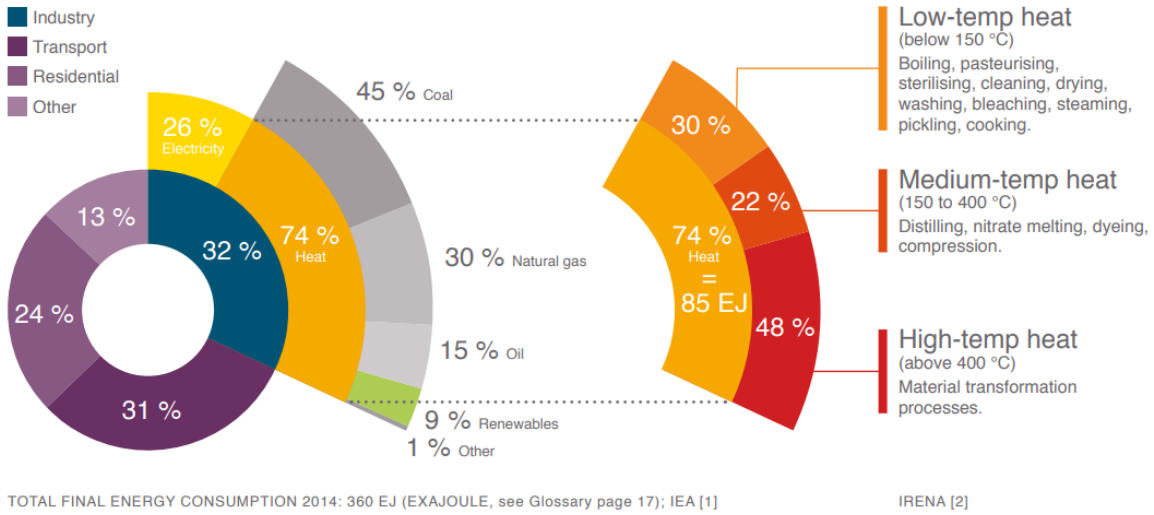

Figure 1-2: Image showing that heat represents three quarters of industrial energy demand worldwide taken from Solar Payback (2017)

Steam is typically generated by fossil fuel combustion in steam boilers. Industrial heat constitutes most of the direct industrial CO_2 emitted each year owing to the fossil fuel combustion. Despite this fact, industrial heat is often missing from energy analyses and research focused on CO_2 reduction [IEA (2018)]. The IEA identifies among others, five key pillars of decarbonisation for the industry [IEA (2021)]:

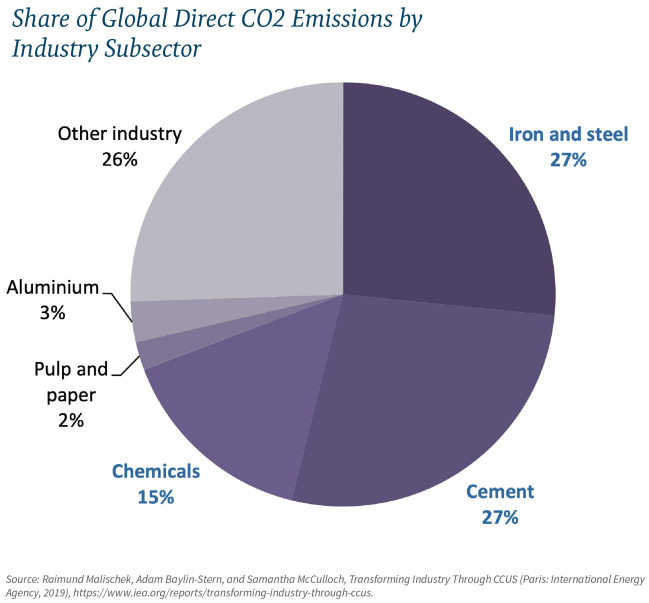

Figure 1-3: Image showing the share of various industrial sub-sectors to the global CO_2 emissions from industry taken from Naimoli and Ladislaw (2020)

1. Renewable energy
2. Hydrogen and Hydrogen based fuels
3. Energy efficiency
4. Carbon Capture and Storage (CCS)
5. Electrification of process industry from renewable power

Power generated by renewable energy (VRE) shall play a key role in achieving net zero emissions by 2050. The Roadmap for the net zero power predicted by IEA [IEA (2021)], suggests a share of 90% power by the VRE. However, the nature of this energy is intermittent due to the variability of the source. Thus, back up power is needed to stabilize the grid. Large potential to provide low and medium temperature steam using biomass combustion (up to 400 °C) exist by fixed or fluidized bed boilers. The efficiency of bio-based steam generation ($75 \sim 90$ %) is however, lower than fossil fuels [IRENA (2015)]. Apart from these, renewable sources like solar thermal and geothermal energy can be directly applied for industrial heat generation if the distance between the heat source and end user is sufficiently close.

Alternative technology suggested is hydrogen and hydrogen based fuels. However, large scale deployment of hydrogen based technologies also depends on a large scale hydrogen generation by electrolysers from renewable power [IEA (2021)].

Electrification of the process sector, also like hydrogen depends largely on power produced by VRE. Heat pumps can also be used to convert electricity into process heat. Industrial heat pumps can only supply low temperature process heat (60 to 100 °Celsius) [IRENA (2015)]

and thus are typically used for space heating and cooling, along with other low temperature applications indicated in figure 1-2.

Fossil fuelled power plants with carbon capture and storage (CCS) can prove to be an attractive solution as a back-up for renewable power to stabilize the grid. Not only for the future, but CCS is also a solution for the present situation, where the existing power generation assets have a long term of their service life left before being decommissioned to meet climate goals. Hence, Carbon Capture and Storage, is one of the options that can play a key role in decarbonisation and is the chosen topic of study and theme of this thesis.

Figure 1-4 shows the different methodologies to generate carbon-free heat for the industry using the key pillars of decarbonization.

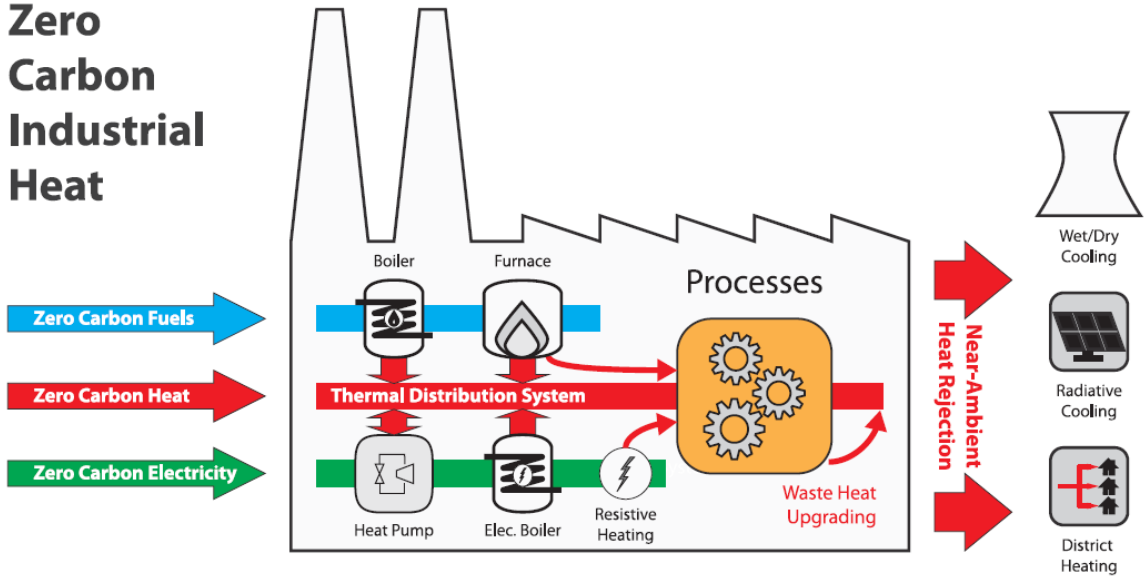

Figure 1-4: A schematic representation of technologies to enable zero-carbon industrial heat through the utilization of zero-carbon fuels, zero-carbon heat, electrification of heat, and better heat management technologies taken from Thiel and Stark (2021)

1-2 Combined Heat and Power: Theoretical background

Combined heat and power or Co-generation is an efficient method to reclaim the heat lost from the electricity generating systems and apply it to the industrial process heating needs. As mentioned in [CODE2 Project], in 2012, 51.8% of the electricity in the Netherlands was produced by CHP. In 2017, approximately 68% of district heat production came from combined heat and power (CHP) plants in the Netherlands.

When compared to separate generation of heat and power, a CHP requires lesser fuel energy for the same heat and power outputs. This can be illustrated by figure 1-5. Because electricity can be transmitted across great distances more easily than heat, industrial co-generation

facilities are generally located close to the place where the thermal energy will be used. These facilities are also scaled to meet the heat requirements of a specific process. If the quantity of electricity generated is below the local requirement, the balance must be purchased from the local grid. Conversely, if a surplus of electricity is generated, it can be sold to the grid. This makes industrial process heat requirement a primary product, and power output a secondary product of the CHP. A typical example of this scenario is at Dow, ELSTA, where the complete heat output is delivered for process, and part of the electricity is sold to the grid.

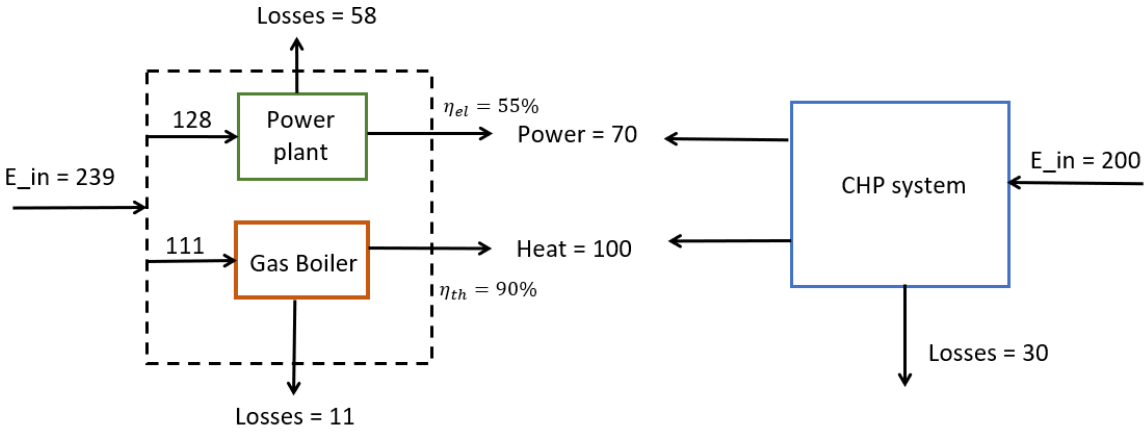

Figure 1-5: Efficiency comparison of CHP and separate heat and power generation

In the example figure 1-5, the reference efficiency values for the power plant and the boiler are taken as 55% and 90% respectively, which are typical of the current technologies available for power and heat generation. It can be seen that CHP is definitely more efficient than separate generation owing to the heat recovery from the gas turbine power plant exhaust.

1-2-1 CHP: Prime mover

The major components of a CHP system are an engine (prime mover), generator, and a heat recovery steam generator. The characteristics and performance of a CHP depends on the prime mover selected, which is a gas turbine in this study. The major advantage of gas turbine systems is the high grade heat available from its exhaust gases. The simplest configuration of gas turbine CHP is shown in figure 1-6.

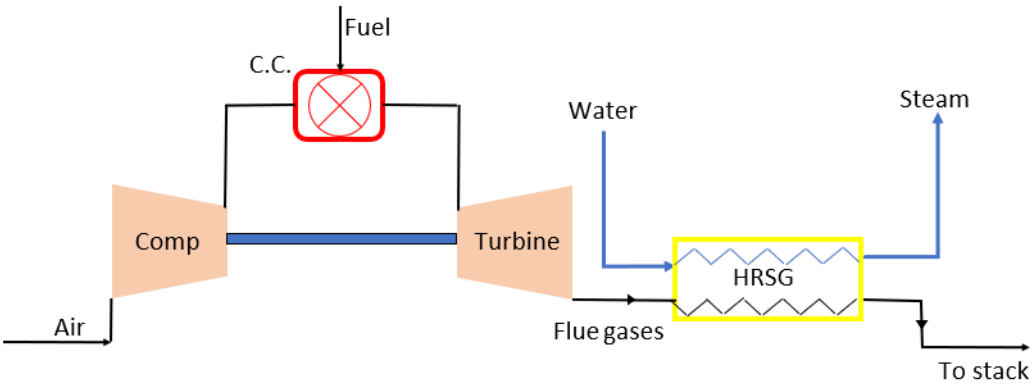

Figure 1-6: Simplified flow diagram of a CHP

Sometimes, a duct burner for supplementary firing is also included between the Gas turbine exhaust and the HRSG system so that it can generate additional steam beyond the quantity that the gas turbine exhaust heat can provide.

1-3 Review of carbon capture and storage technologies

1-3-1 Classification of CCS

Carbon capture technologies focus on separation of CO_2 from other condensable or non-condensable gases which form a part of the working fluid in the power cycle. Figure 1-7 shows classification of the different technologies available:

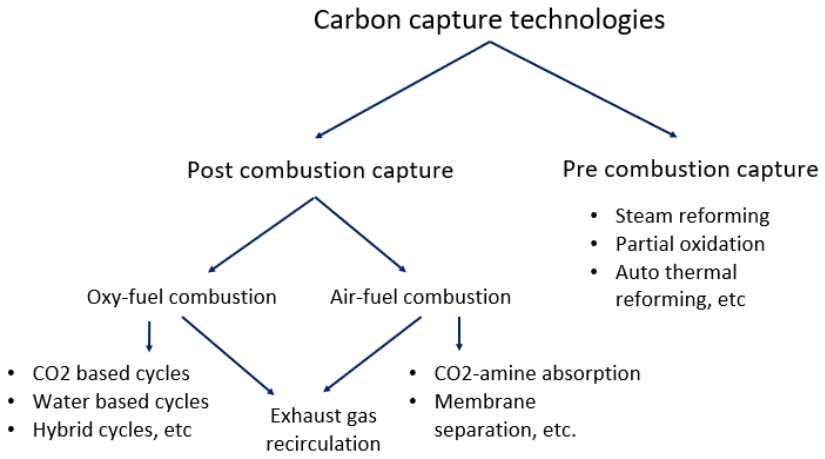

Figure 1-7: Classification of carbon capture technologies

The primary differentiation is based on whether carbon dioxide is removed from the flue gases after combustion (Post combustion capture) or from the fuel before combustion (Pre-combustion capture). For post combustion capture, the oxidizer in the combustion chamber can be oxygen or air. The air-fuel category is based on thermodynamic Brayton cycle whereas the oxyfuel category is based on advanced oxyfuel cycles. Figure 1-8 illustrates the concepts of these technologies.

In exhaust gas recirculation, a part of the exhaust gases from the HRSG is recirculated back to the compressor of the gas turbine. It is a transition between air-fuel and oxy-fuel combustion. Figure 1-9 shows the locations of different capture technologies on a process flow diagram of a CHP.

1-3-2 Theory of CCS

Post combustion CO_2 capture utilizes the concept of reactive absorption. In post combustion capture, the CO_2 from the flue gas of the plant generated by combustion of fossil fuels are absorbed into the solvent by a chemical reaction. The solvent is later regenerated to remove the CO_2 which is later transported and stored. This method suffers from a disadvantage of large energy requirement for the solvent regeneration. Moreover, the energy requirement is an inverse function of CO_2 concentration in the flue gas which is very low at gas turbine exhaust

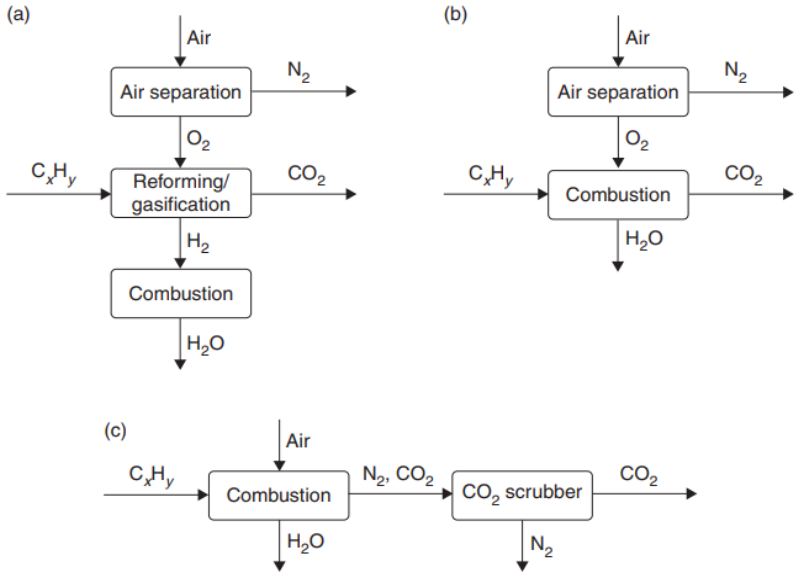

Figure 1-8: Carbon capture technologies. (a) Pre-combustion capture, (b) oxy-fuel processes and (c) post-combustion processes taken from Soothill et al. (2013)

due to the presence of nitrogen in the flue gas. This nitrogen comes from the high excess air ($100 \sim 300\%$) used in the combustion chamber since nitrogen acts as a diluent to lower the flame temperature and ensure that the design turbine inlet temperature is achieved. To avoid nitrogen from acting as a barrier in carbon capture, three solutions are possible.

1. Remove CO_2 before nitrogen (air) enters the system, i.e., CO_2 must be removed from the fuel before combustion - Pre-combustion capture.

2. Increase the concentration of CO_2 in the exhaust gases by recirculating the CO_2 containing gas back to the GT. - Exhaust Gas Recirculation (EGR)

3. Removing nitrogen from the air before it enters the combustion chamber, i.e. using pure O_2 as the oxidizer.- Oxy-fuel combustion.

1-3-3 Current status of carbon capture technologies

Figure 1-10 shows the development of the commercial CCS facility over the past decade. Today, there are 65 commercial CCS facilities. CCS facilities currently in operation can capture and permanently store around 40 Mt of CO_2 every year. There are another 34 pilot and demonstration-scale CCS facilities in operation or development and eight CCS technology test centres [Page et al. (2020)].

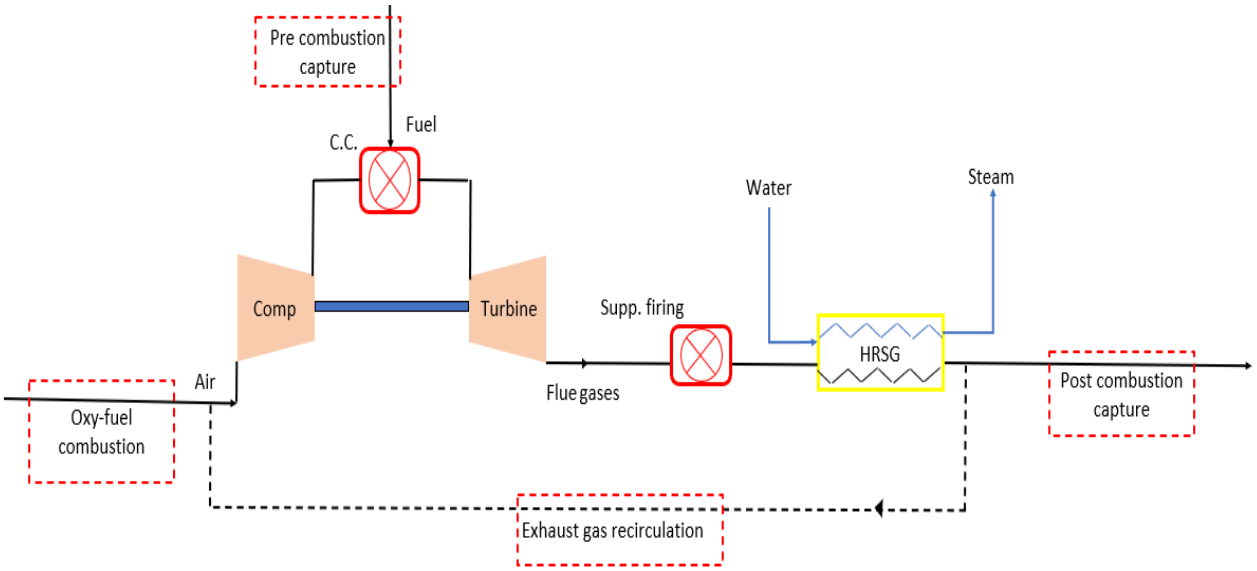

Figure 1-9: Image showing locations of different capture technologies on a process flow diagram of a CHP

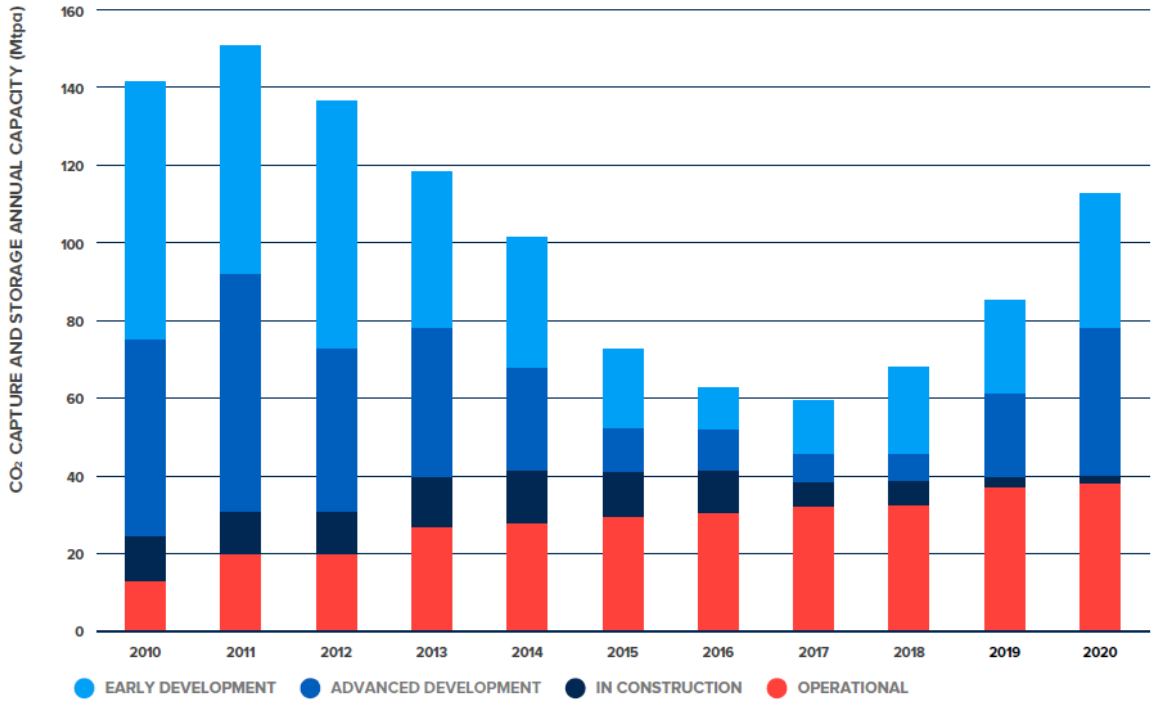

Figure 1-10: Year wise development of the commercial CCS facility over the past decade, taken from Page et al. (2020).

1-4 Research scope

The scope of this thesis includes:

- Design, modeling and thermodynamic evaluation of the different carbon capture and storage technologies discussed (broadly, post-combustion capture, pre-combustion capture and oxy-fuel combustion), for a natural gas combined heat and power gas turbine plant. New concepts are designed and proposed for the oxy-fuel combustion technique.
- A relative comparison of these techniques at fixed design conditions and constant heat and power output. The options will be compared based on thermodynamic performance (overall CHP efficiency and CHP electric efficiency), CO_2 emissions, Levelized Cost of Electricity (LCOE), and power flexibility.
- Finally, based on the results of the comparative analysis, a retrofit solution is proposed to realise a best-performing theoretical concept in an actual power generation scenario.

This study is done for a typical CHP installation at Dow, ELSTA. A constant process steam demand of 400 tonnes/hr at 90 bar and 326 °C is used throughout this study. As discussed, flexibility is the key for future CHP generation, this thesis also deals with the Off-design analysis of several options.

1-5 Research questions

The following research questions will be answered during the course of this thesis:

1. How is the thermodynamic performance of a CHP plant affected by the introduction of post-combustion capture at both, design and off-design?
2. How can the performance of a CHP with post combustion capture be improved?
3. How can a cycle with pre-combustion capture be designed and optimized? What is the effect on thermodynamic performance of introducing pre-combustion capture?
4. What are the different thermodynamic CHP cycle configurations and working fluids for oxy-fuel combustion in gas turbines?
5. How do the different configurations compare to each other at different design conditions? Which configuration suits best to the design condition studied in this thesis?
6. What is the economic performance of the studied cycles?
7. Can an existing air breathing CHP installation be retrofitted to operate on CO_2 as the working fluid? If yes, how can this be achieved?

1-6 Report structure

This section covers in brief, the scope of the thesis by elaborating on the contents and the flow of the report.

Chapter 2 discusses the modelling and thermodynamic analysis of a CHP cycle with post combustion carbon capture, and two different variants of exhaust gas recirculation. Results are analysed at both Design and off-Design conditions.

In chapter 3, CHP configuration with pre-combustion capture is developed and optimized, with the performance analysed again, at design and off-design.

In Chapter 4, novel CHP cycle configurations are developed and different working fluids are studied for the Oxy-fuel combustion concept. These cycle concepts are compared to each other at different design output conditions. Best performing cycles are selected for further comparison with the post combustion and pre combustion concepts studied in Chapters 2 and 3.

This comparison is drawn in chapter 5, where the thermodynamic comparison of different zero carbon technologies is also supplemented with an economic analysis.

It is concluded in chapter 5 that CO_2 as a working medium is a very promising option for low cost CO_2 capture & storage for a CHP installation. Consequently, in Chapter 6, it will be analysed if an air based gas turbine cycle can be retrofitted to Oxy-fuel CHP cycle with CO_2 working fluid. Different modifications to the gas turbine for a successful retrofit will also be proposed.

Finally, Chapter 7 summarises all the important findings from all the chapters of this thesis and answers the posed research questions. Some future recommendations are also proposed.

Chapter 2

CHP with Post combustion capture

2-1 Introduction

Technologies for separation and capture of CO_2 from flue gas streams are based on different physical and chemical processes including absorption, adsorption, membranes, and cryogenics. The choice of a suitable technology depends on the characteristics of the flue gas stream, which depend mainly on the power plant technology [Rao and Rubin (2002)].
Rao and Rubin and Wang et al. have shown that CO_2 absorption systems are the most suitable for combustion based power plants for the following reasons:

1. CO_2 absorption is a mature technology which is commercially available and is in use today.
2. It is an end-of-pipe technology. Thus, it can be retrofit into existing power plant systems without major modifications.

CO_2 absorption can be of two types: Physical absorption and chemical absorption. As chemical absorption is the chosen CO_2 capture technique in this chapter, it is discussed in detail. In reactive/chemical absorption, the CO_2 molecules react with the amine solution to form a weakly bonded chemical compound. CO_2 is later recovered from the solution by allowing reverse reaction (stripping) and regenerating the solvent at high temperatures. Figure 2-1 shows a simplified process diagram for chemical absorption. The flue gas from the HRSG is cooled before it enters the absorber. The equilibrium solubility of CO_2 in the amine solution increases with decreasing temperature of the flue gas [Kohl and Nielsen (1997)]. Kwak et al. (2012) finds that 40 °C is the optimum flue gas entry temperature. As high temperature reverses equilibrium, the temperature of the stripper is maintained sufficiently high for amine regeneration and CO_2 liberation [Abu Zahra (2009)]. These high temperatures in the stripper are achieved by supplying heat (in the form of steam from the HRSG) to generate steam in the reboiler which acts as a stripping gas. Therefore, CO_2 capture by amine absorption is an energy intensive process, and thereby a source of CO_2 itself. In consequence, we shall focus

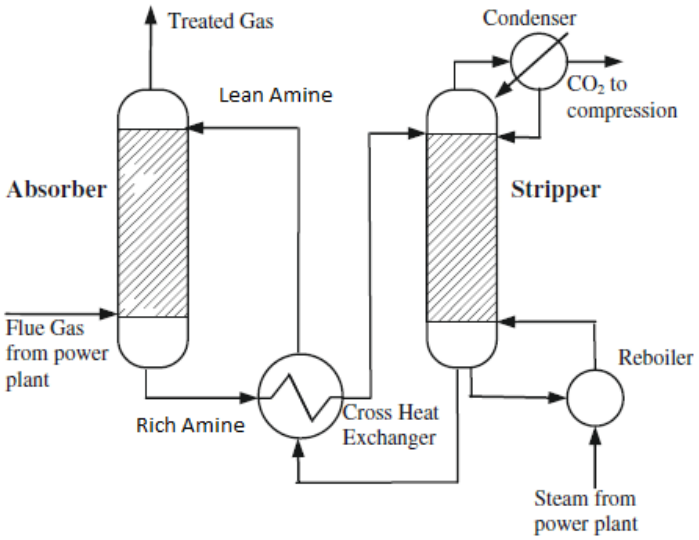

Figure 2-1: Simplified process flow diagram of chemical absorption process for post-combustion CO_2 capture

on minimizing reboiler duty to make the carbon capture process, and hence the complete system more efficient. The CO_2 rich flue gas from the gas turbine followed by a cooler enters the absorber at the bottom and treated gas leaves from the top. The rich amine solution from the absorber passes through the cross heat exchanger where it gains heat from the lean amine solution from the stripper. The high temperature (around 100-140 °C) rich amine solution enters the stripper at the top and releases CO_2 into the steam generated in the reboiler. The stream containing CO_2, steam and traces of amine leaves the stripper from the top into a partial condenser where gaseous CO_2 is sent to the compression train while the condensed water is returned to the stripper as a reflux.

In physical absorption, the CO_2 is captured by diffusion of CO_2 molecules in the sorbent and the sorbent is regenerated by flashing at low pressures. The diffusion of CO_2 in amines takes place by Henry's solubility. According to Henry's law, the solubility of the gas in the absorbent is proportional to the partial pressure of the acid gas (CO_2) in the flue gas mixture.

$$\text{Solubility} = k_{gas} \cdot p \tag{2-1}$$

where k is the Henry's constant and p is the partial pressure of the CO_2 in the gas. Figure 2-2 shows a clear distinction about when physical or chemical absorption is applicable based on partial pressure of CO_2 in the gas.

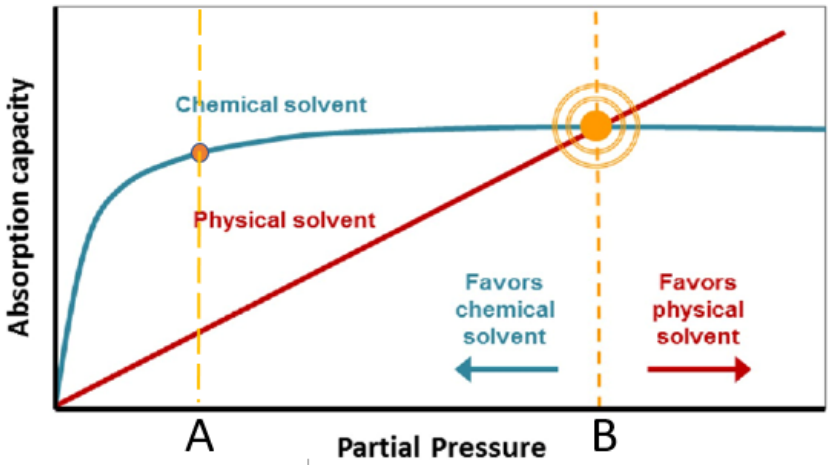

Figure 2-2: Absorption capacity of physical and chemical absorption with respect to CO_2 partial pressure in the gas, taken from Espinal et al. (2013).

It can be seen that for partial pressures to the right of point B, physical absorption is favored over chemical absorption. Stewart (2014) suggests that this point (B) is around 3.5 bars which is approximately 100 times higher than the CO_2 partial pressure in the gas turbine exhaust gas ($\sim$ 3.5 kPa). Hence, the exhaust gas needs to be pressurized to a very high value (such that the CO_2 partial pressure in the gas is above point B), if physical absorption has to be applied for gas turbine exhaust gas treating. This makes physical absorption inefficient for post combustion capture. Thus CO_2-amine (chemical) absorption is the most commonly used post combustion capture technology and will be studied in this chapter.

2-1-1 Exhaust Gas Recirculation (EGR)

As it can be seen in figure 2-2, after a certain point A, chemical absorption becomes insensitive of the CO_2 partial pressure. Below point A, the CO_2 partial pressure is so low that it hinders mass transfer of CO_2 into the amine solution. With less CO_2 being transferred, the absorption reaction is inhibited and thus chemical absorption becomes less efficient. This range is typical of CO_2 partial pressure in gas turbine exhaust gases where CO_2 concentration is around 3% by volume. Thus amine scrubbing of CO_2 is less advantageous at low CO_2 partial pressures and high amount of energy is needed for its regeneration. Li et al. (2011) gives a relation between the regeneration heat required and CO_2 concentration in figure 2-3.

Figure 2-3 also suggests that the heat duty is lower and relatively insensitive to CO_2 concentration above 7 $\sim$ 8%. This provides a motivation for increasing CO_2 mole % at the capture inlet which can be achieved by recirculating the CO_2 containing exhaust gas back to the GT.

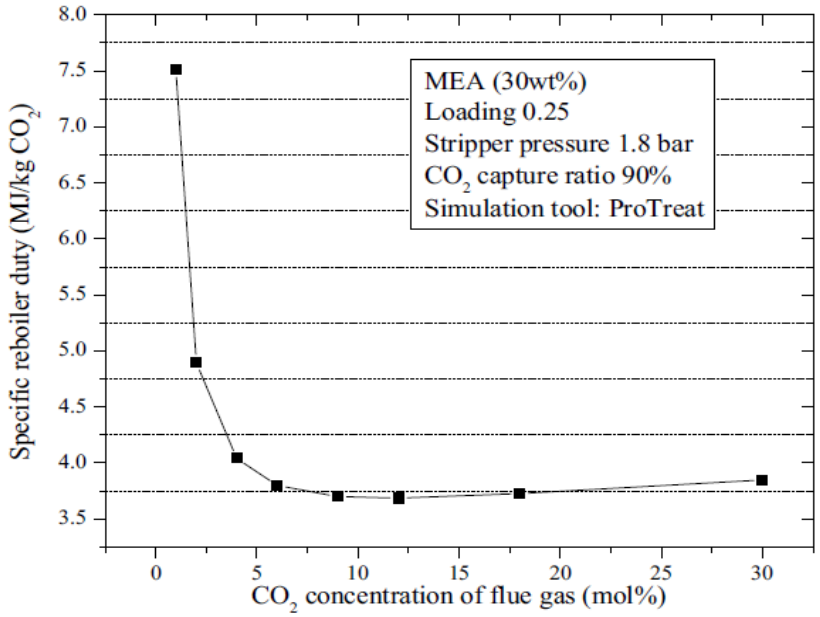

Figure 2-3: Reboiler heat duty as a function of CO_2 concentration taken from Li et al. (2011)

The following sections will deal with the thermodynamic cycles developed on the discussed concepts namely:

1. CHP with post combustion capture
2. CHP with post combustion capture and Cooled exhaust gas recirculation.
3. CHP with post combustion capture and Uncooled exhaust gas recirculation

2-2 CHP with post combustion capture

A simplified process flow diagram of a CHP integrated with the absorption unit is shown in figure 2-4 with the capture unit highlighted by red dotted lines. Steam for the regeneration is generated in the HRSG at 90 bar and expanded in the steam turbine before it enters the reboiler. A GE 9F gas turbine is employed for this case.

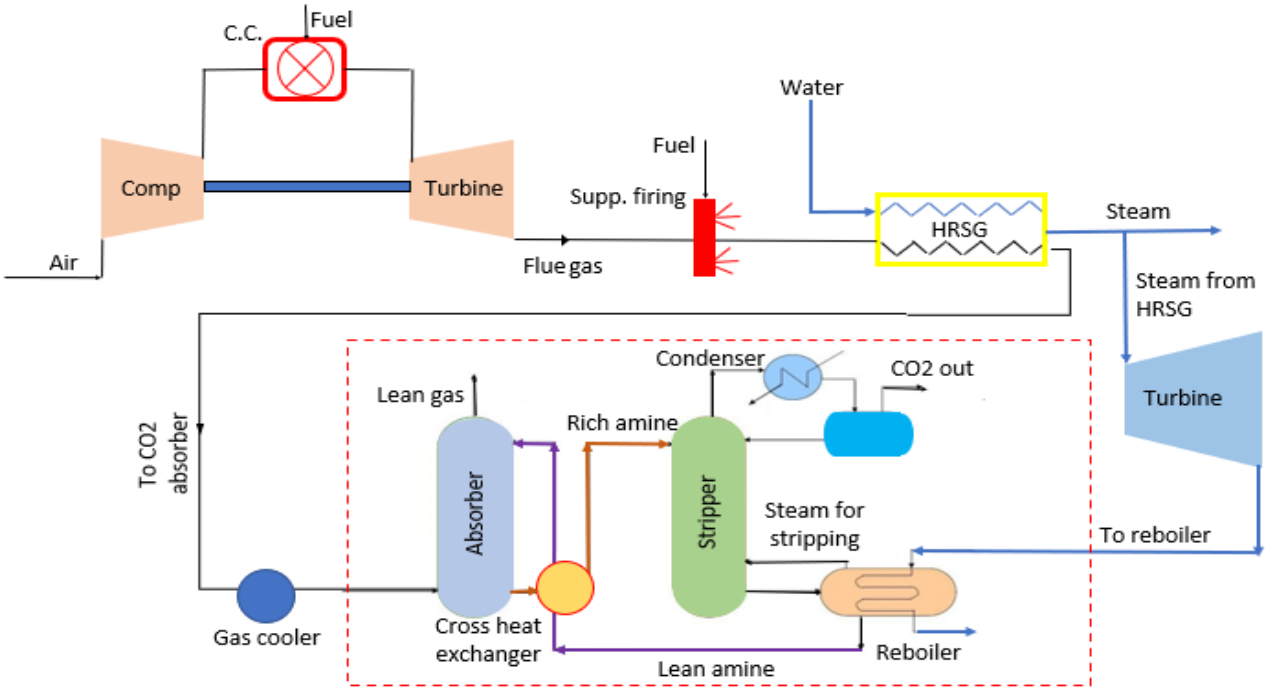

Figure 2-4: Process flow diagram of CHP with post combustion capture using amine stripper

2-2-1 Design and Off-Design parameters

The standard control (IGV+ TIT) for gas turbine is used, in that the load is reduced by IGV (Inlet Guide Vane) control until its limit of a minimum mass flow rate is reached. For further load reduction, the TIT (Turbine Inlet Temperature) is reduced at constant mass flow rate. The reader is referred to Appendix A for the theory on load control in gas turbines by IGV and TIT methods. Table 2-1 shows the mass flow rate and TIT values at different gas turbine loads.

Gas Turbine Load	100	90	80	70	60	50	40	30	20	10
Compressor Inlet mass flow (kg/s)	596.5	546.3	506.4	466.7	450.5	450.5	450.5	450.5	450.5	450.5
Gas Turbine Inlet Temperature (°C)	1267.9	1267.9	1267.9	1265.7	1204.6	1103.2	998.0	888.1	771.9	647.4

Table 2-1: Controlled parameters: Compressor inlet mass flow and Turbine Inlet Temperature for different part loads

2-2-2 Results and Discussion

For the basic operations at Off-Design in the standard Inlet Guide Vane control + Turbine Inlet Temperature control, the reader is again referred to Appendix A. Figure 2-5 shows the CHP electric efficiency and the CHP Total energy efficiency (TEE) at design and Off-Design for standard IGV+TIT control.

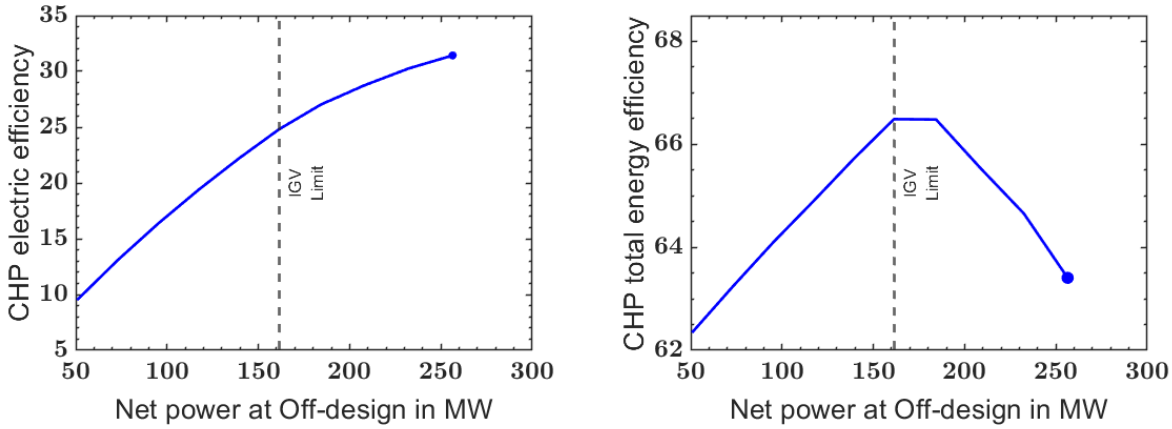

Figure 2-5: Image shows CHP electric efficiency [left] and CHP Total Energy Efficiency (TEE) [right] with Net power at Off-Design. Design point shown by dot at full load

1. The total energy efficiency increases for IGV operation and decreases for the TIT operation. The major contributor to the energy loss is the heat required by the reboiler for CO_2 capture. Hence it is expected that the total energy efficiency follows an inverse trend of the energy associated with CO_2 capture. The energy required by CO_2 capture is in fact an inverse function of the CO_2 concentration at the capture inlet as already discussed in 2-1-1 and validated by figure 2-6. Hence, it can be concluded that the total energy efficiency directly depends on the CO_2 mole percent at exhaust.

2. In right figure 2-6, it can be seen that the CO_2 concentration increases in the IGV operation and decreases for the TIT operation. This occurs as in IGV, increase in duct burner firing increases the CO_2 concentration at absorber inlet and in TIT, reduction in gas turbine firing lowers the CO_2 concentration. Thus, at part load, IGV control improves fuel utilization while TIT control deteriorates it.

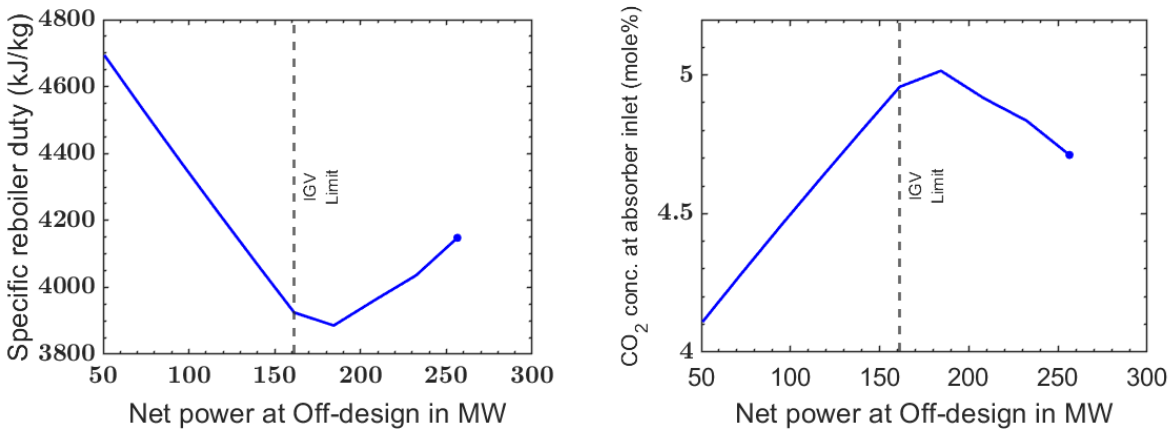

Figure 2-6: Image shows Specific reboiler duty [left] and CO_2 concentration at absorber inlet [right] with Net power at Off-Design. Design point shown by dot at full load

2-3 CHP with Post Combustion Capture and Cooled Exhaust Gas Recirculation

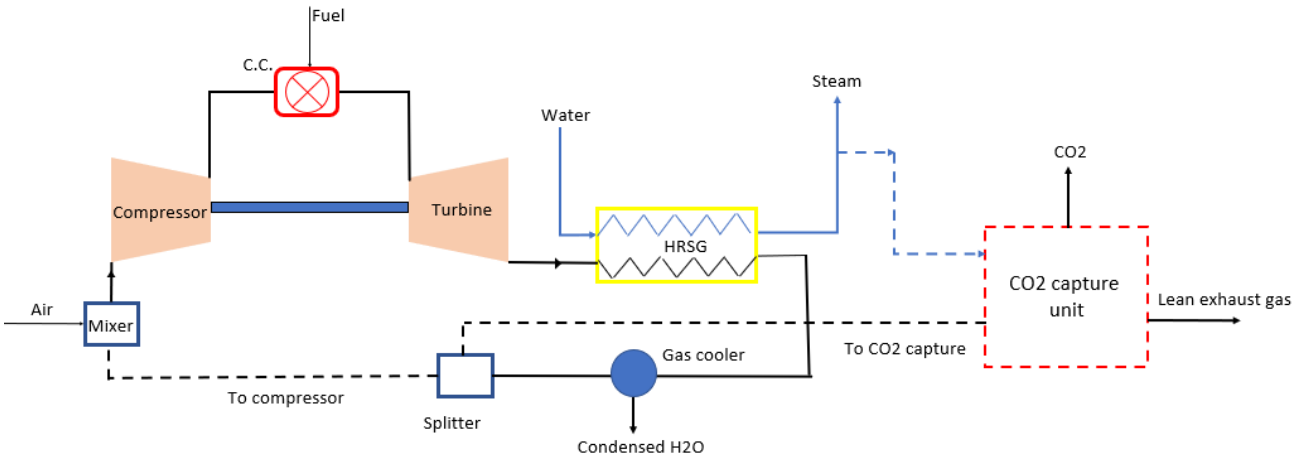

Figure 2-7: Process flow diagram of CHP with post combustion capture and cooled exhaust gas recirculation

A simplified process flow diagram of a CHP with with Post Combustion Capture and Cooled Exhaust Gas Recirculation is shown in figure 2-7. The exhaust gas from the HRSG is cooled and water is condensed before it is recirculated back to the gas turbine. The cooled recirculated gas is mixed with air in order to maintain the design mass flow rate at GT inlet. At Off-Design, the mass flow rate of the gas at inlet is governed by the part load control technique employed [Refer Appendix A]. Bolland and Mathieu have simulated this condition at full load and they have concluded that cooled EGR for a combined cycle gas turbine plant does not offer any major improvement in the electric performance at full load. In this section, it is analysed if the same conclusion is valid for a combined heat and power plant.
When the amount of exhaust gases recirculated and mixed with fresh air increases, the O_2 concentration at GT inlet decreases. ElKady et al. and Rokke and Hustad show that the minimum O_2 concentration at gas turbine inlet must be around 15% for stable combustion. This limits the maximum EGR ratio. The maximum EGR ratio in this case was determined to be 35%. For this study, there is no recirculation at design, but the increasing recirculation is simulated as an Off-Design condition as discussed in the next section.

2-3-1 Design and Off-Design parameters

Table 2-2 shows the Off-Design input cases for cooled exhaust gas recirculation. EGR ratio is defined as the ratio of the gas recirculated to the total mass flow of gas at exhaust. Case 1 to 8 correspond to the Off-design conditions with increasing EGR ratio, starting from 0 recirculation at a design load of 100%. From cases 9 to 16, the standard control (IGV+TIT) is adopted for load reduction at a constant maximum recirculation ratio.

Case	1	2	3	4	5	6	7	8
Gas Turbine Load (%)	100	100	100	100	100	100	100	100
EGR ratio	0	0.05	0.1	0.15	0.2	0.25	0.3	0.35

Case	9	10	11	12	13	14	15	16
Load	90	80	70	60	50	40	30	20
EGR ratio	0.35	0.35	0.35	0.35	0.35	0.35	0.35	0.35

Table 2-2: Off-Design input parameters for Post combustion capture with Cooled Exhaust gas recirculation

2-3-2 Results and Discussion

1. The dotted red lines in figures 2-8 and 2-9 represent EGR operation. When the EGR ratio is increased at Off-Design, in table 2-2 from column 1 to 8, the total energy efficiency increases at a constant load equal to design load in figure 2-8. This is a result of increasing CO_2 concentration at absorber inlet due to higher flue gas recirculation at constant net power as shown in right figure 2-9. As the gas is cooled before recirculation up to the design compressor inlet temperature, the gas turbine mass flow rate does not change from design and thus, the power output with increasing EGR is constant. The CHP Total Energy Efficiency (TEE) increases at constant power until the maximum recirculation, after which, its trend follows that for IGV operation (in table 2-2, column 9 to 12).

2. Another observation is that the TEE is higher at the design condition with no recirculation compared to the case with only post combustion capture (difference shown by separate blue and yellow dots at design point). This is a result of cooling and condensing the combustion generated H_2O from the gas before it enters the absorber at design. H_2O condensation increases the CO_2 concentration at the absorber inlet as shown in right figure 2-9.

3. Further observation of figure 2-8 reveals that in TIT operation, the decrease in TEE is actually flat even though the CO_2 concentration in TIT operation decreases rapidly as shown by right figure 2-9. The negligible sensitivity of the TEE to the CO_2 concentration can be explained by figure 2-3. As the reboiler duty itself is less sensitive to the CO_2 concentration between 7 to 9 mole %, the TEE is unaffected. This can also be validated from figure left 2-9.

It can be concluded that cooled exhaust gas recirculation improves the design as well as part load efficiency.

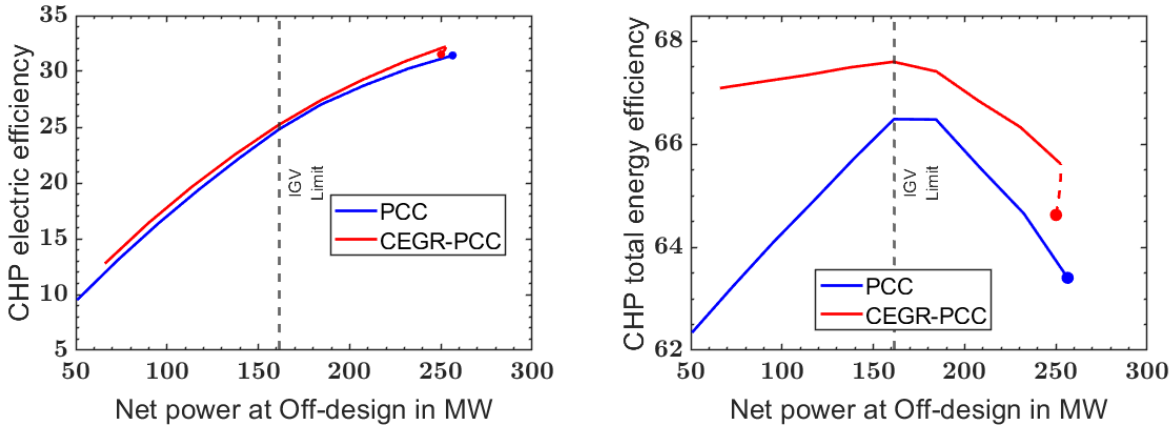

Figure 2-8: Image shows CHP electric efficiency [left] and CHP Total Energy Efficiency (TEE) [right] with Net power at Off-Design for Post combustion capture(PCC) and Post combustion capture with cooled Exhaust gas recirculation (CEGR-PCC). Design points shown by dots at full load

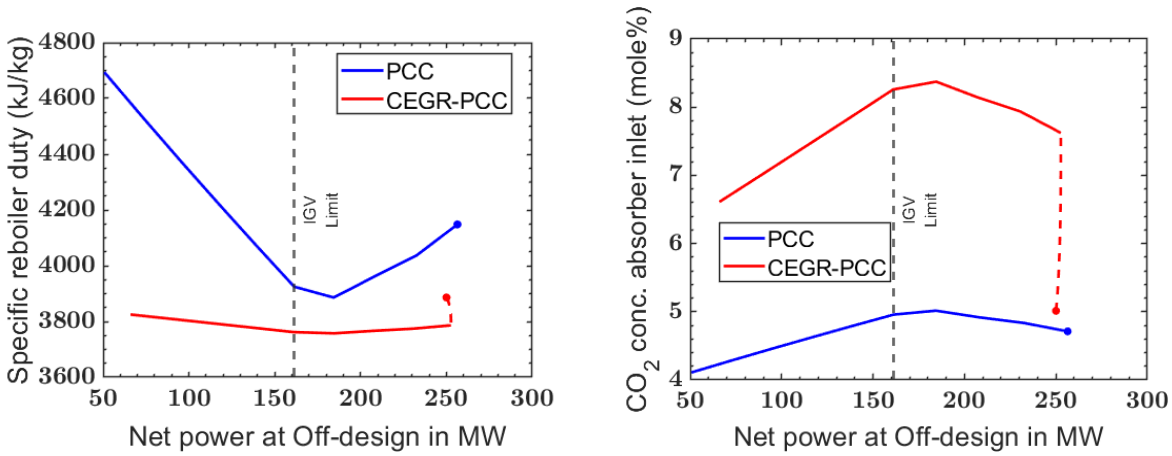

Figure 2-9: Image shows Specific reboiler duty [left] and CO_2 concentration at absorber inlet [right] with Net power at Off-Design for Post combustion capture (PCC) and Post combustion capture with cooled EGR (CEGR-PCC) case. Design points shown by dots at full load

2-4 CHP with Post Combustion Capture and Uncooled Exhaust Gas Recirculation

Figure 2-10 shows a simplified process flow diagram for the Uncooled EGR case. Exhust gas recirculation without cooling reduces the GT inlet mass flow rate as explained in detail in Appendix A, and can be used to control the GT load. In figure A-6, it is shown that EGR has the highest part load efficiency for a CHP. Therefore, it is both an efficient load control and an efficient CO_2 capture technique. The reader is referred to Appendix A for theory of Off-Design operation with EGR.

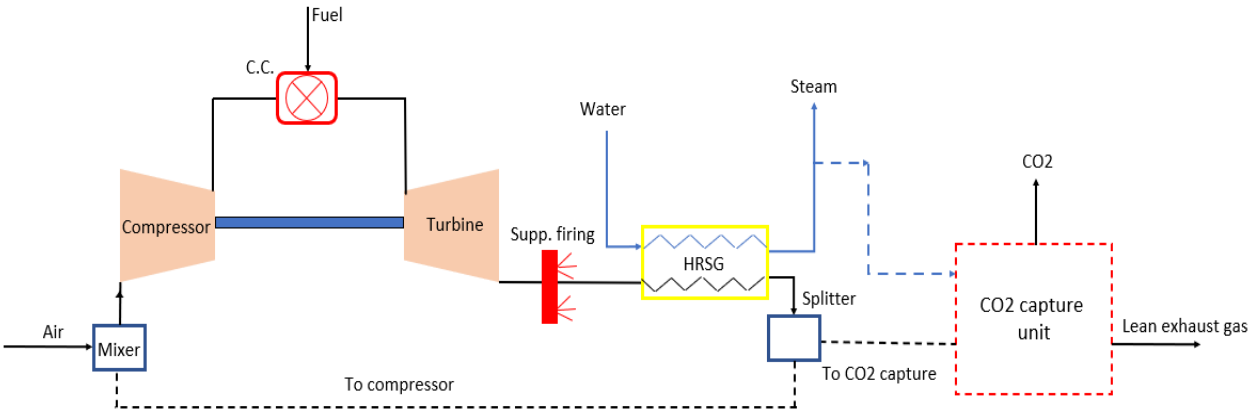

Figure 2-10: Process flow diagram of CHP with post combustion capture and uncooled exhaust gas recirculation

2-4-1 Design and Off-Design parameters

Table 2-3 gives the Off-Design parameters for uncooled exhaust gas recirculation. Rows 1 and 2 (Load and EGR ratio) are inputs given to the model while the inlet temperature to the compressor is calculated by the model.

2-4-2 Results and Discussion

1. Dotted lines in figures 2-11 and 2-12 represent EGR operation. For increasing exhaust gas recirculation from 0% to 35%, the net power delivered reduces even at full load and the TEE increases as shown in right figure 2-11. Power decreases as a result of lower mass flow rate due to higher temperature than design at compressor inlet.

2. As energy is lost by heat rejection from the system due to cooling and condensing in cooled EGR, its effect of reducing the TEE dominates below a part load power value of 2.25 MW where uncooled EGR is more efficient.

Case	1	2	3	4	5	6	7	8
Gas Turbine Load (%)	100	100	100	100	100	100	100	100
EGR ratio	0	0.05	0.1	0.15	0.2	0.25	0.3	0.35
Compressor Inlet Temperature (°C)	46.1	46.8	47.6	48.5	49.5	50.6	51.8	53.2

Case	9	10	11	12	13	14
Load	90	80	70	60	50	40
EGR ratio	0.35	0.35	0.35	0.35	0.35	0.35
Compressor Inlet Temperature (K)	53.3	53.4	53.5	52.9	52.1	51.3

Table 2-3: Off-Design input parameters for Post combustion capture with Uncooled Exhaust gas recirculation

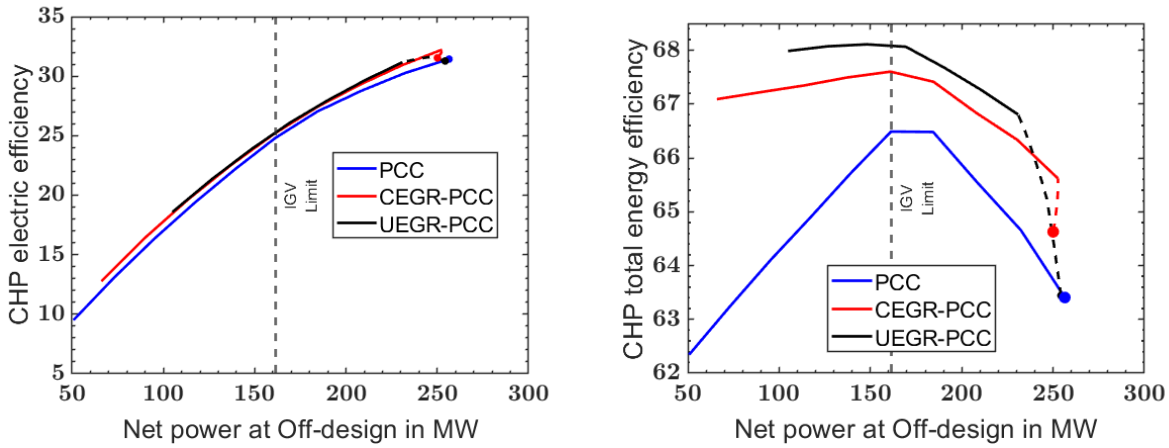

Figure 2-11: Image shows CHP electric efficiency [left] and Total Energy Efficiency with Net power at Off-Design for Post combustion capture (PCC), cooled EGR (CEGR-PCC) and uncooled Exhaust gas recirculation (UEGR-PCC). Design points shown by dots at full load

3. Also, the minimum limit of part load power for uncooled EGR is lower than for cooled EGR. For the cooled EGR case, due to H_2O condensation before recirculation, the O_2 concentration at compressor inlet is higher than uncooled EGR at the same recirculation ratio. As the O_2 concentration before combustion decreases continuously with decrease in power, the limit of minimum O_2 concentration at combustor inlet for the uncooled EGR case is attained at a load value higher than the cooled EGR case. So, very deep part load operation is limited for the uncooled EGR case.

4. Slopes of the TEE curves for EGR cases are lower than the Post Combustion Capture (PCC) case in both IGV and TIT operation (TEE curves are flatter for EGR). This is due to the fact that in EGR, the CO_2 concentration is in the higher range where the reboiler heat duty is less sensitive to the CO_2 concentration.

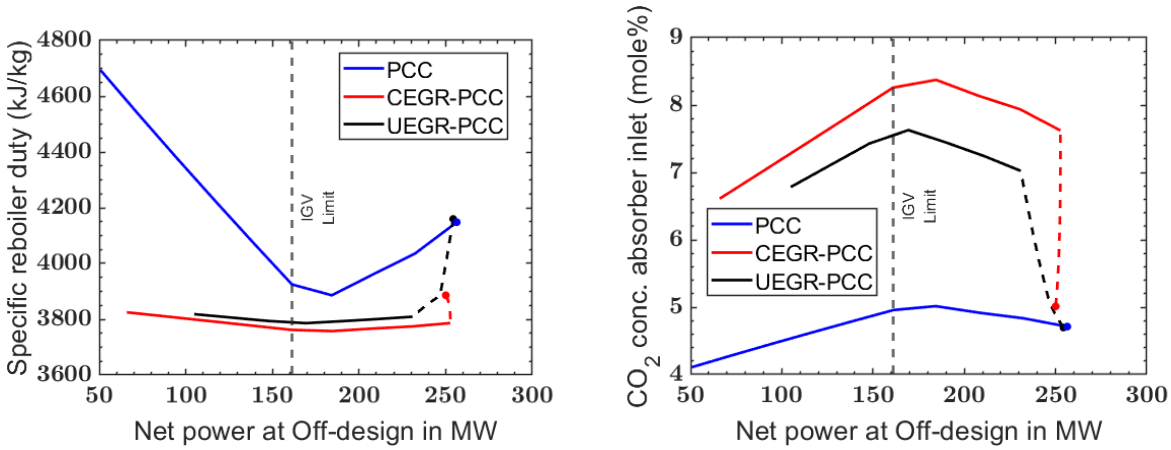

Figure 2-12: Image shows Specific reboiler duty [left] and CO_2 concentration at absorber inlet [right] with Net power at Off-Design for Post combustion capture (PCC), cooled EGR (CEGR-PCC) and uncooled EGR (UEGR-PCC) case. Design points shown by dots at full load

2-5 Summary

Some important observations from the figures 2-11 and 2-12:

1. **In IGV mode:** EGR gives highest efficiency magnitude for a particular load while PCC gives highest efficiency gain per unit reduction in power. The efficiency increase is flatter for EGR than for PCC.

2. **In TIT mode:** The efficiency drop is flatter for EGR than for PCC. EGR gives the highest efficiency magnitude. The problem of efficiency deterioration in TIT control makes deep part load control inefficient in PCC.

3. In this thesis, it is observed that the control combination of EGR + IGV + TIT offers best efficiency at part loads for CHP with post combustion carbon capture. Similarly, in the paper by [Steimes et al.], it has been reported that the optimum control combination for a CHP without capture is EGR + TIT + IGV.

Chapter 3

CHP with Pre combustion capture

In this chapter, the performance of a gas turbine system fired by hydrogen generated from methane will be studied as a potential carbon dioxide reduction technique. This technique concentrates on the conversion of fuel rather than on exhaust or oxidizer, therefore much lower quantities of working fluid is required to be conditioned which reduces equipment costs and energy requirement [Lozza and Chiesa (2002)]. The benefit of pre-combustion capture is based on the conversion of carbon fuel to carbonless fuel.

First the pre-combustion capture cycle design proposed in this thesis will be discussed, followed by its parametric settings. Finally, a discussion on cycle performance will conclude the study for this chapter.

3-1 Cycle description

Figure 3-1 shows the process flow diagram of a Pre-combustion carbon capture CHP system. In this technique, the fuel (methane or natural gas) is converted to syngas which consists of H_2, CO_2 and CO. The conversion takes place by either Steam methane reforming, partial oxidation or Autothermal reforming. Steam methane reforming is by far the most mature and commonly used technology for hydrogen production [Basile et al. (2015)], and hence is used in this study. This syngas then undergoes a water gas shift reaction to convert nearly 90 % of CO to CO_2. The reactions are given as:

$$\text{SMR}: \quad CH_4 + H_2O \rightleftharpoons CO + 3\,H_2 \qquad \Delta H^\circ_{298} = 206.0\,\text{kJ/mol} \tag{3-1}$$

$$\text{WGS}: \quad CO + H_2O \rightleftharpoons CO_2 + H_2 \qquad \Delta H^\circ_{298} = -41\,\text{kJ/mol} \tag{3-2}$$

Thus the outlet of WGS contains predominantly H_2 and CO_2, with traces of methane and CO. In this study, H_2 is separated from this stream by physical absorption CO_2 capture. Unlike gas turbine exhaust, the syngas stream has a higher CO_2 partial pressure (around 350

kPa), and hence, physical absorption can be used. The H_2 rich gas is then used as a fuel in the gas turbine. The rest of the operation of the CHP is usual without any modifications except that the working fluid in the gas turbine is majorly water and nitrogen. This modifies the GT operation slightly as studied extensively by [Chiesa et al.]. The steam generated from the GT exhaust at design is in excess to the process demand. This excess steam is expanded in a condensing steam turbine (not shown) delivering extra power.

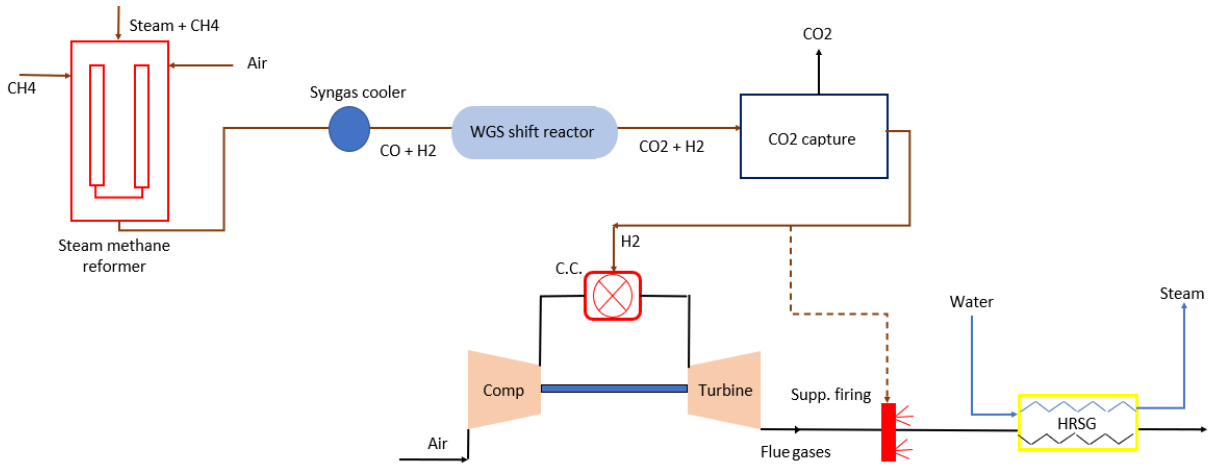

Figure 3-1: Process flow diagram of a simple pre-combustion capture cycle

There are several optimizations proposed to the basic cycle in this thesis to improve thermodynamic performance and lower the CO_2 emissions. They are elaborated in the following sections:

3-1-1 Cycle Optimization 1: H_2-fired Steam Methane Reformer (SMR)

Conventional SMR requires CH_4/fossil fuel firing to increase the temperature in the SMR to the high temperature required by reaction thermodynamics. This makes the SMR itself a source of CO_2 which requires separate treatment. One novelty of the system designed in this thesis is the internally-generated-hydrogen fired SMR which requires a new design of the SMR burner. So, hydrogen is generated in excess to that required by the gas turbine and the duct burner to fire the SMR.

3-1-2 Cycle Optimization 2: Heat integration

There are several heat integration potentials in the cycle that are exploited in this thesis and the cycle is optimized for maximum energy utilization. They are explained below:

3-1-2-1 Syngas recuperator

The syngas from stem methane reformer leaves the SMR at a high temperature of 900 °C and has to be cooled to a lower temperature for the upcoming WGS. This syngas is cooled in

the Syngas recuperator (SR) as shown in figure 3-2 by heating the steam-methane mixture that enters the SMR. Increasing the SMR feedstock temperature would lead to lower fuel requirements for raising the SMR temperature.

3-1-2-2 Low Temperature Preheater

In the WGS reactor, the temperature of the syngas increases, which again needs to be cooled to the CO_2 absorber temperature. This is a low temperature heat which is exchanged with the air going to the SMR in the Low temperature Preheater (LTP) in figure 3-2. Preheating the air entering the SMR again reduces the fuel consumption in the SMR.

3-1-2-3 High Temperature Preheater

The flue gas from the SMR exits at a very high temperature of 1000 °C. The high grade heat from this flue gas is exchanged in the High Temperature Recuperator (HTR) in figure 3-2 with the preheated air coming from the low temperature recupertor. A large amount of high grade heat is thus retained in the cycle.

3-1-2-4 Heat Recovery Steam Generator 1

As the preheated air entering the HTP from the LTP is already heated, the energy from the flue gas leaving the LTP is not utilized completely. Thus the remaining energy from the flue gas is extracted in the HRSG 1 which generates steam for the SMR reaction as shown in the figure 3-2.

The final Process flow diagram after the optimizations is shown in figure 3-2.

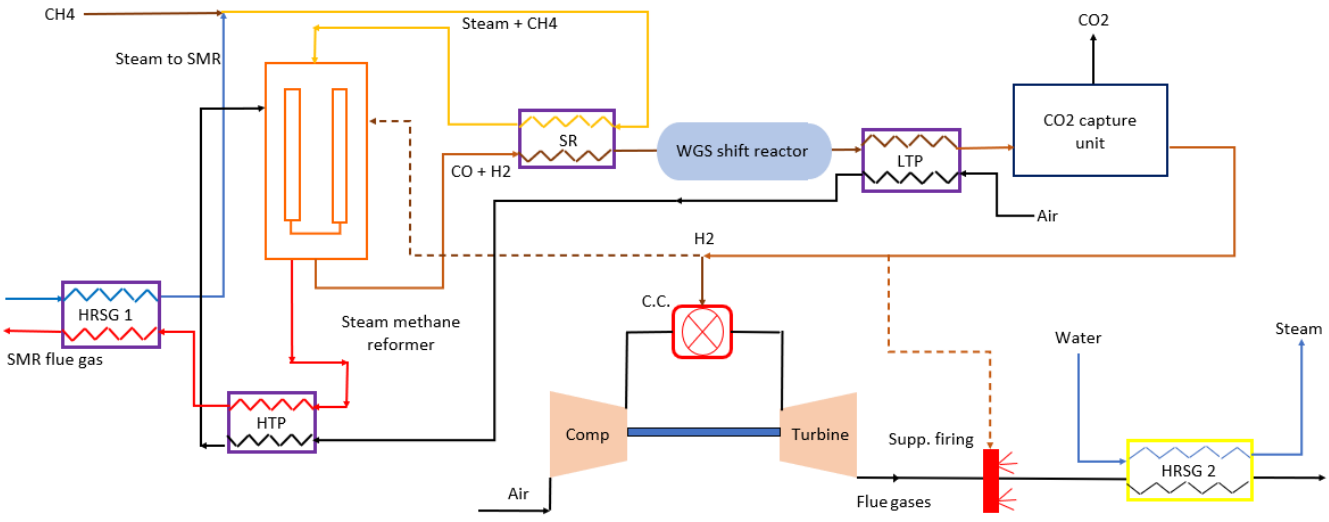

Figure 3-2: Image shows the process flow diagram of the optimised pre-combustion capture cycle.

3-2 Design parameters for the cycle

The process design setting is elaborated in the following paragraphs.

3-2-1 Operating temperature of SMR and WGS

Steam methane reforming reaction is highly endothermic, and the reaction is preferred at high temperatures of 800 to 900 °C. The WGS reaction is an exothermic reaction, hence the shift reactor is maintained at low temperatures. Thus the syngas is cooled between the SMR and the WGS reactor in the Syngas recuperator.

3-2-2 Operating pressure of SMR and WGS

A mole increasing reaction like SMR is favored at low pressures, whereas WGS reaction is independent of pressure. The lowest pressure of operation is limited by fuel pressure desired by the gas turbine combustion chamber which in this case is 30 bar.

3-2-3 Steam to methane ratio (S/C) at the inlet to SMR at design

The methane conversion increases with high steam to carbon ratios, but this comes at the cost of efficiency reduction by generating excess steam than the stoichiometric requirement which is S/C = 1. Madona et al. show that steam to carbon ratios must be high at around S/C = 2.5 $\sim$ 4 to avoid carbon deposition in the reformer.

The table 3-1 shows the final design parameters for the cycle. The reader is referred to the appendix C for details on how the design parameters affect the SMR performance.

Input	Value	Unit
Steam methane reformer		
Syngas outlet temperature	900	°C
Operating pressure	30	bar
Inlet Steam to methane ratio	4:1	–
Water gas shift reactor		
CO conversion	90	%
CO_2 **capture unit**		
CO_2 capture efficiency	95	%

Table 3-1: Design parameters for Pre-combustion capture cycle

3-3 Results and discussion

The performance of the pre-combustion capture cycle is computed for the 9F gas turbine to compare the Pre combustion capture cycle with the post combustion capture cycle.

3-3-1 Design and Off-Design analysis

Figure 3-3 shows the CHP electric efficiency and CHP Total Energy Efficiency (TEE) at Off-Design. The load control technique used for Off-Design analysis is again IGV + TIT control [Refer Appendix A]. The CHP electric efficiency decreases at part load which is typical for IGV+TIT control.

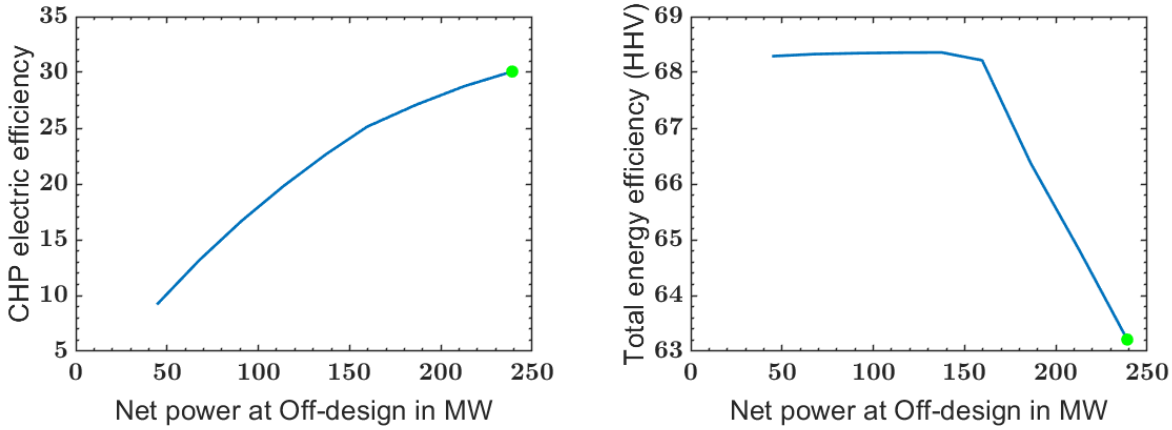

Figure 3-3: Image shows CHP electric efficiency [left] and Energy utilization factor [right] with net power at part load of the gas turbine. Green dots represent the design condition for the GE 9F gas turbine.

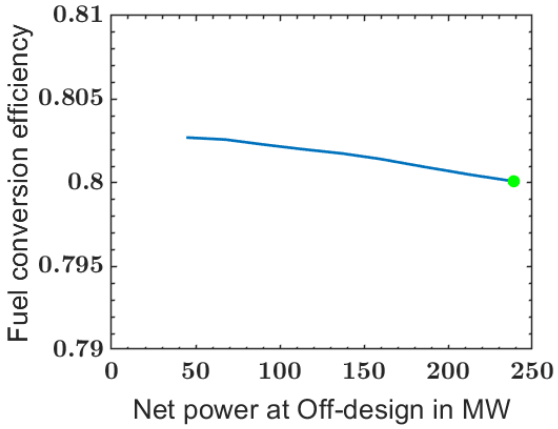

Figure 3-4: Image shows the fuel conversion efficiency with Net power at Off-Design.Green dots represent the design condition for the GE 9F gas turbine

Figure 3-4 shows the LHV fuel conversion efficiency. This is calculated as the ratio of Hydrogen fuel energy (LHV) available at the inlet of the gas turbine to the total CH_4 fuel energy at input to the SMR (percent of input energy converted to useful fuel). The almost constant conversion loss of 20% is due to the fact that the hydrogen generation process in the SMR itself requires energy. As hydrogen is generated at an expense of fuel efficiency, it can also be concluded that H_2-fired SMR is lesser efficient than conventional SMR. The total input

energy loss indicated by the total energy efficiency from the right figure 3-3, comprises of the conversion loss and the stack losses at the HRSG exit. As the conversion loss is constant over the part load range, the shape of the total energy efficiency curve depends on the variation of stack losses in IGV and TIT operation.

Chapter 4

CHP with Oxy-fuel combustion

4-1 Introduction

In chapter 2 we discussed post combustion capture plants as a retrofit solution for decarbonization of the air-based gas turbine industry for combined heat and power applications. As discussed previously, for natural gas fuelled gas turbine installations, CO_2 dilution by nitrogen in flue gas presents a major barrier for energy efficient and cost effective removal of CO_2 from the gas turbine exhaust. As using air as an oxidizer is a source of nitrogen in flue gas, we also proposed a solution wherein N_2 in the flue gas can completely be eliminated by using pure oxygen as an oxidizer in the gas turbine, so called, oxy-fuel firing. This chapter investigates the potential of oxyfuel firing as a decarbonization technique in gas turbine CHP systems.

4-1-1 Gas turbine working fluid selection

Methane burnt with pure oxygen achieves a peak temperature of over 3000K compared to around 2100K achieved with air-fuel combustion where large amount of N_2 acts as a diluent. Thus, with N_2 removed from the oxidizer stream, a new moderator is required to attain a lower flue gas temperature considering the material limits (Turbine inlet temperature specified for a given gas turbine design). One good option is to recirculate the inert gases generated by the engine itself (O_2 depleted flue gas). Recirculating the flue gas makes it possible to easily retrieve carbon dioxide from the flue gas so that H_2O can be condensed and CO_2 can be extracted without any external energy requirement. This condition motivates the study of complete flue gas recirculation. There can be three options for the working fluid of the pure oxygen-methane fired Brayton cycle.

1. Pure CO_2 recirculated
2. CO_2+H_2O recirculated

3. Pure H_2O recirculated

With the above choices for the working fluid, the gas turbine cannot anymore be operated at the design point for conventional air Brayton cycle. This means that the cycles have to be designed for the new working fluid.

Apart from the conventional working fluids mentioned above, supercritical state of the CO_2 working fluid is also studied in this chapter. The density of a fluid near and above its critical point can reach very high values (even close to its liquid phase density). A supercritical CO_2 cycle is essentially a Brayton cycle that takes advantage of this property of the working fluid at the beginning of compression to minimize the compression power requirement. Careful observation would lead to the finding that utilizing high density fluid state for low compression work input and low density state for high expansion output is a favorable characteristic of the Rankine cycle. Thus, a supercritical Brayton cycle retains the advantages of a Rankine cycle and a conventional Brayton cycle and overcomes the limitations of both.
In summary, we aim to analyse the effect of different working fluids and cycle configurations on the gas turbine CHP performance.

4-2 Modelling Approach

The following novel cycle configurations were developed in this thesis and will be studied in this chapter:

- Pure CO_2 cycle without recuperation
- CO_2-steam cycle without recuperation
- Split CO_2-steam cycle with partial recuperation
- Supercritical CO_2 (s-CO_2) cycle with partial recuperation
- Pure CO_2 -with bottoming s-CO_2 cycle without recuperation

All the cycles are compared at the same TIT fixed based on material limits, and same overall pressure ratio for comparison purposes. The following steps show the modelling procedure adopted:

1. First we consider only a power cycle. For the cycle calculations in power mode, there is no heat recovery process heat generation (no duct burner firing and the HRSGs act as coolers for a fixed mass flow rate). The values at design for the thermodynamic state parameters (for eg. p,T) are fixed to maximize the net electric efficiency. As η_e is independent of the mass flow rate, any value of design mass flow rate can be selected at this point. In the next step, we shall convert the power cycle to a CHP cycle.
2. For the mass flow rate selected in step 1, the duct burner firing required to meet the constant process demand is calculated. This step is repeated for different mass flow rates at design that leads to the calculation of CHP performance at different power to heat ratios. Thus, the mass flow rate at design is fixed by the power to heat ratio desired at design. For this study too, a constant process steam demand of 400 t/h at 90 bar and 326 °C is required from the CHP cycle.

A calculation routine for a typical Oxyfuel cycle is discussed in Appendix B, section B-1. For all the cycles described in this chapter, parametric analysis pertaining to only step 1 is shown. Step 2 is similar for all the cycles and hence briefly discussed in Appendix B, section B-1.

4-2-1 Thermodynamic gas property models

For the supercritical CO_2 cycle, REFPROP is used to compute fluid properties. For all other cycle concepts, gas property functions are calculated from pure fluid gas functions of each of the components, added together using mole fractions as weighting factors. The components are treated as ideal gases and the program augments the ideal gas relations as necessary for extreme cases like higher partial pressure of H_2O in a gas mixture, etc. The property models are tested for accuracy by [Thermoflow Inc].

4-3 Pure-CO_2 cycle without recuperation

4-3-1 Conceptual modelling

Figure 4-1 shows the process flow diagram for the CO_2 cycle with pure O_2-CH_4 firing. If the H_2O in the flue gas mixture is condensed and the CO_2 is recirculated back to the gas turbine until a steady state is reached, a Brayton cycle with working fluid dominant in CO_2 is obtained.

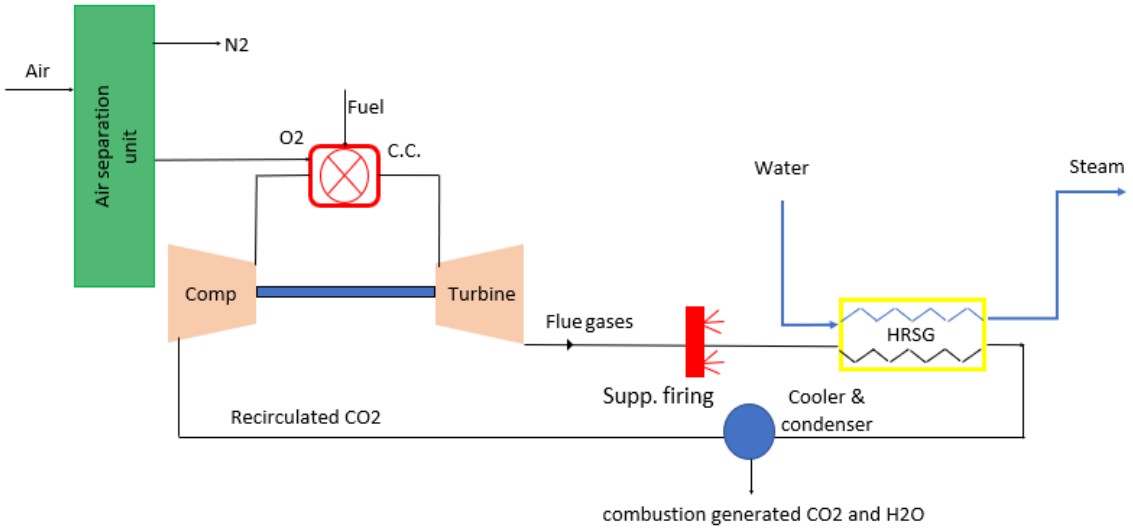

Figure 4-1: Process flow diagram of the CO_2 cycle

4-3-2 Parametric analysis

Table 4-1 shows the fixed inputs to the model and a corresponding description about how they are set.

Parameter	Basis of setting	Value	Unit
Compressor Inlet pressure	Ambient	1	bar
Compressor Inlet temperature	By gas composition desired at compressor inlet	20	°C
Turbine inlet temperature	Material limits	1127	°C
Turbine inlet pressure	Parametric analysis	40	bar
Turbine exhaust pressure	Atmospheric	1	bar

Table 4-1: Model input parameters for CO_2 cycle

At a fixed pressure, the amount of H_2O condensed from the flue gas before compressor entry depends on the temperature of the stream. This temperature must be kept as low as possible to condense all the H_2O and obtain pure CO_2 cycle. At 20 C, nearly all water is condensed such that the gas composition at compressor entry is 97.6% CO_2 by mole.
A parametric analysis has also been performed where the effect of pressure ratio on gas turbine

efficiency and power is compared with air case. Figure 4-2 shows the net cycle efficiency for only power mode for the same TIT, compressor inlet temperature and pressure, and mass flow conditions.

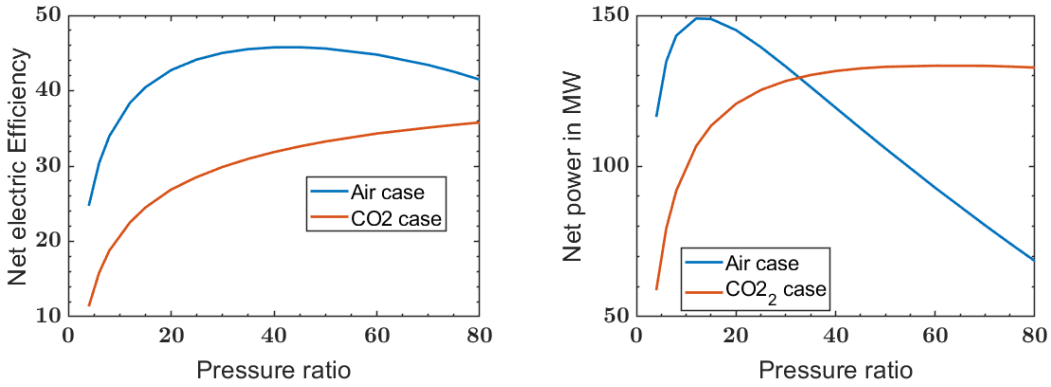

Figure 4-2: Image shows for CO_2 and air the net cycle efficiency [left] and net power [right] with increasing pressure ratio

Thus, for the same electric efficiency, the CO_2 cycle requires a higher pressure ratio due to the lower ratio of specific heats of CO_2. A pressure ratio of 40 is selected as it gives maximum efficiency for the air cycle and although for the CO_2 cycle the efficiency increases, there is no gain in power beyond a pressure ratio of 40. This pressure ratio and TIT is fixed for all the cycles that are studied.

4-4 CO_2-steam cycle without recuperation

4-4-1 Conceptual modelling

The process flow diagram of CO_2 + steam cycle is shown in figure 4-3 and is same as the CO_2 cycle with a different cooler exit temperature.

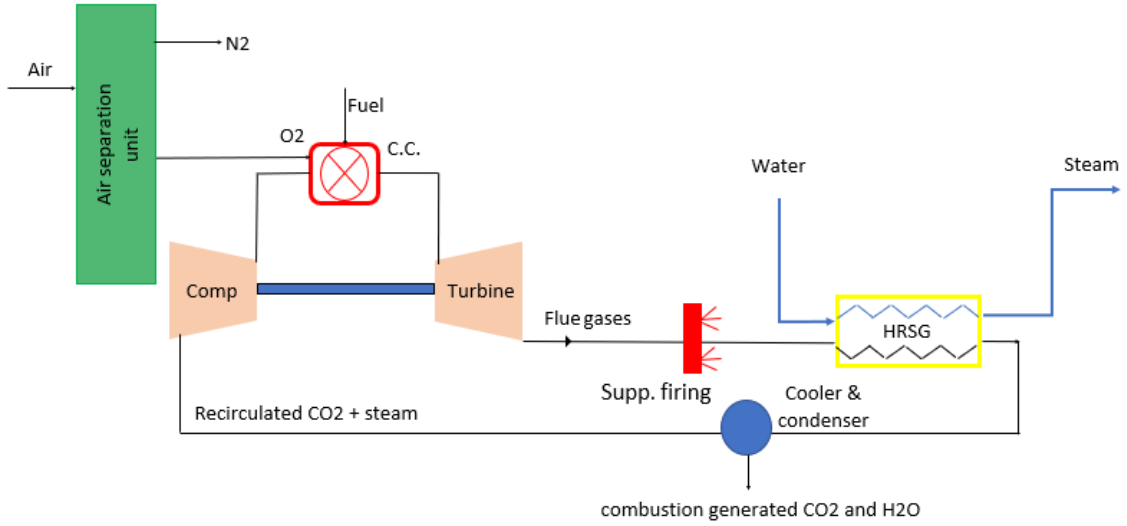

Figure 4-3: Process flow diagram of the CO_2+ steam cycle

Unlike CO_2 cycle, for the CO_2 + steam configuration, H_2O in the flue gas is not condensed completely and the compressor inlet temperature is fixed by the steam to CO_2 ratio desired at the inlet. Thus, as compressor inlet temperature increases, the steam content in the inlet mixture increases. This will have effects that form the motivation to study this configuration.

4-4-1-1 Motivation

1. When a pure CO_2 working fluid cycle and a steam CO_2 mixture working fluid cycle are compared at the same temperature ratio and pressure ratio, the net specific work obtained with CO_2 steam mixture is higher than pure CO_2 due to its different gas properties (R and γ).
2. As the temperature at compressor inlet increases, the compressor work required for the same pressure ratio increases. For the same TIT, the Carnot efficiency of the cycle decreases.
3. Also, the specific heat at constant pressure of the gas mixture increases as we move towards higher steam content. For the same mass flow rate and ΔT in the combustion chamber, more fuel is required for CO_2+Steam cycle.

These conflicting arguments lead to the conclusion that a cycle model is required to test the dominance of the above effects on cycle performance in comparison to pure CO_2.

4-4-2 Parametric analysis

The table 4-2 shows the input parameters for the CO_2 + steam cycle model after design optimizations. A parametric analysis of net electric efficiency with pressure ratio and mole

Parameter	Basis of setting	Value	Unit
Compressor inlet temperature	By mole fraction of steam at inlet	50	°C
Mole fraction of steam at inlet	By parametric analysis	12.58	%
Turbine inlet temperature	Material limits	1127	°C
Turbine inlet pressure	Same as CO_2 for common comparison basis	40	bar
Turbine exhaust pressure	Atmospheric	1	bar

Table 4-2: Model input parameters for CO_2+ Steam cycle

percent steam in the inlet mixture is performed. Note that the chosen value of steam content will directly affect the compressor inlet temperature. As shown in the performance map

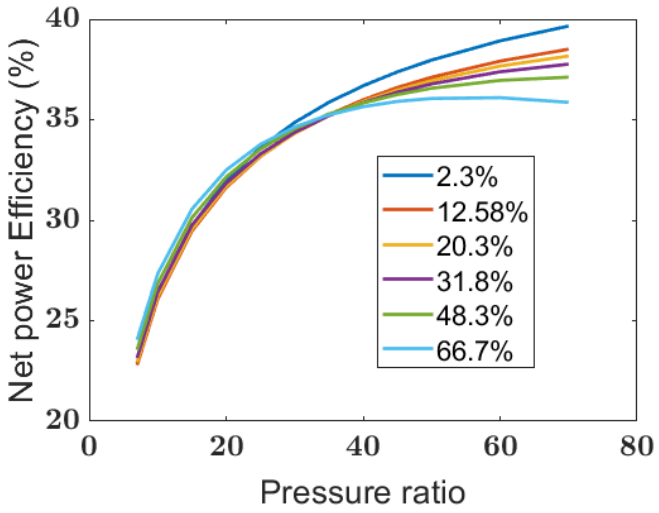

Figure 4-4: Efficiency map of CO_2+Steam cycle for different inlet steam content (in %) and pressure ratio. Curve with 2.3% steam represents the CO_2 cycle

in figure 4-4 at pressure ratios lower than 30, there is no significant difference in the net cycle efficiency compared to the CO_2 cycle (The curve with 2.3% steam represents the CO_2 cycle). However above pressure ratio of 30, the net electric efficiency drops as the steam content increases for a specific pressure ratio possibly because the effect of increase in inlet temperature and C_p dominates over the effect of higher specific work due to steam addition at higher pressure ratios. A steam content of 12.5% at inlet is selected for this study.

4-5 Split CO_2-Steam cycle with partial recuperation

4-5-1 Conceptual modelling

In this thesis, an attempt was made to improve the net cycle efficiency of the CO_2-Steam cycle. Figures 4-5 and 4-6 shows three proposed modifications to the CO_2 steam cycle at the turbine exhaust to improve cycle efficiency. In the no split configuration, the energy

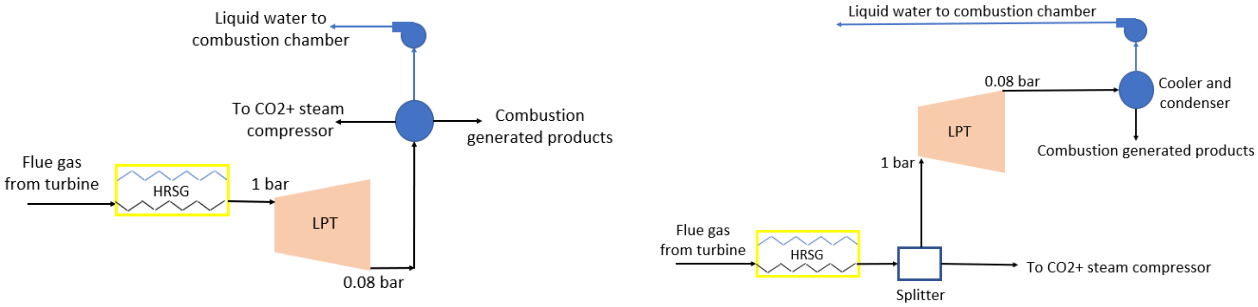

Figure 4-5: Left image: No split configuration. Right image: Split after HRSG configuration

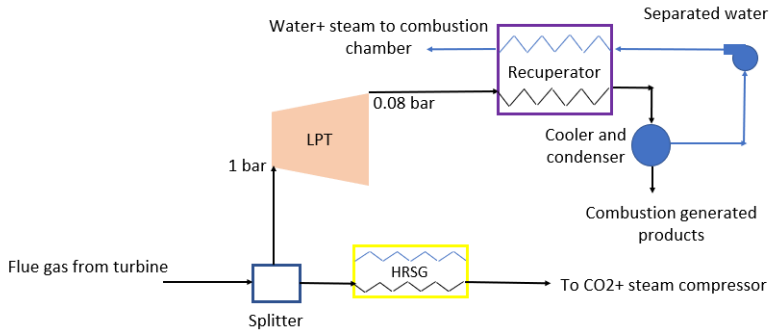

Figure 4-6: Split before HRSG with partial recuperation configuration

from the gas turbine exhaust is recovered to generate process heat before the gas stream is expanded in a turbine and later cooled and condensed. The water condensed out is pumped to the combustion chamber, the amount of steam+ CO_2 mixture formed during combustion is removed from the cycle and the remaining mixture is compressed to the combustion chamber pressure. In CO_2-Steam split before HRSG configuration, the high enthalpy HPT exhaust stream is split before one stream enters the HRSG and the other is expanded until 0.08 bar. High grade heat energy still available at this turbine exhaust is recovered by heating the water going to the combustion chamber. The power cycle efficiencies of the three configurations are compared to the CO_2-steam cycle without recuperation in table 4-3. These efficiencies are computed at the same pressure ratio of the main (high pressure) turbine, same TIT and same mass flow. The best performing CO_2 -Steam split before HRSG configuration is selected for further analysis. The process flow diagram of the split CO_2- Steam cycle is shown in figure. 4-7.

Cycle concept	Power cycle efficiency (%)
CO_2-Steam	30.87
CO_2-Steam No split	28.69
CO_2-Steam Split before HRSG with partial recuperation	39.62
CO_2-Steam Split after HRSG	32.2

Table 4-3: Power cycle efficiency comparison of different concepts

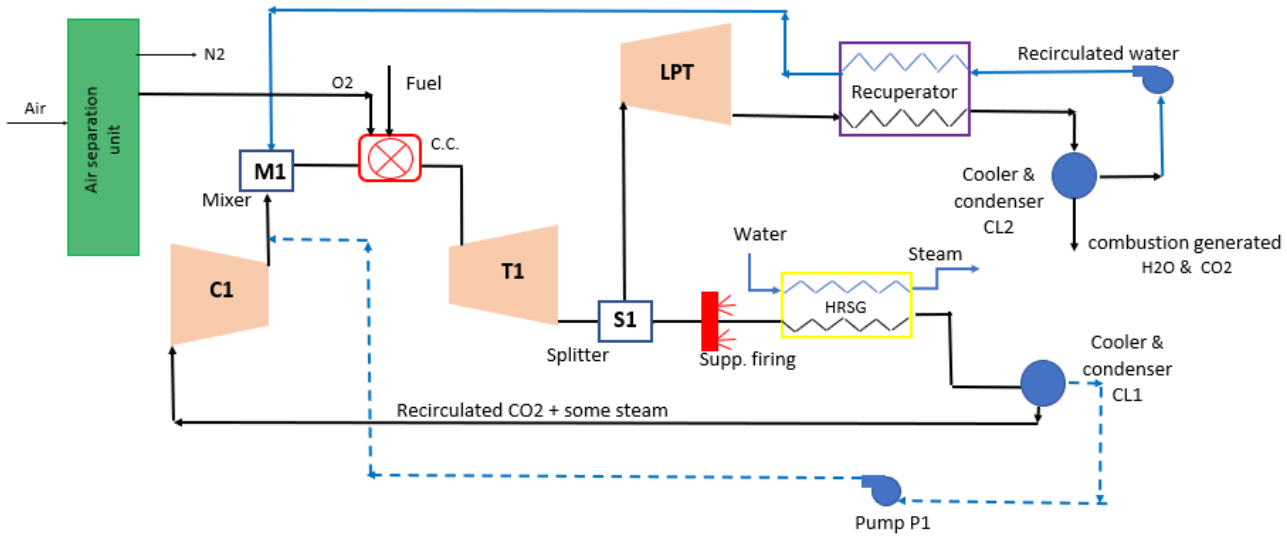

Figure 4-7: Process flow diagram of the CO_2+ Steam Split with partial recuperation cycle

In this concept, the gas expanded from 40 bar until 1 bar consisting of CO_2+steam is split into two streams. One stream is cooled to the compressor C1 inlet temperature and later compressed until 40 bar. The other stream is expanded further until 0.08 bar, cooled further to ambient conditions so that water and CO_2- steam mixture can be separated. The mass flow of the separated CO_2 steam mixture is exactly same as that generated during combustion. The separated water (from CL2) is pumped before it enters the combustion chamber. The concept of this cycle is partly similar to the S-GRAZ cycle by [Sanz et al.]. The gas entering the compressor C1 is cooled in an HRSG which generates the process demand for the CHP cycle, followed by cooler CL1. The cooler CL1 exit temperature decides the amount of water going through the pump P1. As for all cycles, the emitted CO_2 stream is available from 1 bar, the compression work of the exhausted CO_2-steam stream from 0.08 to 1 bar is also considered in this analysis.

4-5-1-1 Motivation

- The net power efficiency of the CO_2+ steam cycle is augmented by the addition of the low pressure expansion loop for a part of the working fluid as shown in figure 4-7.
- Part of the cycle working fluid is also pumped which appreciably reduces the pressurizing

power requirement leading to an increased efficiency.

- However, water is directly mixed with the high temperature compressed gas reducing the enthalpy at combustion chamber inlet. The specific heat at constant pressure of water is also high, along with the fact that latent heat will have to be supplied in the combustion chamber. Both these effects can lead to very high fuel consumption for the cycle leading to reduced efficiency.

Thus, due to contradicting effects observed also in this configuration, it is modelled and performance is analysed.

4-5-2 Parametric analysis

Table 4-4 shows the input parameters required for this cycle model.

Parameter	Basis of setting	Value	Unit
Compressor inlet temperature/ Condensing temperature	By parametric analysis	100	C
% Water at inlet to the mixer M1	By parametric analysis	40	%
Turbine inlet temperature	Material limits	1127	C
T1 Turbine pressure ratio	Same as CO_2 cycle for common comparison basis	40	-
LPT Turbine exhaust pressure	Lowest possible	0.08	bar

Table 4-4: Model input parameters for Split CO_2+Steam with recuperation cycle

The effect of varying the design compressor inlet temperature and the mixing ratio are evaluated on the net cycle efficiency. Mixing ratio is the ratio of the amount of water from the Recuperator (solid blue line in figure 4-7 to the amount of CO_2+ Steam mixture (solid black line emerging from compressor C1) at the inlet of mixer M1. Note that even though there is no unique cycle pressure ratio for this cycle, we will consider the overall pressure ratio of the cycle as 40 which corresponds to the pressure ratio of the turbine T1 and compressor C1, as any gain in power from other components apart from these (power produced by the LPT expansion loop), will be considered as additional power due to the new working fluid concept of the cycle.

Figure 4-8 shows that there is an optimum compressor inlet temperature/ CL1 exit temperature for all the mixing ratios. This temperature determines the liquid water content through pump P1 (shown in dotted blue lines). The optimum temperature occurs as temperature increases from 50 °C, the water condensed and pumped from cooler CL1 decreases, so lesser and lesser energy is required in the combustion chamber for evaporation of water. This happens until a temperature where no water is condensed and further increase in temperature leads to higher compression energy eventually lowering the efficiency as the temperature is increased.

It can also be seen from the same graph that as the mixing ratio increases, the efficiency increases. This is due to the fact that although the fuel required for evaporation increases with increased water content, the effect of increase in net power output due to lower compressor

work required and larger portion of working fluid expanded until 0.08 bar dominates. A mixing ratio of 0.4 (40%) is selected as at higher mixing ratios, the electric efficiency is high such that very low energy is available for the process heat generation and unacceptable duct burner temperatures would be required.

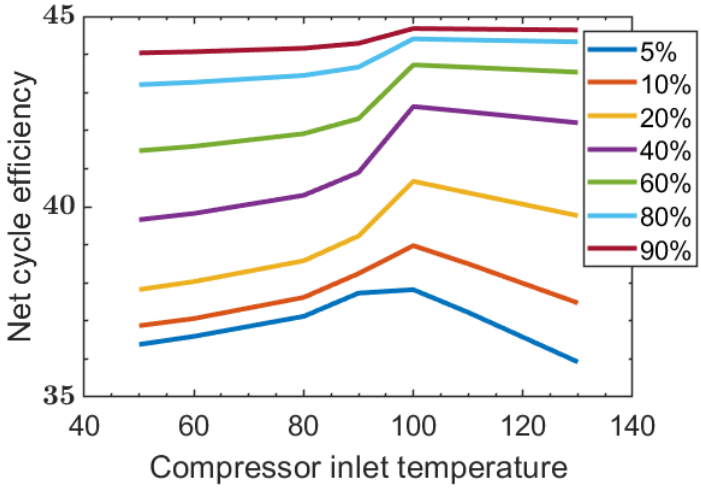

Figure 4-8: Plot for compressor inlet temperature vs Net power cycle efficiency at different mixing ratios (represented here as % water at inlet to the mixer M1)

4-6 Supercritical CO_2 cycle with partial recuperation

4-6-1 Conceptual modelling

This cycle design is similar to the Allam cycle [Allam et al. (2014)]. The process flow diagram of the supercritical CO_2 cycle for this analysis is shown in figure 4-9.

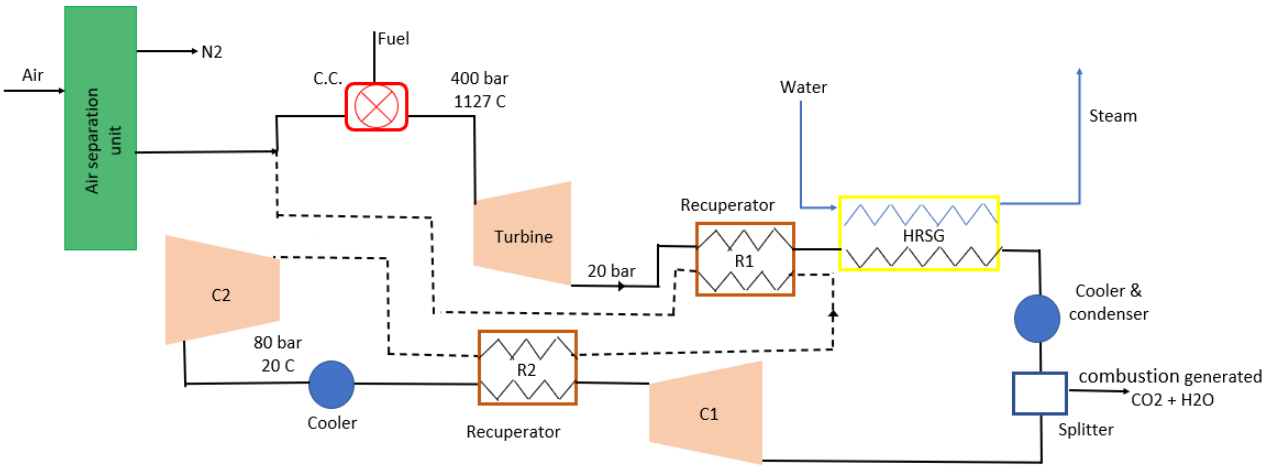

Figure 4-9: Process flow diagram of the supercritical CO_2 cycle

4-6-1-1 Partial recuperation

The supercritical CO_2 power cycle is highly recuperated which gives the cycle its high efficiency. However for CHP, very large recuperation cannot be utilized as the aim is to recover high grade heat for industrial processes for which large enthalpy at the exhaust is required. With complete recuperation, very high duct burner firing is required for process generation. The limit is that the process heat demand has to be supplied completely by additional firing leading to decoupling between power and process cycles and tending to separate generation (no waste heat utilization). In partial recuperation, the recuperator and the HRSG are placed in series after the gas turbine. Due to the high enthalpy of gas available at exhaust, the temperature of gas at recuperator exit can be set to satisfy the process demand. Thus, unlike other cycles where the duct burner firing is controlled to meet process demand at different design mass flow rates, in this cycle, the recuperator exit temperature is the control parameter. At higher power to heat ratios, higher mass flows through the cycle. Thus, lower temperature at HRSG inlet is required. Therefore higher heat is available for recuperation and the cycle efficiency increases at higher power to heat ratios.

4-6-2 Parametric analysis

Table 4-5 refers to the input parameters for the supercritical CO_2 cycle concept. As in literature, the cycle parameters are optimized for a fully recuperated cycle, the inputs in this

thesis for partially recuperated cycle are set by parametric analysis. Figure 4-10 shows the effect of the C1 compressor inlet temperature on the net power cycle efficiency.

Parameter	Basis of setting	Value	Unit
Sub-critical compressor (C1) inlet temperature	By parametric analysis	20	C
Super-critical compressor (C2) inlet temperature	Minimum possible to reduce compression power	20	°C
Turbine inlet temperature	Material limits	1127	°C
Turbine inlet pressure	By parametric analysis	400	bar
Turbine exhaust pressure	By parametric analysis	20	bar

Table 4-5: Model input parameters for supercritical CO_2 cycle

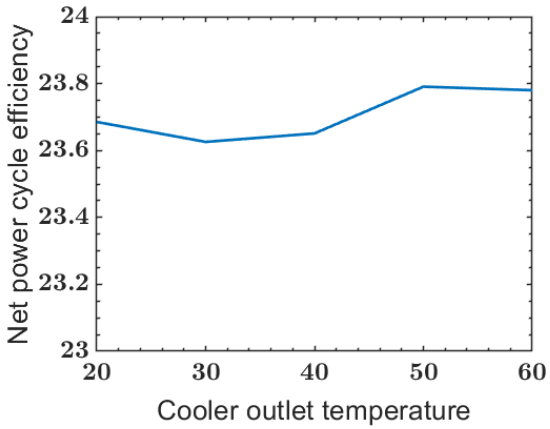

Figure 4-10: Net power cycle efficiency with cooler outlet/ C1 compressor inlet temperature

The main deduction from figure 4-10 is that the s-CO_2 cycle efficiency is insensitive to the temperature at the inlet of the subcritical compressor (C1) in the range 20 to 60°C. The very low efficiency of 23% arises as only 9% of energy available at turbine exhaust is being recuperated.

4-7 Pure CO_2 -bottoming s-CO_2 cycle without recuperation

4-7-1 Conceptual modelling

In this cycle, the electric efficiency of the CO_2 cycle is improved by bottoming the cycle with a completely closed supercritical CO_2 cycle. The process flow diagram for the cycle is shown in figure 4-11. The bottoming closed cycle is initially charged with CO_2, and flows at a design mass flow rate that is determined by the topping cycle design mass flow rate to maximize the heat exchanger effectiveness.

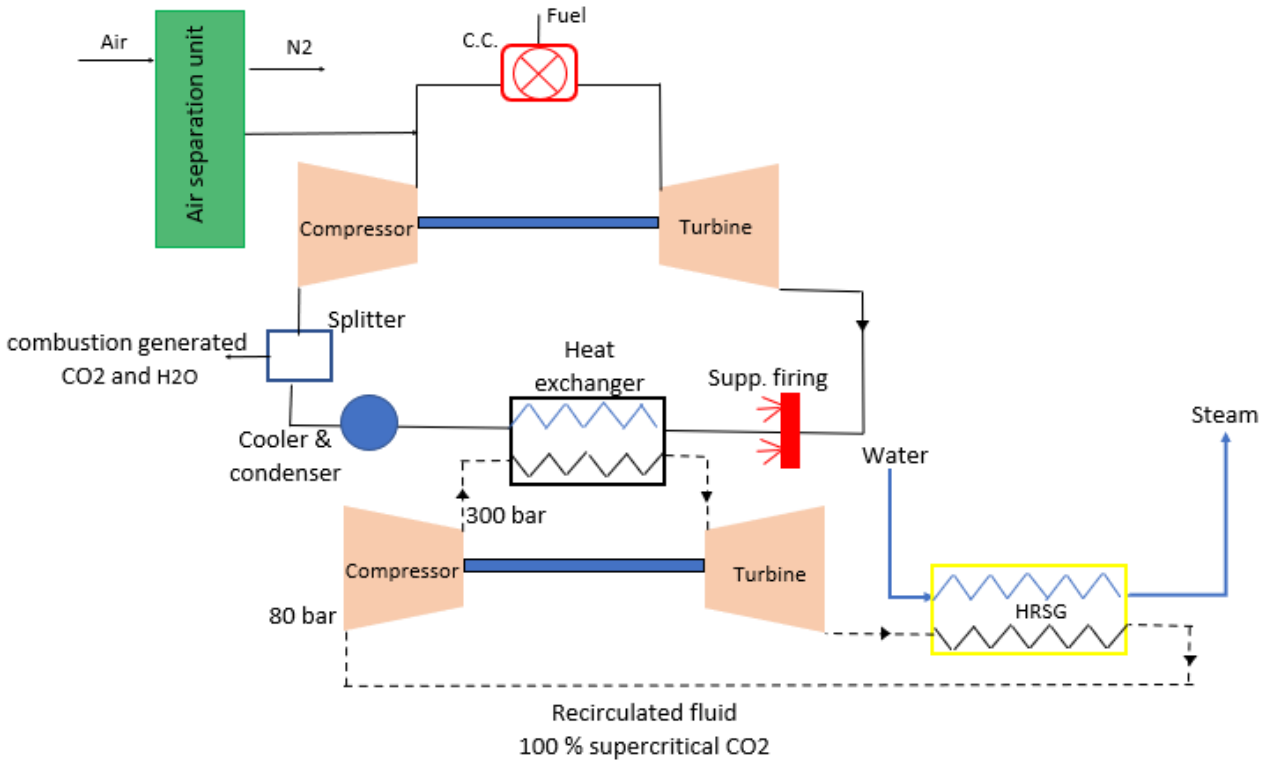

Figure 4-11: Process flow diagram of pure CO_2- bottoming s-CO_2 cycle

4-7-2 Parametric analysis

The main cycle design parameters are given in table 4-6. The exhaust pressure of bottom cycle turbine is set at 80 bar for the following reasons:
1. Gain in efficiency due to high density of CO_2 at compressor inlet is only obtained at a compressor inlet pressure of 80 bar (near critical pressure).
2. Expanding until lower pressures would lead to very low enthalpy available at turbine exhaust, thus leading to impractical duct burner temperatures required to meet the CHP demand.
The compressor inlet temperature of 40°C was set based on optimization for maximum electric efficiency.

Parameter	**Basis of setting**	**Value**	**Unit**
CO_2 compressor inlet temperture	By parametric analysis	40	°C
CO_2 Turbine inlet temperature	Material limits	1127	°C
CO_2 Turbine pressure ratio	By parametric analysis	40	–
s-CO_2 compressor inlet temperature	Minimum possible to reduce compression work	20	°C
s-CO_2 Turbine inlet pressure	From literature	300	bar
s-CO_2 Turbine exhaust pressure	From literature	80	bar

Table 4-6: Model input parameters for pure CO_2- bottoming sCO_2 cycle

4-8 Results and interpretation

4-8-1 Power-mode performance

Figure 4-12 shows the net power cycle efficiency for power cycles optimised for CHP (cycles obtained in step 1 of the modelling approach in section 4-2) with pressure ratio. The dotted line representing 40 bar represents the design point for all power cycles. In left figure 4-12, it can be observed that the net power efficiency improves for the CO_2 cycle and CO_2 steam cycle by adding the s-CO_2 bottom cycle and the split configuration respectively. The low efficiencies in power mode for all the cycles is a consequence of not utilizing part of the high grade heat at turbine exhaust for power generation purpose, but instead reserving it for process generation. Maximum heat could be utilized to boost electric efficiency by, for example employing recuperation or adding a bottoming steam cycle. Table 4-7 shows the difference in electric efficiencies for not employing the rejected heat for power generation in the cycle concepts at design overall pressure ratio and same TIT. For the detailed process flow diagrams of the modifications given in table 4-7, the reader is referred to the Appendix B.

Base cycle in power mode	**Modifications used to utilize maximum waste heat for power**	**Optimised for power (η_{el})**	**Optimised for CHP (η_{el})**
Air cycle without capture	Bottoming steam Rankine cycle	59	45
CO_2	Bottoming steam Rankine cycle	46	30.4
CO_2-Steam	Bottoming steam Rankine cycle	45.6	29.7
Split CO_2-Steam	Complete recuperation by further heating the water entering the combustion chamber	44.5	39.62
supercritical CO_2	Complete recuperation	48	23.65
CO_2-bottom s-CO_2	Recuperating bottoming cycle turbine exhaust heat for further power generation (Refer PFD B-6)	47.4	40.37

Table 4-7: Comparison of electric efficiencies for a) Cycles optimised for power and b) Cycles optimised for CHP

Right figure 4-12 shows the same table 4-7 in a bar graph format. The main conclusion from right figure 4-12 is that the maximum cycle efficiency when the cycles are optimised for power and CHP occurs for Air Combined cycle without carbon capture (59% and 45% respectively). With Oxy-fuel combustion and carbon capture, the maximum electric efficiency is lower owing to the energy requirement of the ASU. As can be seen from table 4-7, the penalty for employing s-CO_2 cycle for CHP is very high.

4-8-2 CHP-mode performance

CHP performance is computed for cycles after also completing step 2 given in the modelling approach in section 4-2. Figure 4-13 represents the CHP electric efficiency and CHP Total Energy Efficiency (TEE) with Power to Heat ratio (P2H) at design. The CHP electric performance at a given P2H (left of figure 4-13) varies from the power mode electric performance (figure 4-12) due to the different additional input energy required by the duct burner for different cycles at different power to heat ratios.

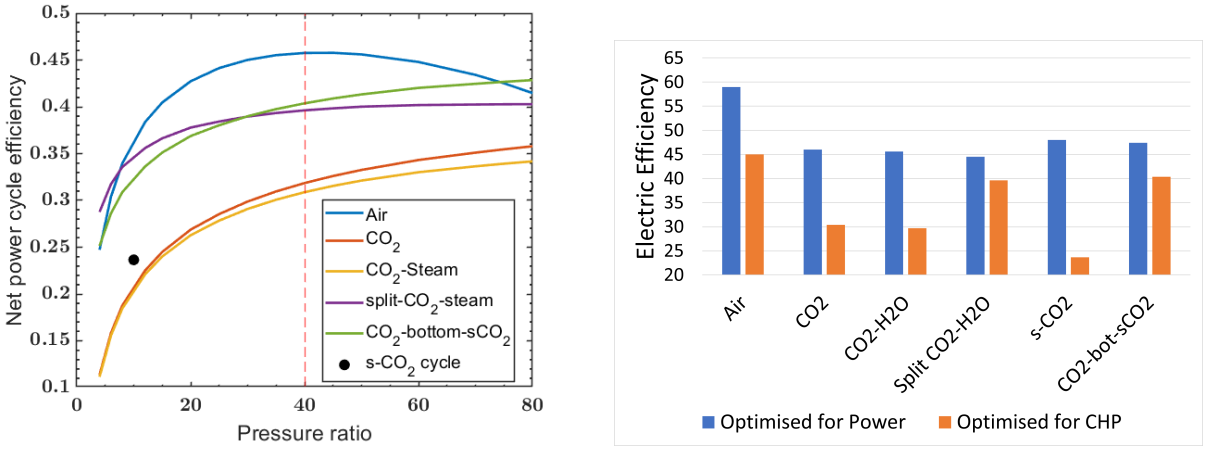

Figure 4-12: Left: Comparison of net cycle efficiency for different cycle concepts optimised for CHP with pressure ratio. The design line of 40 bar pressure at turbine inlet common for all is shown in dotted red. Right: Comparison of electric efficiencies of cycles optimised for CHP to that optimised for power.

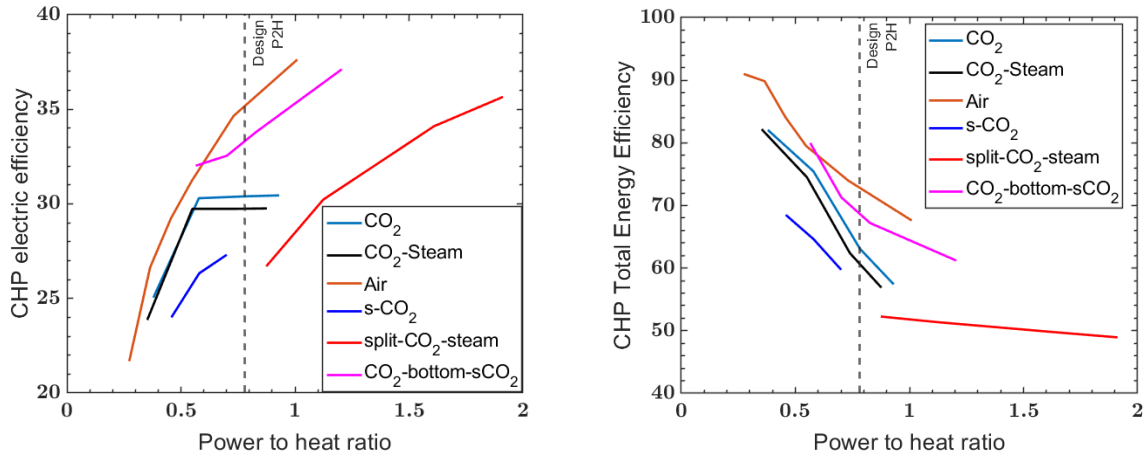

Figure 4-13: Image shows CHP electric efficiency [left] and CHP Total Energy Efficiency [right] with increasing design point power to heat ratio

The design power to heat ratio (P2H) is chosen as a typical number of 0.78 based on the design P2H of the post combustion and pre-combustion capture cycles. At this P2H, the top three performing cycles (from figure 4-13) are Air cycle without capture, CO_2 cycle with bottoming sCO_2 cycle and pure CO_2 cycle, respectively. The poor performance of the Split CO_2-Steam cycle in CHP mode is due to a very high duct burner firing required as a result of part of the gas turbine exhaust heat being utilized for power generation. Although the CHP performance of CO_2 cycle with bottoming sCO_2 cycle is better compared to all cycles with carbon capture, it will not be considered for further analysis due to the complexities involved with closed CO_2 cycle at supercritical states, and lack of author's knowledge on the feasibility of such a cycle.

This analysis suggests a superior performance of the air cycle without carbon capture compared to the CO_2 cycle with carbon capture. It is also evident from the previous chapters that post combustion and pre-combustion carbon capture techniques for air cycles are energy intensive. So, it is also important to compare the Oxy-fuel CO_2 cycle to them at a fixed design point Power to heat ratio, so as to have a common basis of comparison.

4-8-3 Discussion on the general trend of CHP performance

As it is evident from the general trend for the working range of power to heat ratio in figure 4-13 that the CHP TEE decreases and CHP electric efficiency increases for increasing power to heat ratio for all the cycle concepts. As power to heat ratio tends to higher values, the CHP cycle tends to a power cycle. As power to heat ratio tends to very low values, the CHP cycle tends to a boiler. If the data obtained in left figure 4-13 is extrapolated to high power to heat ratios, after a point, the CHP electric efficiencies will not change with increasing power to heat ratio such that the cycle efficiency values will be same as figure 4-12. This is evident from figure 4-13, as the CO_2 cycle and CO_2+ Steam cycle electric efficiencies are flat after a P2H of 0.5. This happens as after a certain high mass flow rate (and thus, also a high power to heat ratio), no duct burner firing is required to satisfy the process demand. At that point, the gas turbine exhaust heat is just enough to supply the process heat completely. Therefore, beyond that point (at a further higher mass flow rate or P2H), the TEE reduces due to higher stack losses. This phenomena governs the shape of the curves in figure 4-13. Maximizing the CHP electric efficiency gives utmost value to power and pushes the system to operate at high power to heat ratios (power cycle regime) without considering the energy utilization from the cycle which is also important for a CHP. Maximizing Total Energy Efficiency does not consider that power is a more valuable contribution to the energy utilization and focuses only on increasing the energy utilization by dragging the system to operate in the boiler regime.

Thus, like the power cycle has net thermal efficiency, there is no single thermodynamic criteria for optimization of CHP cycles.

The design space for working range of power to heat ratios is different for different applications. For a high grade heat recovery application like this case, the general design space is at a lower power to heat ratio (0.78 in this case). For a low grade heat recovery application like district heating, the design space is at higher power to heat ratios.

4-8-3-1 Comparative analysis

If figure 4-13 is referred to carefully, at a design power to heat ratio of 0.78, the waste heat from the pure CO_2 cycle is not recovered completely. This can be witnessed by the constant electric efficiency and reducing CHP efficiency after a P2H of 0.5. Thus, the pure CO_2 cycle has a potential for a higher electric efficiency with added heat recovery at this design P2H of 0.78 either by recuperation or by generating extra steam and expanding in a steam turbine, thus producing additional power from the extra waste heat. By implementing the latter option, the electric efficiency of the cycle increases to 33.7%. This modified pure CO_2 cycle will be considered for further analysis. The next chapter deals with the comparison of the post combustion capture, pre combustion capture and Oxy-fuel cycles extensively.

4-9 Summary

1. The top performing cycles (with respect to CHP electric efficiency and total efficiency) are Air cycle without capture, CO_2 cycle with bottoming sCO_2 cycle and pure CO_2 cycle, respectively. The next chapter compares air cycle with carbon capture and pure CO_2 cycle with carbon capture. CO_2 cycle with bottoming sCO_2 cycle is not studied further as the cycle is highly complex for the scope of the thesis.

2. At a typical power to heat ratio of 0.78, the CO_2 cycle performance is further improved by heat recovery for power generation.

3. There is no unique thermodynamic parameter that can be maximized to get the optimum CHP cycle unlike power cycles which has net thermal efficiency as a universal parameter. This is mainly because the outputs of a CHP cycle are non homogeneous (power and heat).

Chapter 5

Comparative analysis of selected cycles

In the previous chapter, the Oxy-fuel CHP cycle with CO_2 was identified as a potential zero-carbon CHP technology. However, in comparison to an air-cycle without capture, it offered a lower thermodynamic performance. It then becomes important to compare the Oxy-fuel CHP cycle with air-cycle including capture, as we have already seen in chapters 2 and 3 that introducing carbon capture reduces the thermodynamic performance of the air CHP cycle. In this chapter, a simplistic techno-economic comparison of the air cycle with different capture techniques and the Oxyfuel-CHP cycle with CO_2 working fluid is performed.

5-1 Methodology for economic analysis

In this study, the Levelized cost of electricity (LCOE) and the cost of CO_2 avoided are used as economic performance parameters. Figure 5-1 shows the common system boundary for all the cycles considered in this analysis:

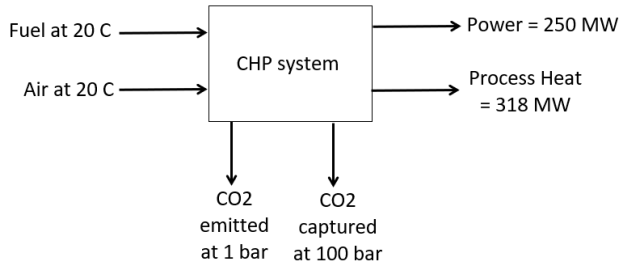

Figure 5-1: Image shows the common system boundaries considered for all the selected cycles

The LCOE is a fundamental calculation used in the preliminary assessment of an energy-producing project. It is a measure of the average net present cost of electricity generation for a generating plant over its lifetime and is calculated as the ratio between all the discounted costs over the lifetime of an electricity generating plant divided by a discounted sum of the actual energy amounts delivered.

$$\text{LCOE} = \frac{\text{NPV of Total Costs Over Lifetime}}{\text{NPV of Electrical energy produced over lifetime}} \tag{5-1}$$

Description of costs:
In this analysis the following costs incurred for electricity generation are taken into account:

1. Capital costs taken from table 5-2
2. Fixed and variable (fuel) operating costs taken from table 5-3
3. Additional cost of natural gas required in a cycle compared to a boiler without capture generating same amount of process heat. This gives the additional fuel required to generate power from the cycle. The cost of natural gas is taken as 35 EUR/MWh from [Naturalgas-price]
4. Additional cost of CO_2 captured from the cycle compared to a reference boiler without capture generating same amount of process heat. The CO_2 capture cost includes the cost of CO_2 compression, CO_2 transport and CO_2 storage. This accounts to 46 EUR/tonne CO_2 taken from [Sam Lamboo and Lensink (2021)].
5. Additional cost of CO_2 emitted from the cycle compared to a reference boiler without capture generating same amount of process heat. This cost is a negative cost as the CO_2 emitted from a cycle with capture unit is always lower than that from a natural gas boiler without capture. The present value of the carbon cost is 54 EUR/tonCO_2 taken from [Carbon-price].

Thus the LCOE can be calculated as:

$$\text{LCOE} = \frac{\text{I} + \sum_{\text{t=1}}^{\text{n}} \frac{\text{F}_\text{t}+(\text{O\&M})_\text{t}+\text{C}_\text{t}^\text{em}+\text{C}_\text{t}^\text{cap}}{(1+\text{r})^\text{t}}}{\frac{\text{E}_\text{t}}{(1+\text{r})^\text{t}}} \tag{5-2}$$

where,

I_t = Total Capital costs in M€
F_t = Additional Fuel costs (Variable operation costs) in M€ in year t
$(\text{O\&M})_\text{t}$ = Fixed Operation and maintenance costs in M€ in year t
$\text{C}_\text{t}^\text{em}$ = Additional Cost of CO_2 emitted M€ in year t
$\text{C}_\text{t}^\text{cap}$ = Additional Cost of CO_2 captured M€ in year t
E_t = Electrical output in MWh in year t
r = Discount rate

Note that all the costs except Capital costs are calculated in relation to a natural gas boiler with the same process generation. This is because, the goal of this study is to compare CHP cycles that have heat as a primary product and additional power as a secondary product. Therefore, the levelized cost of electricity, in this study represents the cost of additional electricity generated from the CHP plants (Marginal cost of electricity).The LCOE is calculated at a discount rate of 7% and the lifetime of the plants are assumed to be 15 years.

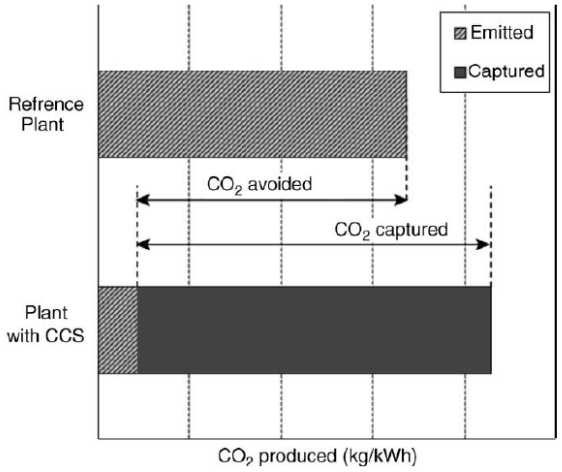

Figure 5-2: Image shows the difference between CO_2 captured and CO_2 avoided

Next, the cost of CO_2 avoided is calculated. Cost of CO_2 avoided is defined as the additional cost of electricity (LCOE) incurred due to the deployment of CCS per unit tonne of CO_2 avoided. The concept of CO_2 avoided can be understood from left figure 5-2.

$$CO_2 \quad \text{avoided} \quad \text{cost} = \frac{\text{LCOE}_{\text{CCS}} - \text{LCOE}_{\text{Ref}}}{\text{CO}_2{}^{\text{emitted}}_{\text{Ref}} - \text{CO}_2{}^{\text{emitted}}_{\text{CCS}}} \tag{5-3}$$

where, subscript Ref refers to a reference CHP without capture and CCS refers to a case of CHP with CCS.

For calculating the LCOE, Capital expenditure and operating expenditure of the CHP plants based on the selected cycles are estimated with a very simplistic approach. A general procedure for estimating the costs is followed as explained:

1. First, a cost estimate of the base case CHP plant is made using data from the literature as discussed in table 5-1.
2. Then, the cost of additional elements of the selected cycles are added to the cost estimated in step 1. The costs of these additional elements are also calculated from the data available in literature.

Having discussed a broad explanation of how economic analysis is performed in the study, in the next section, first, the thermodynamic analysis is discussed, followed by an economic analysis, followed by a flexibility analysis.

5-2 Results

5-2-1 Thermodynamic analysis

In this section, the CHP electric efficiency and the CHP total efficiency for selected cycles namely: the post combustion capture, post combustion capture with EGR, Pre-combustion

capture and Oxyfuel CO_2 cycles are compared at Design point. Figure 5-3 shows the results. Figure 5-4 shows the CO_2 emissions from the selected cycles. Results show a slightly superior

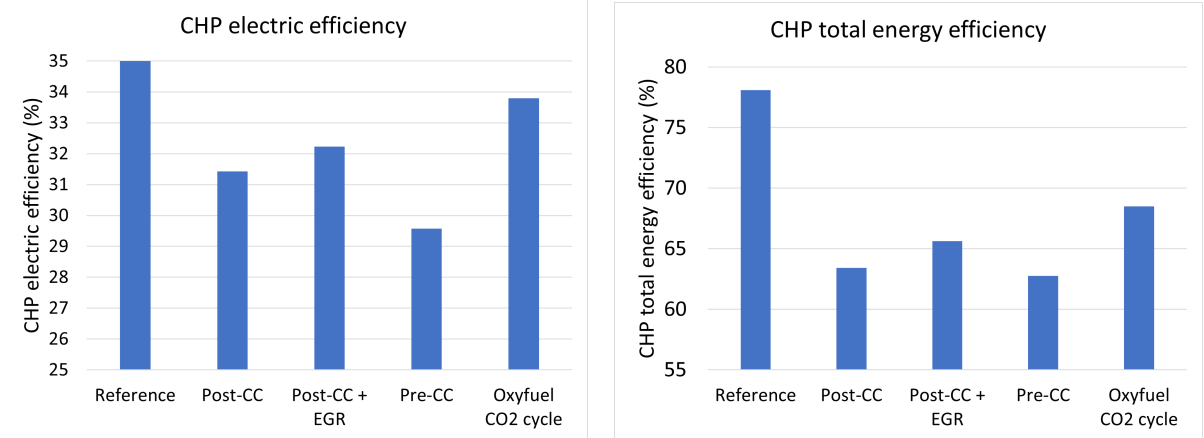

Figure 5-3: Left: Image shows CHP electric efficiency and Right: Image shows CHP total efficiency for different CHP cycles with carbon capture

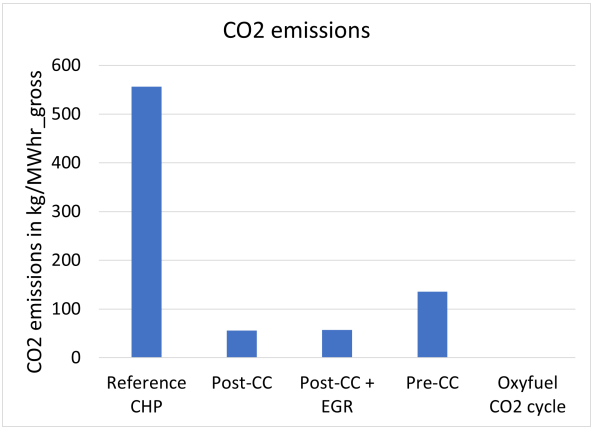

Figure 5-4: Image shows CO_2 emissions from the respective cycles

thermodynamic performance of the Oxy-fuel CO_2 cycle compared to others. Another observation is that, for an air-CHP cycle without capture, the CHP electric and CHP total efficiency at design P2H of 0.78 is 35% and 79% respectively. However, with capture and exhaust gas recirculation, the maximum electric efficiency and CHP total efficiency attainable is 33.7% and 69% without considering CO_2 compression. This represents a drop of 1.3% points and 10% points respectively due to capture.

5-2-2 Economic analysis

5-2-2-1 CAPEX estimation

In Rezvani et al. (2009), a CAPEX estimate of an NGCC power plant of 380 MW net power output is made. In this thesis, the cost estimate of base case CHP is simplified by subtracting

the CAPEX as well as the output of a steam turbine, and CAPEX of a condenser from the CAPEX of the NGCC. Then, table 5-1 is obtained corresponding to a base-case CHP.

Net power output	MW	243
WH-Boiler	M€	23
HX+ Cooling	M€	11
Pumps	M€	1
Piping	M€	1
GT	M€	86
Duct Burner	M€	2
Misc	M€	0
Indirect	M€	28
Total	M€	152
Specific Investment	€/kW	627.4

Table 5-1: CAPEX estimate for base case CHP taken from Hu and Ahn (2017) and IEAGHG (2015)

Table 5-2 refers to the additional expenditures incurred by adding additional components to the standard base case CHP components to represent the selected cycles. Exhaust gas recirculation reduces the CAPEX by upto 9% due to smaller CO_2 capture unit required for reduced gas flow rates. Figure 5-5 shows a bar graph of the CAPEX for the different cycles. Oxy-fuel cycle with CO_2 is the most economic option while Pre-combustion capture with hydrogen generation on site is expensive.

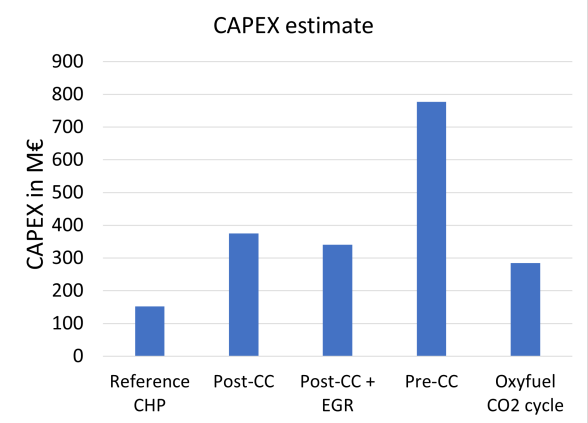

Figure 5-5: CAPEX of values of the selected cycles

5-2-2-2 OPEX estimation

The operating expenditure of the selected cycles is computed by adding the variable fuel costs to the fixed operating and maintenance costs. The fixed Operating costs are obtained from literature and the variable fuel costs are determined from the cycle analyses (mass and energy balance) performed in this thesis. Table 5-3 gives the values of the fixed and variable costs

Cycle	Added/Modified elements	References	Comments	CAPEX computation
Post combustion CO_2 capture	Steam turbine, CO_2 Chemical absorbption unit, CO_2 compressor	Hu and Ahn (2017), Almansoori et al. (2021)	Data shows an average increase of 180 M€ to the base CHP by addition of the capture and compressor unit. Additional 43 M€ is added for the steam turbine	152+180+43 = 375 M€
Post combustion CO_2 capture+ EGR (40%)	Steam turbine, CO_2 Chemical absorbption unit, CO_2 compressor, EGR system	Hu and Ahn (2017)	Data estimates a CAPEX reduction of 9% with EGR of 40% with respect to Post combustion capture for a plant output of 577 MW. The same percent reduction is used in this work.	375*0.91 = 341 M€
Precombustion capture with SMR and Heat integration	SMR, WGS, CO_2 capture unit, CO_2 compressor, Heat exchangers	Jakobsen and Åtland (2016), IEAGHG (2017)	CAPEX data is available for 20 t/h and 8.9 t/h of H_2 output. The former was chosen for this study	152+625 = 777 M€
CO_2 Oxy-fuel cycle	Gas Turbine, ASU, Flue gas condenser, CO_2 compressor	IEAGHG (2015), Rezvani et al. (2009)	Data from two sources show an increase in the CAPEX by 64% and 87.5% compared to NGCC for an Oxy-fuel CO_2-based combined cycle for GT output of 243 MW and 500 MW respectively. The latter value is used in this study to be on a safer side.	152 *1.875 = 285 M€

Table 5-2: CAPEX estimation for the selected cycles

for the selected cycles. As fuel costs dominate the variable operating costs, no other variable costs are considered. The natural gas price of 35€/MWh is used from [Naturalgas-price]. The histogram in figure 5-6 shows that the lowest OPEX is for Oxy-fuel cycle with CO_2 again. This is due to the fact that it has a higher energy efficiency and thus requires lesser fuel for the same power.

Cycle	Fixed Operating cost	Reference	Variable operating (Fuel) costs	Total OPEX (M€/year)
Base case CHP	16	IEAGHG (2015)	181	197
Post combustion capture	16+21.5 = 37.5	Almansoori et al. (2021)	238	275
Post combustion capture + EGR (40%)	16+21.5 =37.5	Hu and Ahn (2017)	228	266
Pre combustion capture	16+47 = 63	Jakobsen and Åtland (2016)	232	294
Oxyfuel CO_2 cycle	32.5	IEAGHG (2015)	239	271

Table 5-3: Table gives the fixed operating and maintenance costs obtained from literature and the variable operating costs (only fuel) obtained from cycle energy balance

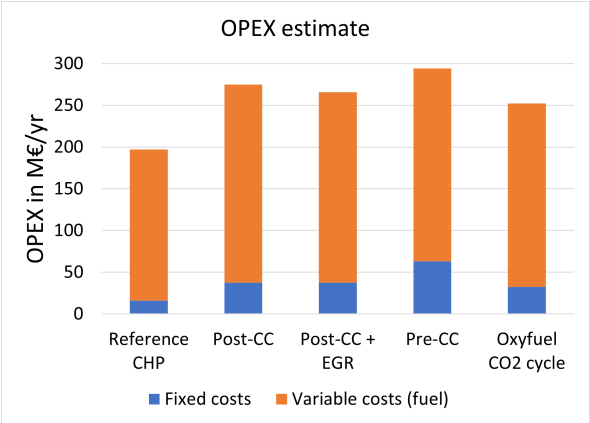

Figure 5-6: Image showing break up of total Operating costs for the selected cycles

5-2-2-3 LCOE computation

The left figure 5-7 shows the LCOE for the selected cycles with the minimum cost for Oxy-fuel CHP with CO_2, primarily because of its higher electric and CHP efficiency at the given Power to heat ratio. Also, a sensitivity analysis for the cost of CO_2 emitted has been performed. It is varied from the current price of 54 EUR/tonCO_2 to 200 EUR/ton and its effect on the LCOE is studied. As shown in right figure 5-7, the marginal cost of electricity decreases with increasing cost of CO_2 emitted. This is a result of negative CO_2 emissions from the selected CHP plants when compared to a natural gas boiler delivering the same process heat. So, increasing the cost of CO_2 emissions imposes higher costs on a boiler without capture and relatively gives more and more benefit to a CHP equipped with CCS.

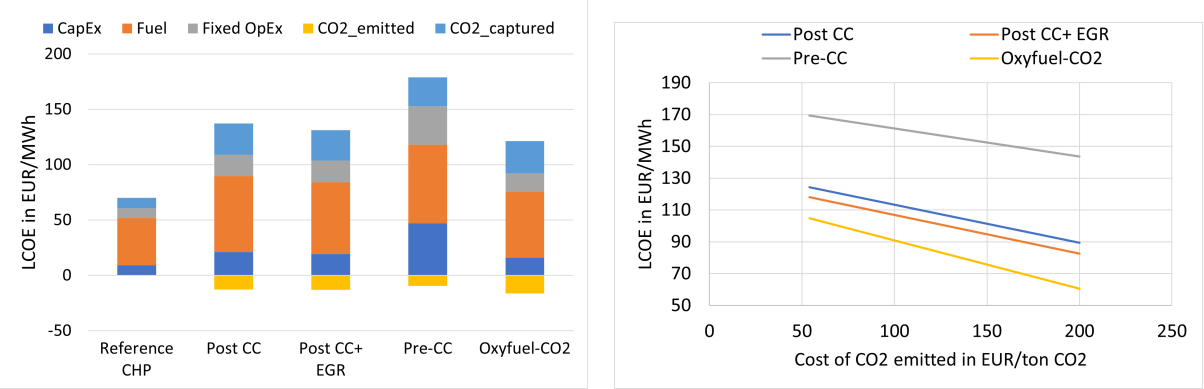

Figure 5-7: Left: Image shows LCOE for the selected cycles. Right: Image shows the sensitivity of CO_2 emitted cost on the LCOE for the selected cycles

Next, the LCOE is used to calculate the cost of CO_2 avoided. Right figure 5-8 shows the cost of CO_2 avoided for different options, with again, Oxy-fuel CHP cycle with CO_2 leading.

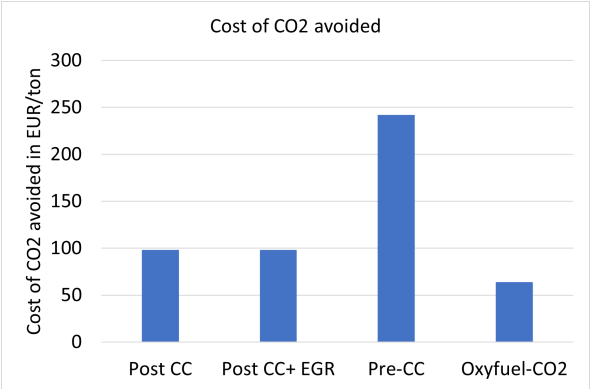

Figure 5-8: Image shows the calculated cost of CO_2 avoided

5-2-3 Flexibility analysis

The CHP plant studied in this thesis will have to produce power even at times when the power generation costs are higher than the revenues due to the constant heat demand that has to be supplied by the CHP. For such times, it is beneficial to operate the plant at minimum load, given that it's performance does not deteriorate at part loads. Thus, it becomes important to study the part load performance (flexibility) of the CHP. In this study, the quantification of flexibility is made by analysing two simple performance indicators at Off-Design: CHP Total energy efficiency and CO_2 slope at part load.

The CO_2 slope is the slope of the graph of CO_2 emissions vs power at off design. For example, at full load, this value corresponds to:

$$CO_2 \quad \text{slope} = \frac{{CO_2}^{100\%\text{Load}} - {CO_2}^{90\%\text{Load}}}{\text{Power}^{100\%\text{Load}} - \text{Power}^{90\%\text{Load}}} \tag{5-4}$$

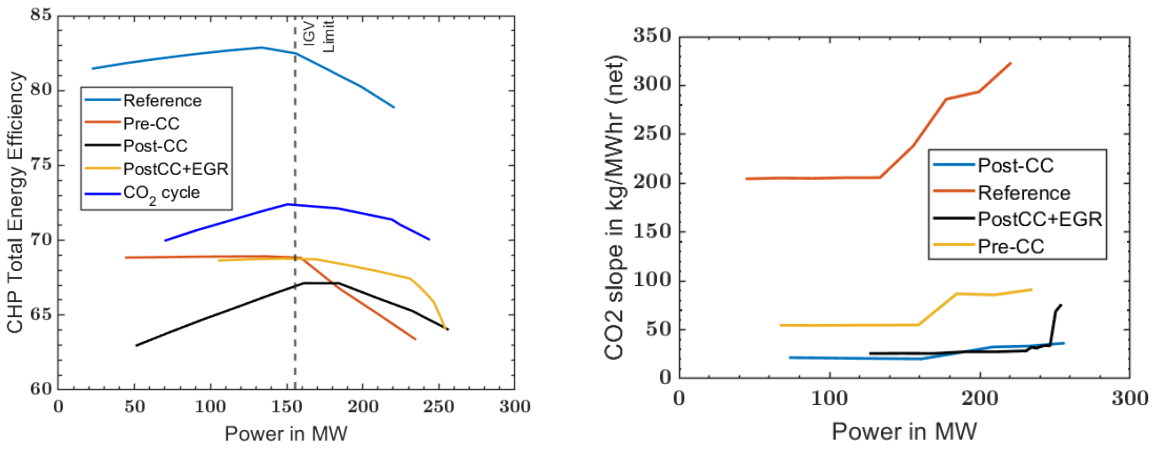

Figure 5-9: Left: Image shows CHP Total Energy Efficiency with Power at Off-Design. Right: Image shows CO_2 slope with Power at Off-Design

For the Off-Design calculations, standard IGV+TIT control combination is used for all cases except Post combustion capture with EGR. The CHP efficiency is an indirect indicator of the impact of flexible power production on natural gas consumption. It can be seen from left figure 5-9 that although the magnitude of efficiency is always higher for Oxy-fuel cycle at part loads, the post combustion capture with EGR has a flatter characteristic indicating that it maintains relatively constant performance at varying loads.

Right figure 5-9 shows the impact of power reduction from design on reduction in CO_2 emissions. For EGR operation, the highest slope occurs near design point where the part load control technique is EGR. This shows that in the EGR off-design mode, reduction in power leads to steep reduction in CO_2 emissions, and thus, is beneficial. Also, for pre-combustion capture and the reference case, steeper CO_2 reduction is obtained in IGV control mode.

5-3 Summary

1. A thermodynamic, economic and flexibility analysis was performed for four selected cycles, namely: Post combustion capture, Post combustion capture with EGR, Pre combustion capture and Oxyfuel CHP cycle with CO_2 working fluid.

2. As stated in chapter 4, CHP cycle without capture has a superior thermodynamic performance compared to Oxyfuel CHP cycle with CO_2, however, the latter has a higher thermodynamic performance after the introduction of CCS in the air cycle.

3. The study shows that Oxyfuel CHP cycle with CO_2 is indeed a more suitable option for future carbon-free CHP both in technical and economic sense.

Chapter 6

Retrofit analysis of an air compressor for CO_2 operation

In chapter 5, it is concluded that Oxyfuel CHP with CO_2 working fluid is promising concept for zero carbon CHP. However, a major drawback with Oxyfuel cycles is that new component designs would be required for turbomachinery, combustion and heat exchanger systems. Industries that aim to go carbon neutral in a few years without stranded assets are instead interested in "converting" existing CHP systems to zero carbon systems rather than building a new project from scratch. Thus the goal of this chapter is to get a first order estimate of whether an air designed gas turbine can be operated in complete CO_2 mode in a stable manner. If it cannot, what modifications could be proposed such that it operates close to the design point with CO_2 working fluid.

6-1 Introduction

For retrofitting an original installation, the major change for the installation would be the change of working fluid (CO_2) as compared to air for which the components are designed. The main components of a CHP are the compressor, combustion chamber, turbine and heat recovery steam generator. For oxy-fuel combustion, the combustion chamber must necessarily be redesigned. Considering turbomachinery, the operational limits for a turbine are decided mainly by the material. Thus, the turbine operates satisfactorily over a wide range of operating conditions. However, for a compressor, the operational limits are decided by the onset of instabilities in compressor operation, namely surge and stall. Thus a changing the working fluid is more critical for a compressor than a turbine. Moreover the turbine is subjected to very high temperatures which necessitates more frequent replacements of turbine parts in comparison to the compressor. On the other hand, compressor has a greater functional life left before it is replaced or discarded. This motivates the reason for first estimating compressor performance for a retrofit analysis in this thesis.

6-1-1 Structure

The switch to CO_2 working fluid is considered as an off-design operation because the design of the compressor is unaltered, instead, this work investigates if an existing designed compressor is suitable for CO_2 working fluid, where suitable means that the compressor can operate with CO_2 without the risk of instabilities. A GE 9E gas turbine model will be evaluated for this retrofit.

1. In section 6-2, A methodology is proposed to obtain the operating point for extreme off-design conditions like change in working fluid to CO_2 with standard maps that implicitly assume air as the default working fluid.

2. Then the theory behind compressor operation at this off-design operation is discussed in section 6-3.

3. In section 6-4, the results at Off-Design operation are presented and interpreted. We shall finally conclude if it is possible to operate the compressor at this off-design condition.

4. In section 6-5, the modifications required in gas turbine operation to force the compressor operation at the design point are proposed followed by a discussion on the effect of those modifications on the CHP cycle. The final conclusions are presented in section 6-6.

6-1-2 Introduction to Non-dimensional compressor characteristics

The compressor performance, depends on certain parameters based on physical laws. When this physical relation is non dimensionalised, it forms certain non dimensional groups that independently govern the compressor performance. For a compressor, the performance is defined by the pressure ratio delivered, its isentropic efficiency or the temperature ratio across the compressor. The relevant non dimensional groups that govern the performance are flow Mach number, rotational Mach number, Reynolds number and ratio of specific heats:

$$\frac{\mathrm{P_{02}}}{\mathrm{P_{01}}}, \eta_{\mathrm{isen}} = \mathrm{f}\left(\frac{\mathrm{ND}}{\sqrt{\gamma \mathrm{RT}}}, \frac{\mathrm{m}\sqrt{\mathrm{RT}}}{\mathrm{D^2 p}\sqrt{\gamma}}, \mathrm{Re}\right) \tag{6-1}$$

Where $\frac{\mathrm{P_{02}}}{\mathrm{P_{01}}}$ is the overall pressure ratio, m is the mass flow, N is the rotational speed, p and T are inlet pressure and temperature respectively, D is the characteristic diameter, Re is the Reynolds number and η_{isen} is the isentropic efficiency. When the relation in 6-1 is plotted in two dimensions with non dimensional mass flow (flow Mach number) on x axis, pressure ratio on y axis, non dimensional speed (rotational Mach number) as a parameter and isentropic efficiency as islands, it makes a compressor map. Each point in the map implicitly defines completely the velocity triangles for all blade and vane rows in terms of Mach numbers. This means that the compressor performance does not depend individually on the parameters but on the non-dimensional groups they form. However, the definition of the non dimensional groups changes according to the use. For example, for a fixed design of a compressor operating

on air, often D is considered constant and omitted from the non dimensional groups making them semi dimensional.

$$\mathrm{N_{ND}} = \frac{\mathrm{N}}{\sqrt{\gamma \mathrm{RT}}} \quad \mathrm{m_{ND}} = \frac{\mathrm{m}\sqrt{\mathrm{RT}}}{\mathrm{p}\sqrt{\gamma}} \tag{6-2}$$

Where m_{ND} and N_{ND} are semi dimensional mass flow rate and semi dimensional speed respectively. Figure 6-1 shows a typical compressor map.

6-1-3 Assumptions made in this analysis

1. **Effects of change in Reynolds number by switching to CO_2 are ignored.**
   Reynolds number is one of the non dimensional parameters on which the compressor performance depends. The Reynolds number in conventional air compressor operation is high to the extent that any change in Reynolds number with change in operating conditions does not have significant impact on the performance. The performance is only affected below a certain limiting Reynolds number (2.2×10^5) [Horlock (1958)]. Over the operating range of the compressor, the kinematic viscosity for CO_2 is lower than air. Thus if the changes in velocity profile through the compressor are not very significant, the Re for CO_2 operation will always be higher than air operation and we can assume that any change in Reynolds number does not influence the performance.

2. **The compressor characteristics do not change for CO_2 operation.**
   In this thesis, it is assumed that the compressor characteristics do not change with a change in working fluid. Thus, the compressor map is fixed for a certain designed compressor for this analysis.

6-2 Proposed Methodology

Generally, gas turbine component maps are generated with the assumption that the working fluid by default is air, hence, R and γ are usually omitted from the non dimensional groups. Also in most of the gas turbine simulation packages, it is not possible to change the gas properties to simulate an off-design condition with a different working fluid. This section provides a generic approach using dimensional analysis to find the off design operating conditions with a different working fluid, without actually changing the working fluid properties. General gas turbine simulation packages use different mathematical extrapolation schemes to obtain off design operating points far away from the design point. As a similar condition is expected in this work, if the characteristics at this extreme off-design condition are not accurate, it may lead to faulty results. However, there is no method to check the validity or accuracy of the maps except for detailed models and tests. We assume for now that the map is at least first order accurate in this off-design operating regime.

Conventionally, the following steps are followed to find an off design operating point for an industrial gas turbine given the compressor and turbine maps [Saravanamuttoo et al. (2001)].

1. With the ambient conditions and gas properties known, select a constant speed line ($\frac{N}{\sqrt{\gamma RT}}$ line) on which the gas turbine should operate.

2. Select a point on the selected non dimensional speed line and obtain the mass flow rate and pressure ratio at that point. Check if the pressure ratio and mass flow pair at that point is consistent with the turbine characteristics. If yes, this is the operating point. If no, repeat the procedure for a new point on the non dimensional speed line. In other words, find the operating point iteratively.

To locate the off design operating point with CO_2 working fluid on the compressor map, a similar procedure is followed. Pressure loss in the combustion chamber and mass flow addition due to fuel and oxygen are not considered in this analysis.
Table 6-1 shows the values of the parameters used to locate a point on the map at both design and off design.

Parameter	**Unit**	**Value at Design (Air)**	**Value at Off-Design (CO_2)**
N	rpm	3000	3000
T_{01}	K	288	288
TIT	K	1451	1451
R	J/kgK	287	188
γ	-	1.4	1.293
p_{01}	bar	1.0132	1.0132
m	kg/s	407.2	To be evaluated
Pressure ratio	-	13.07	To be evaluated

Table 6-1: Table shows the values of the parameters used to locate a point on the compressor map at both design (Air) and off design (CO_2) cases.

With the information in the table above, the non-dimensional speed can be calculated at off-design using equation 6-2. This gives an increase of 28% compared to the design point. However, if the map in figure 6-1 is observed carefully, there is no non dimensional speed line corresponding to 1.28 times the value at design. Without the non dimensional speed line, it is not possible to obtain the off-design operating point by just looking at the map. Hence, to locate the off-design point some manipulative steps are described as follows:

1. We make use of the fact that compressor performance does not depend individually on parameters given in table 6-1 but on the non dimensional groups they form. This means that the compressor performance does not depend individually on the specific gas constant and ratio of specific heats but on their effect on the non dimensional mass flow and non dimensional speed. So an artificial/hypothetical value of the compressor inlet temperature is given as an input to any gas turbine simulation package, such that the non dimensional speed is same as the case with lower R for CO_2 and ambient inlet temperature. As long as the non dimensional parameter values are the same for the CO_2 and the artificial case, the performance of the compressor will be the same for both. Note that this reduction in temperature is only a numerical manipulation, in reality, only R lowers for CO_2 operation and temperature does not change to give the same non-dimensional speed line. In this study, this artificial temperature shall be called as T_{pseudo} which can be calculated as shown below:

$$\frac{N}{\sqrt{\gamma_{co2} R_{co2} T_{amb}}} = \frac{N}{\sqrt{\gamma_{air} R_{air} T_{pseudo}}} \tag{6-3}$$

$$T_{pseudo} = \frac{\gamma_{co2} R_{co2} T_{amb}}{\gamma_{air} R_{air}} \tag{6-4}$$

2. With this artificial inlet temperature given as input and all other parameters same as in table 6-1, the software simulates this off-design condition and plots a point on the map that should theoretically lie on a non dimensional speed line corresponding to CO_2 operation. This point will be called as 'pseudo point'. The map with pseudo point plotted is shown in figure 6-1.

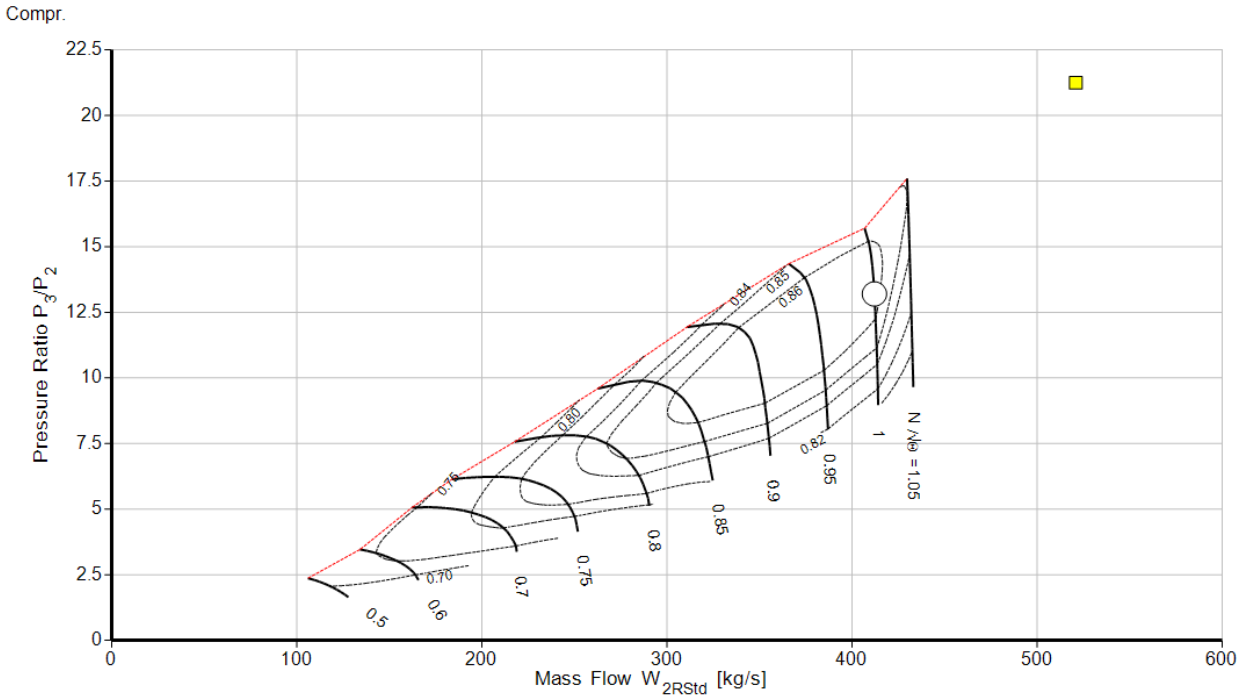

Figure 6-1: Compressor map with Design point for the GE 9E gas turbine in white circle and pseudo Off-design point in yellow square

3. It is to be noted that the pseudo off-design point shown in the figure only lies on the same non dimensional speed line as real CO_2 working fluid case, but it does not give the actual values of mass flow and pressure ratio. The actual mass flow rate for CO_2 operation can be calculated from the pseudo mass flow rate using the equation 6-5 below.

$$\frac{m_{pseudo}\sqrt{R_{air} T_{pseudo}}}{p_1 \sqrt{\gamma_{air}}} = \frac{m_{act}\sqrt{R_{co2} T_{amb}}}{p_1 \sqrt{\gamma_{co2}}} \tag{6-5}$$

Where, the left hand side of the equation is the output non dimensional mass flow at the yellow point in figure 6-1 given as an output by the software routine when T_{pseudo} is given as input inlet temperature and all other off-design inputs taken from table 6-1. The actual mass flow rate can be found as:

$$m_{act} = \frac{m_{pseudo}\sqrt{R_{air} T_{pseudo}}\sqrt{\gamma_{co2}}}{\sqrt{\gamma_{air}}\sqrt{R_{co2} T_{amb}}} \tag{6-6}$$

Substituting equation 1,

$$m_{act} = \frac{\gamma_{co2}}{\gamma_{air}} \cdot m_{pseudo} \tag{6-7}$$

4. The above equation gives a relation between the pseudo mass flow rate obtained from the software and the actual mass flow rate. Once the actual mass flow is known, the pressure ratio is obtained from the turbine equation. The algorithm of the simulation package will try to calculate the pressure ratio from the pseudo mass flow rate and air properties and input TIT. Whereas the actual pressure ratio must be calculated from the actual mass flow rate and CO_2 properties and the input TIT. Thus the pressure ratio given by the software is not the true value. As TIT is the only input parameter, An artificial TIT input is fixed such that the pressure ratio computed by the software corresponds to the actual pressure ratio. This is elaborated in the following equations:

$$\frac{m_{pseudo}\sqrt{R_{air}TIT_{pseudo}}}{p_3^{computed}\sqrt{\gamma_{air}}} = \frac{m_{act}\sqrt{R_{co2}TIT_{act}}}{p_3^{act}\sqrt{\gamma_{co2}}} \tag{6-8}$$

For the pressure calculated by the software to be equal to the actual pressure at turbine inlet, i.e, $p_3^{computed} = p_3^{act}$, after algebraic manipulations and substitution of equation 6-7, TIT_{pseudo} should be such that,

$$TIT_{pseudo} = \frac{\gamma_{co2}R_{co2}}{\gamma_{air}R_{air}} \cdot TIT_{act} \tag{6-9}$$

where TIT_{act} is the actual turbine inlet temperature of 1451K as shown in table 6-1.

Parameter	**Unit**	**Real Off Design value**	**Artificial Off Design value**
N	rpm	3000	3000
T_{01}	K	288	175.07
TIT	K	1451.7	882.46
R	J/kg	188.9	287
γ	-	1.293	1.4
m	kg/s	407.7	To be evaluated
Pressure ratio		13.10	To be evaluated

Table 6-2: Table shows the real off-design inputs and the artificial off-design inputs (for simulating the case with CO_2 operation but with air properties)

Table 6-2 refers to the real off-design inputs and the artificial off-design inputs which by theory should both represent the CO_2 operating point. The figure 6-2 shows the real off-design point for CO_2 operation with a yellow plus symbol in relation to the design point and the pseudo operating point.

5. To summarise, by setting the inputs as given in the table 6-2 for artificial Off design calculations, an operating point for CO_2 operation will be obtained without actually changing the working fluid properties to CO_2 properties. This is the significance of dimensional analysis that shows changing the working fluid to CO_2 is equivalent to

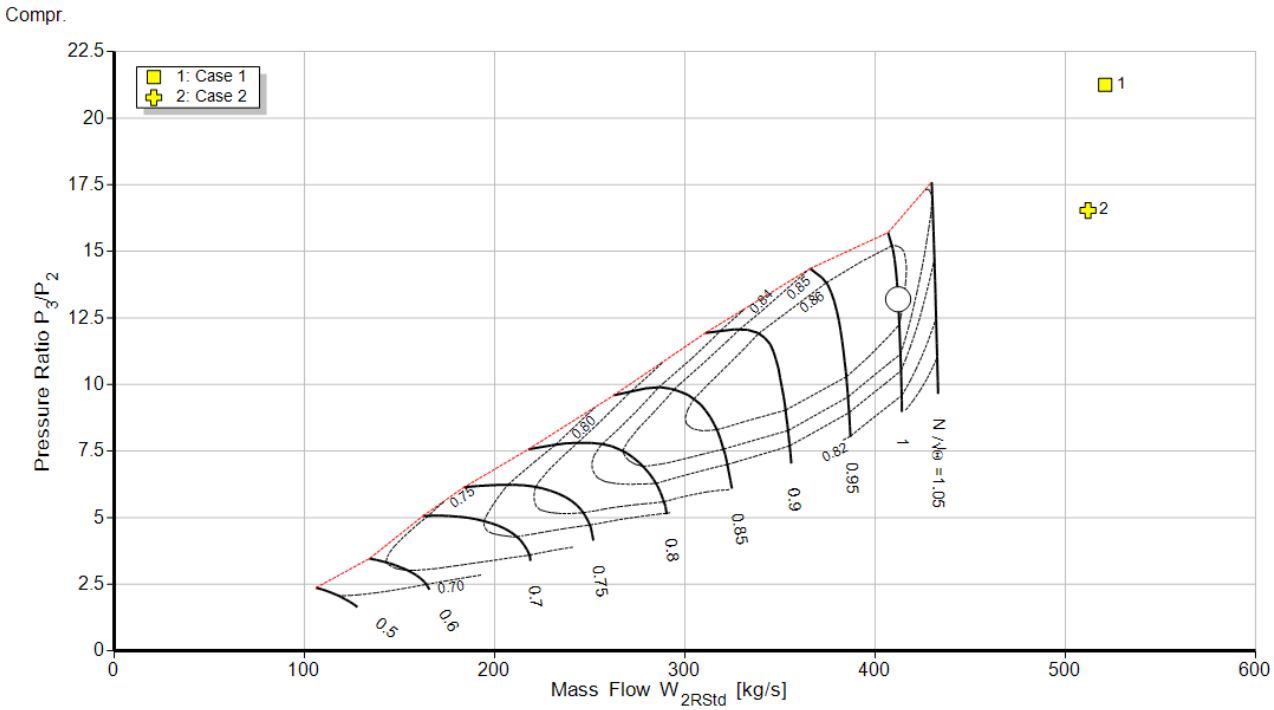

Figure 6-2: Compressor map with a) Design point in white circle b) pseudo Off-design point in yellow square and c) real Off-Design point with yellow plus symbol

operating the gas turbine on air with a compressor inlet temperature of 175 K and TIT of 882.46K. Flowchart 6-3 summarises the above procedure used to simulate the Off-Design operating condition artificially.

Once the pressure ratio and mass flow rate are also determined, all other parameters of table 6-4 at off design can be determined.The results are presented in section6-4.

6-3 Theory of compressor performance at Off-Design

In this section we shall investigate how a compressor physically responds when CO_2 is used as a working fluid instead of air. The following table 6-3 shows the parameters at off-design at the inlet to the first stage that are different than design.

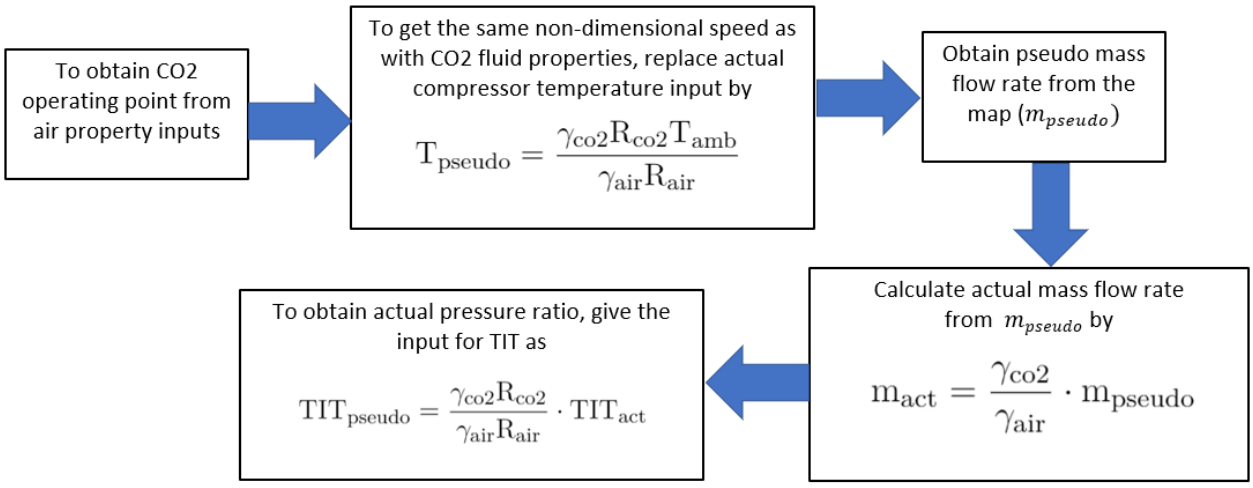

Figure 6-3: Flowchart to obtain CO_2 operating point artificially with air properties and pseudo temperatures as inputs

Parameter	**Unit**	**Comparison with Design point**	**Reason**
p_1, T_1	bar, K	Same	Governed by ambient conditions
Cx_1	m/s	Same	This is an initial assumption which is later addressed in section 6-4-1
U	m/s	Same	Neither the rotational speed nor the design changes
ρ_1	kg/m^3	Higher	For same pressure and temperature at inlet, density of CO_2 is higher due to a lower specific gas constant
m_1	kg/s	Higher	m= ρAV, for higher density and constant area and inlet axial velocity, higher mass flow rate.

Table 6-3: Table shows the parameters at off-design at the inlet to the first stage of the compressor in relation to design values

where, $p_1, T_1, \rho 1$ are compressor inlet conditions. Cx1 is the inlet axial velocity and U is the tangential blade velocity. Referring to the table 6-3, it can be evaluated that as Cx and U at inlet are same as design, so the flow coefficient (Cx/U) through the first stage is also same as design. This should lead to the same loading coefficient for the first stage. This is shown on the first stage compressor characteristics in left of figure 6-4. However although the loading coefficient is same as design for the first stage, the pressure ratio is higher. This can be shown by equation 6-10 which just rewrites the loading coefficient (ψ) in terms of pressure rise through the stage.

$$\psi = \frac{\Delta P}{\rho U^2} \tag{6-10}$$

where ΔP is the pressure rise through a stage and ρ is the stage inlet density which is higher at the first stage inlet. So even though the loading coefficient can be same as design, we expect that the pressure rise through the first stage is higher. Right figure shows Cx vs pressure rise per stage for constant rotational speed and density as a parameter. Higher pressure rise

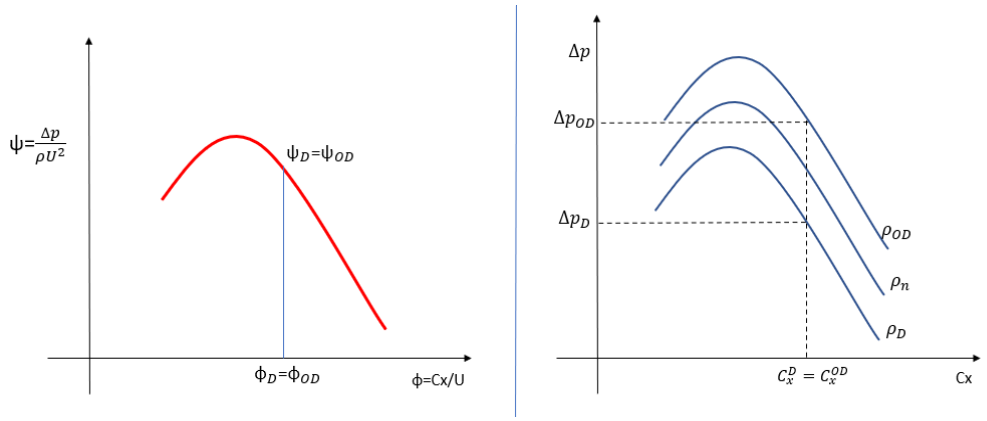

Figure 6-4: Left: Stage characteristics (flow coefficient vs loading coefficient for the first compressor stage. Right: Pressure rise per stage characteristics vs axial velocity at inlet for constant rotational speed at different inlet densities. Subscripts D stands for design and OD stands for Off-Design

leads to a higher density rise through the first stage compared to design. So, a higher density compared to design is expected at the second stage inlet.

The axial velocity at the second stage inlet is given by $\mathrm{Cx}_2 = \frac{\mathrm{m}}{\rho_2 \mathrm{A}_2}$ where m is the mass flow rate constant throughout the compressor, A is the inlet area of second stage, and Cx_2 is the axial velocity at second stage inlet. Due to a higher density at second stage inlet than design, the axial velocity through the second stage reduces. For the same U, this means a larger loading coefficient for the second stage . Referring to equation 6-10 and applying it to the second stage, both the effects of increased density and increased loading coefficient combine to give a pressure rise higher than the design pressure rise for the second stage. This phenomena repeats stage after stage and we can expect that the later stages could reach a point where,

$$\frac{\partial \Delta P}{\partial \phi} = 0 \tag{6-11}$$

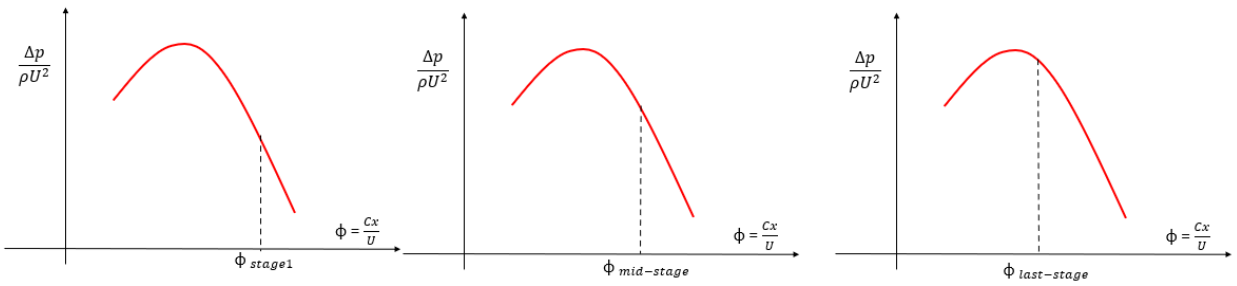

Figure 6-5: $\Psi - \phi$ plot for successive compressor stages (First stage to last stage from left to right)

This point might signify an inception of instabilities in the compressor as the slope of the characteristics reverse. To understand how this point might lead to an unstable operation, the

reader is referred to Horlock (1958). This process can be illustrated by figure 6-5. Note that we can only estimate that there is a risk of instabilities with CO_2 operation with a very low level of certainty. It is possible that even after crossing the point, some stages are stalled but the compressor can still operate in a stable manner. Another main point is that, matching a compressor with the turbine greatly affects the flow behaviour in the compressor. So the theory presented in this section can prove to be baseless without validation with actual off design calculations for a gas turbine. This is done in the next section.

6-4 Results and discussion

Table 6-4 is obtained after the generic methodology described in section 6-2 is implemented on the commercial software GasTurb.

Parameter	**Symbol**	**Unit**	**Design value**	**Off-Design value**	**Deviation from design (%)**
Mass flow rate	m	kg/s	407.7	601	+ 47.4
Pressure ratio	PR	-	13.1	16.4	+ 24.9
Inlet axial velocity	Cx	m/s	166.8	161.4	- 3.3
Inlet absolute Mach number	M_1	-	0.5	0.61	+ 24.2
Exit axial velocity	Cx_n	m/s	145.4	90.5	- 37.8
Compressor isentropic efficiency	η_c	%	86.3	68.5	- 20.7

Table 6-4: Off-Design values for CO_2 operation obtained by implementing the proposed methodology in GasTurb

In the subsection 6-4-1, the consistency of the results presented in table 6-4 with the theory presented in section 6-3 is evaluated.

6-4-1 Interpretation of results

1. The initial assumption made in section 6-3 of same inlet axial velocity as design can be considered valid as the change in inlet axial velocity is negligible (3% lower than design). The underlying theory behind this assumption was that for the same rotational speed and choked compressor stages (mass flow is uninfluenced by pressure ratio), the inlet axial velocity is essentially constant.

2. From the table, the overall axial velocity through the compressor reduces. This validates the prediction made in section 6-3 that with CO_2 as the working fluid, axial velocity at each stage exit reduces. This leads to a reduced axial velocity at the inlet of each successive stage which in turn leads to a positive incidence at the rotor stage inlet as shown in figure 6-6. Increased positive incidence at the rotor inlet leads to stalling.

3. As it can be seen from the table, the inlet Mach number has increased due to a lower sonic velocity of CO_2 at the same inlet temperature. The graph in figure 6-7 shows that as Mach number at inlet increases, the allowable range of incidence reduces.

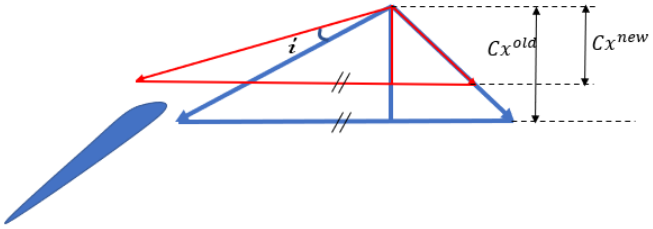

Figure 6-6: Figure shows inlet velocity triangle for a rotor stage with a) Design velocity triangle in blue (Cx at design as Cx^{old}) and b) Off design velocity triangle with reduced inlet axial velocity in red (Cx at off- design as Cx^{new}). Incidence is shown as the difference between the blade angles at design and off-design.

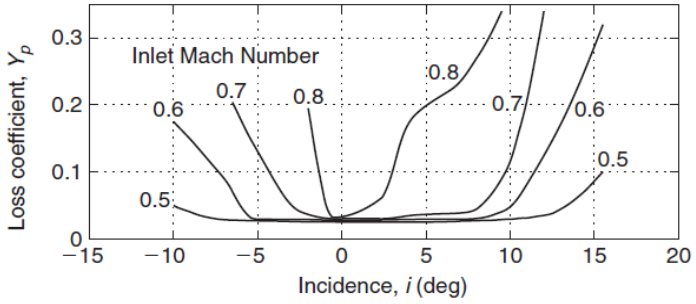

Figure 6-7: Loss coefficient as a function of incidence and inlet Mach number taken from Dixon and Hall (2013)

This makes the risk of stalling even higher. Figure 6-7 also suggests that increased Mach number leads to increased blade losses, which could be one of the reasons for the lower isentropic efficiency of the compressor.

Although a risk of instabilities in the compressor is estimated with a very low level of uncertainty, we decide to claim that the gas turbine cannot be operated at this off-design point. If the same gas turbine still has to be used, then the modifications proposed in the next section are required.

6-5 Possible solution to force compressor operation at design point

In this section, a method is proposed which enables the compressor to operate at its design point in CO_2 mode. A unique point on the compressor map defines unique velocity triangles in terms of Mach numbers and hence unique compressor behaviour. So the compressor performance will be the same as design performance if it operates at the design point on the

map even with CO_2 working fluid. There is an increase in the non dimensional speed by 28% due to a lower R for the CO_2 case. This drives the off-design operating point away from the design point. So at first, we consider a solution such that the operating parameters are so manipulated that they lead to a non dimensional speed same as the design non dimensional speed. We consider the expression for the full non dimensional speed ($\frac{ND}{\sqrt{\gamma RT}}$) Here, we choose to increase the compressor inlet temperature such that the product γRT is same as design. However increasing inlet temperature to reduce the non dimensional speed by 28% leads to a temperature of 473K at the compressor inlet. Even though at this point the compressor isentropic efficiency will be same as design, this is a highly inefficient technique as the thermal efficiency of the gas turbine cycle is drastically reduced for the same turbine inlet temperature due to a reduction in the Carnot efficiency of the cycle. This technique leads to a non dimensional speed line same as design but the operating point is still away from the design operating point as shown in the figure 6-8.

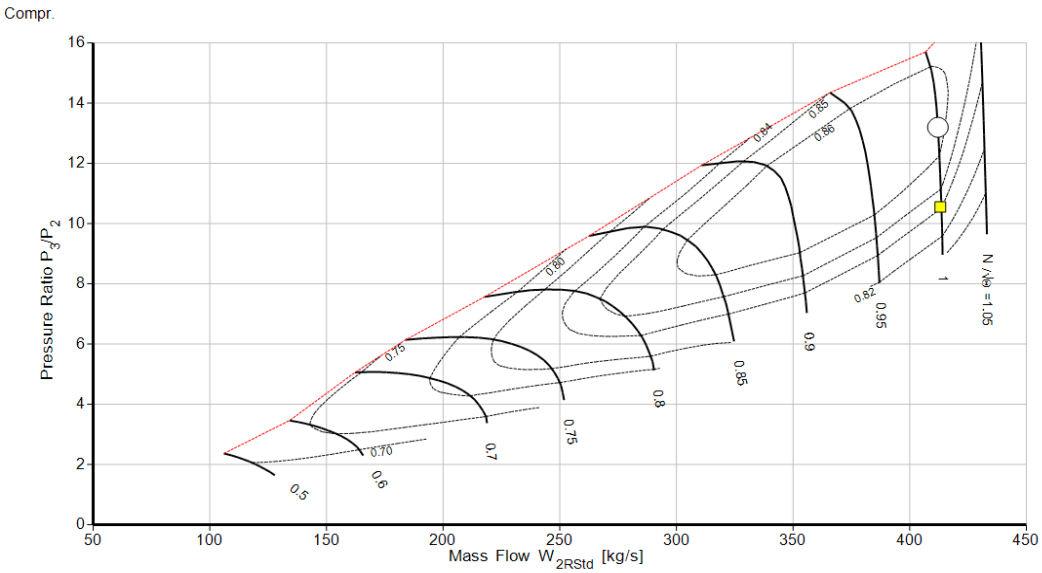

Figure 6-8: Map showing Off design operating point in yellow with manipulated compressor inlet temperature such that both off-design and design points are on the same non dimensional speed line

This occurs because the increase in compressor inlet temperature does not affect the gas turbine pressure ratio in any way. The gas turbine pressure ratio is decided by the turbine and only depends on the inlet stagnation conditions, gas properties and mass flow rate at turbine inlet. For the turbine, the following equation holds at both design and off-design,

$$\frac{\mathrm{m}\sqrt{\mathrm{RT}}}{\mathrm{p}\sqrt{\gamma}} = \mathrm{const} = \mathrm{f}(\mathrm{A_{throat}}) \tag{6-12}$$

Where m is the mass flow rate through the turbine, R,T,p are conditions at turbine inlet and $\mathrm{A_{throat}}$ is the first turbine rotor throat area. As shown in figure 6-8, for a constant TIT and non dimensional speed, even though the mass flow rate is almost close to the design mass flow

(choked compressor stages), the pressure at turbine inlet is lower due to lower R for CO_2. To obtain a pressure ratio same as the design pressure ratio at the same mass flow rate and the specific gas constant for CO_2, the Turbine inlet temperature required would be as higher than 2000 K. This is practically impossible considering the material limitations.
The turbine equation is governed by choking conditions at the first stage turbine nozzle throat. It is to be noted that the constant on the right side of 6-12 is a function of the first stage turbine nozzle throat area, which is fixed by a fixed design and therefore was considered a constant in this analysis. So another option is to change the turbine characteristics itself by changing the first stage nozzles which in turn fixes the constant of equation 6-12. We attempt to find a right hand side constant such that the design pressure ratio is achieved. This leads to a turbine throat area of 0.247 sq.m. compared to the design value of 0.2068 sq.m. which is an increase by 20%. This is still a valid solution consistent with the goals of this retrofit analysis as it is possible to change the first stage turbine nozzles. As turbine inlet is subjected to very high temperatures, the first stage nozzles are designed to be replaced.

Thus, it seems possible to operate the compressor at design point with CO_2 working fluid by following the two steps discussed above. However, this is achievable at a cost of lower gas turbine thermal efficiency.

6-6 Conclusion

From the above analysis, the following conclusions can be derived:

1. Validation of the assumptions made in this analysis should be done with a high fidelity CFD model, and is left as future work. This analysis provides a very physically simplistic yet powerful approach to test the replacement of CO_2 with air. **This analysis is only a first order estimate and should not be trusted without validation.**

2. For the Off-Design condition of CO_2 as a working fluid, the compressor pressure ratio and mass flow rate are higher than design. There is a risk of stalling of the compressor stages due to building pressure rise in each successive stage. **This leads to a decision that operating at the new off design point is dangerous and therefore should be avoided.**

3. This leads to proposing measures to forcefully operate the compressor with CO_2 working fluid at its design point by manipulating relevant parameters. **A compressor inlet temperature of around 473K and a new turbine inlet nozzles with a throat area of 20% higher than design is required to enable compressor operation at the design point**. Even though it is possible, the gas turbine efficiency is highly compromised due to a higher compressor inlet temperature required.

Chapter 7

Summary and Conclusions

In this thesis, system models have been developed, and results are analysed for different options for zero carbon combined heat and power gas turbine plants. The following options are studied:

1. Post combustion capture: CO_2 is removed from the exhaust gases of the gas turbine.
    - Without exhaust gas recirculation
    - With Cooled exhaust gas recirculation
    - With Uncooled exhaust gas recirculation
2. Pre-combustion capture
3. Oxyfuel combustion: As conventional air Brayton cycle is not applicable to pure O_2-fuel combustion in gas turbines, different cycle working fluids and configurations are proposed. They include:
    - Pure CO_2 cycle without recuperation
    - CO_2+ steam cycle
    - Split CO_2 + steam cycle with partial recuperation
    - s-CO_2 cycle with partial recuperation
    - CO_2 cycle with bottoming s-CO_2 cycle

    The configurations are compared to each other based on thermodynamic performance at different power to heat ratios.

Of all the options, some are selected for further analysis where they are compared based on thermodynamics, economics, and Off-Design performance. The options are compared for a design condition of a power to heat ratio of 0.78 and fixed process steam output of 400 t/h at 326°C and 90 bar.

Finally, although pure CO_2 cycle was found to be a promising solution, new turbomachinery designs are required to realise such a cycle. Therefore, a retrofit analysis is performed to assess if an existing gas turbine can operate on CO_2 working fluid. For this analysis, a methodology was proposed to evaluate the off-design behaviour of a gas turbine for a different working fluid using compressor and turbine characteristics.

Some important results of this thesis are summarised as follows:

1. For a gas turbine CHP system with amine based post combustion capture, cooled exhaust gas recirculation improves the Design point performance, while uncooled exhaust gas recirculation improves the off-design performance.

2. When only Oxyfuel cycles are compared to each other at a typical design power to heat ratio of 0.78, CO_2 cycle with bottoming s-CO_2 cycle shows highest performance (CHP electric efficiency and total energy efficiency), followed by pure CO_2 cycle. As the former is a complex cycle to realize, the pure CO_2 cycle is selected for further analysis.

3. Next, a comprehensive techno-economic comparison of all selected concepts (namely: Post combustion capture, post combustion capture with exhaust gas recirculation, Pre-combustion capture and Pure CO_2 Oxyfuel cycle), conveys that the lowest cost of electricity for the pure CO_2 Oxyfuel cycle. It therefore seems promising as a zero carbon CHP cycle.

4. Finally, the retrofit analysis to assess the suitability of a designed gas turbine to CO_2 operation, shows that a gas turbine can be operated with CO_2, with a different compressor inlet temperature and a larger first turbine inlet rotor area. However, the performance of the gas turbine is seriously deteriorated by these modifications.

5. This analysis predicts a very poor performance of the s-CO_2 cycle for CHP applications, whereas it is very promising as a power cycle concept [Stanger et al. (2015)].

Future Recommendations

The CO_2 cycle with bottoming s-CO_2 cycle developed in this thesis seems a promising solution to both decarbonised power as well as CHP. This configuration can be optimised further for power generation, and the feasibility of a closed supercritical cycle as a bottoming cycle can be assessed to further develop the cycle concept.

The retrofit analysis performed in this thesis using compressor and turbine characteristics is a low fidelity simplistic evaluation. Thus, it is advised to conduct a detailed CFD study and validate the assumptions and the results of this analysis.

Appendix A

Load control techniques in Gas Turbine CHP

A-1 Inlet Guide vane control

Inlet guide vanes are blades at the inlet of the compressor that control the inlet air flow to the compressor and hence to the gas turbine. By turning the IGVs, the flow to the compressor is deviated such that the magnitude of the absolute velocity remains the same but its direction changes. This leads to a decrease in the axial component of the velocity. The air mass flow rate entering the GT is related to the axial velocity component by the following relation:

$$\mathrm{m_a} = \frac{\mathrm{P_1}}{\mathrm{RT_1}} \mathrm{A_1 V_1 cos}\alpha_1 \tag{A-1}$$

where $\mathrm{A_1}$ is the compressor inlet area, $\mathrm{V_1}$ is the inlet absolute velocity, α_1 is the guide blade angle, and $\mathrm{V_1 cos}\alpha_1$ is the axial velocity component. Ideal gas law is applicable hence density is written as $\rho_1 = \frac{\mathrm{P_1}}{\mathrm{RT_1}}$. Inlet guide vanes are closed such that α_1 increases and thus mass flow rate reduces. As the mass flow rate is controlled in IGV, the fuel flow rate is adjusted such that the Turbine Inlet Temperature (TIT) is maintained constant.
In IGV, load can only be reduced up-to around 70% of the full capacity. This limit is dictated by the surge limit in the compressor.

A-1-1 Effect on Pressure ratio and power

We can write a similar relation as equation A-1 for a choked turbine entry:

$$\mathrm{m_3} = \frac{\mathrm{P_3}}{\mathrm{RT_3}} \mathrm{A_3 V_3} \tag{A-2}$$

where subscript 3 stands for turbine inlet condition. Thus as turbine exit pressure (ambient), TIT (T_3), and turbine stator inlet area (A_3) are constant, pressure ratio decreases as mass

flow rate decreases. Note for a choked turbine, inlet velocity V_3 is not a function of pressure ratio but of TIT only ($V = V_{sound} = \sqrt{\gamma RT}$). This effect can also be verified from gas turbine maps as shown in figure A-1.

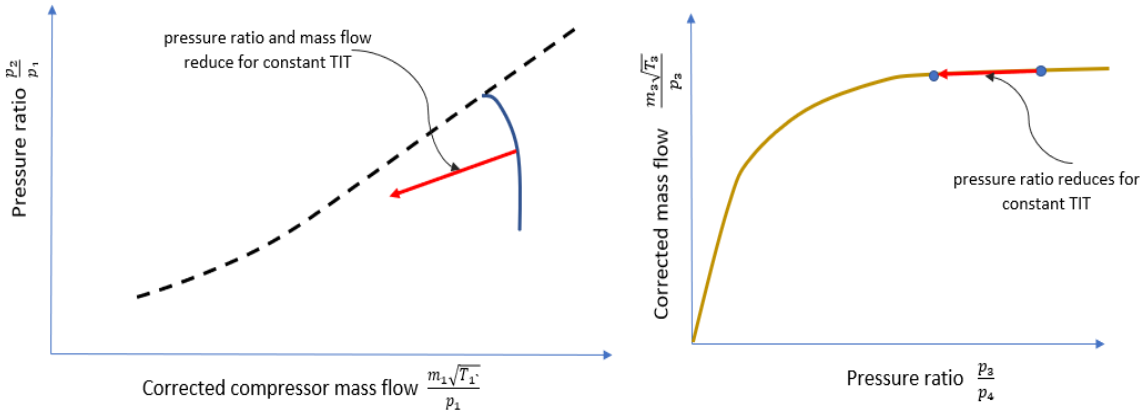

Figure A-1: Compressor map (left) and turbine map (right) showing IGV operation

As mass flow rate reduces, net power output reduces.

A-1-2 Effect on CHP Efficiency

The heat transferred in the HRSG by the gas is given by:

$$Q_{HRSG} = m_{gas} cp_g (T_{DB}^{out} - T_{stack}) \tag{A-3}$$

where T_{DB}^{out} is the duct burner exit temperature. For constant heat demand (Q_{HRSG}), the R.H.S of equation A-3 is also constant. As mass flow rate of gas through the HRSG decreases in IGV, for nearly constant specific heat, the temperature drop across the HRSG increases. Thus, the duct burner exit temperature increases and the stack temperature reduces. This is illustrated by figure A-2.

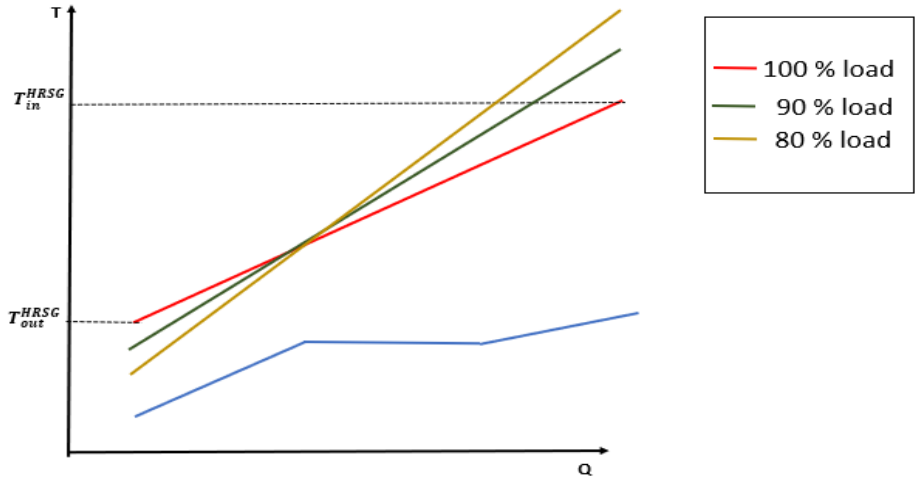

Figure A-2: T-Q diagram of the HRSG with the gas curves in red, green and yellow and the water/steam curve in blue. Red, green and yellow lines represent the slope of the gas curves at 100%, 90% and 80% loads respectively, depicting the increase in duct burner exit temperature and decrease in the stack temperature at part loads.

The stack losses are given by:

$$\mathrm{Q_{stack}} = \mathrm{m_{stack} cp_g (T_{stack} - T_{amb})} \tag{A-4}$$

In equation A-4, as the stack mass flow rate and stack temperature both decrease, the stack losses reduce. Therefore, CHP efficiency increases with IGV control.

A-2 Turbine inlet temperature control

Gas turbine fuel flow rate is varied to control the Turbine inlet temperature. As suggested by equation A-1 the air inlet mass flow rate is a function of compressor geometry ($\mathrm{A_1}$) and inlet thermodynamic conditions ($\mathrm{P_1, T_1}$) only. Thus the turbine mass flow rate is constant (variation in fuel mass flow rate is negligible). This causes the combustion air-fuel ratio to increase and TIT to decrease.

A-2-1 Effect on pressure ratio and power

As TIT changes, the pressure ratio changes by equation A-2. For a choked turbine, the inlet velocity scales with square root of temperature ($V = \sqrt{\gamma RT}$). Thus, using scaling laws, equation A-2 can be rewritten as:

$$\mathrm{m_3} \sim \frac{\mathrm{P_3}}{\sqrt{\mathrm{T_3}}} \tag{A-5}$$

This effect can be seen on the compressor and turbine maps as shown in figure A-3.

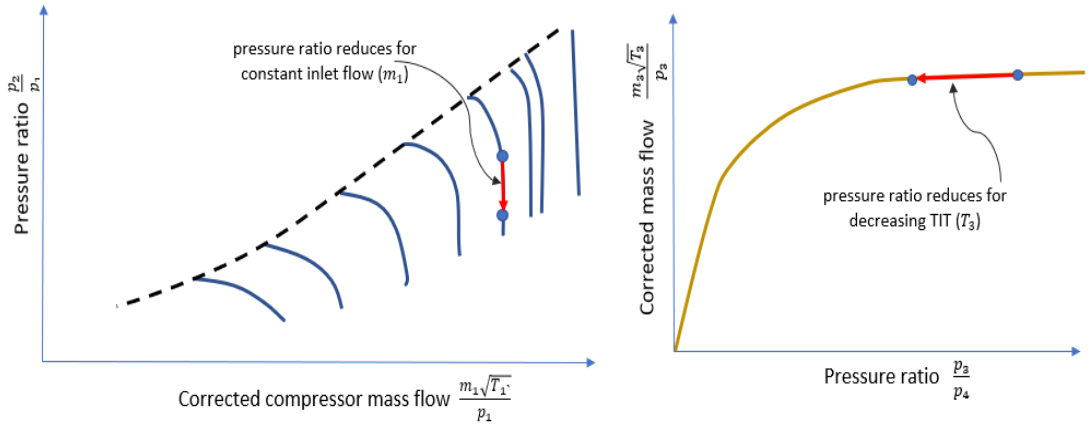

Figure A-3: Compressor map (left) and turbine map (right) showing TIT operation

For constant mass flow rate and turbine exit pressure, pressure ratio decreases when TIT is decreased at part load. The effect of reducing pressure ratio and TIT on the GT cycle is shown in figure A-4.

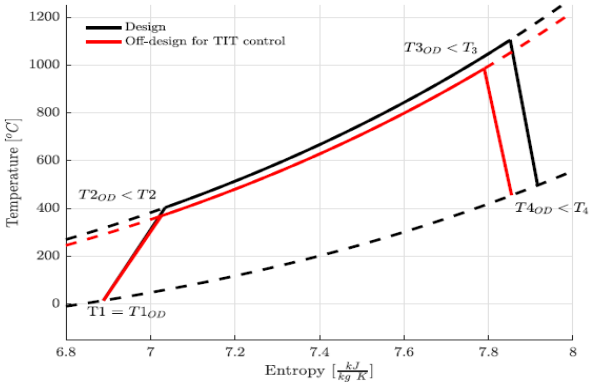

Figure A-4: T-s diagram for a gas turbine with design load shown by a black curve and part load control by TIT shown by red. Image taken from master thesis by Persico (2017)

The area under the closed curve represents the net specific work done by the gas turbine system. As it can be seen that this area reduces for constant GT mass flow, the specific work reduces. Hence, the net power reduces.

A-2-2 Effect on CHP efficiency

As the mass flow rate is constant in TIT operation, the slope of the gas curve in the T-Q diagram for the HRSG does not change for the same heat transferred in the HRSG. Thus the

stack losses are constant through out TIT operation. With the net fuel input to the CHP system decreasing at part loads, constant losses lead to a reduction in the CHP efficiency in TIT operation.

A-3 Exhaust gas recirculation control

In EGR control, as exhaust gases at a higher temperature than ambient are recirculated back to the compressor, the temperature at the inlet of gas turbine increases. From equation A-1 we see that the inlet mass flow scales inversely with the inlet temperature ($m_1 \sim \frac{1}{T_1}$). This causes the GT mass flow rate to decrease. The process diagram for EGR is illustrated in figure A-5

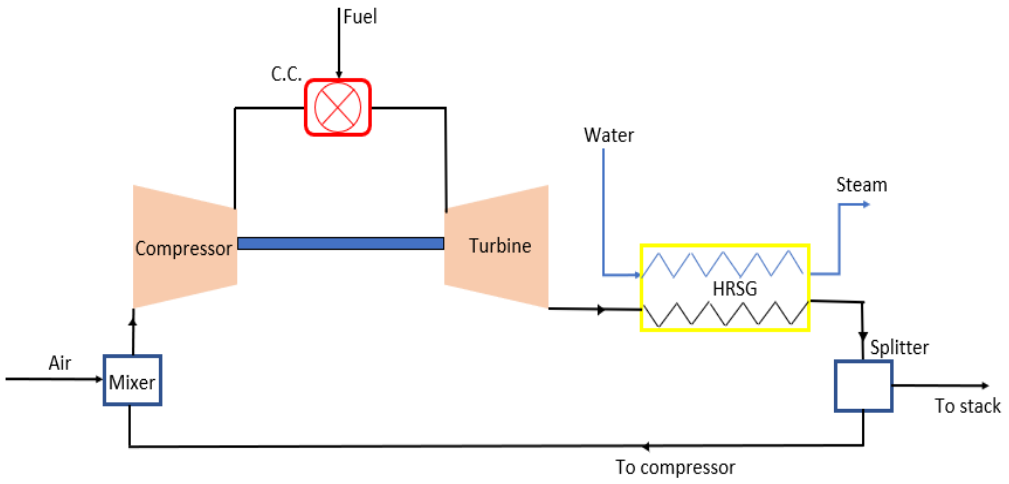

Figure A-5: Process flow diagram of a CHP with exhaust gas recirculation without supplementary firing.

The ratio of amount of the flue gases recirculated to the total flue gas mass flow is defined as the EGR ratio. The EGR ratio is varied to control the mass flow and hence the load. The turbine inlet temperature is maintained constant in EGR by decreasing the fuel flow proportionally to the inlet mass flow such that the air-fuel ratio is constant.
The oxygen content of the flue gases is quite lower than air (around 12%). When these gases are mixed with fresh air at the inlet of the GT, the oxygen content of the GT inlet flow also reduces. According to ElKady et al. (2008), Rokke and Hustad (2005), Bolland and Mathieu (1998), the minimum O_2 concentration required for a stable combustion is around 15 to 16 mole% at the GT inlet. Thus, the maximum EGR ratio is limited by the minimum oxygen concentration at the combustion chamber inlet.

A-3-1 Effect on pressure ratio and net power

In equation A-2, for constant TIT, the pressure reduces with reducing mass flow, just as it happens in IGV control. GT power reduces as the mass flow rate decreases.

A-3-2 Effect on CHP efficiency

The EGR ratio must increase to meet the decreasing load demand at part loads. As EGR ratio increases, the mass flow rate of gas going to the stack reduces. The stack temperature also reduces, the reason being same as in IGV operation (refer section A-1-2, equation A-3 and figure A-2). Thus, the stack losses in EGR operation reduce, which leads to increasing efficiency in EGR operation. However, there is a minimum load below which the EGR ratio cannot be increased further (dictated by minimum O_2 concentration). Beyond this point, IGV or TIT control, or both can be employed for deep part load operations.

A-4 Part load efficiencies

A comparison of efficiencies at part load for the three discussed control techniques are illustrated below. We observe that as we go towards a high efficiency technique, the range of load control reduces.

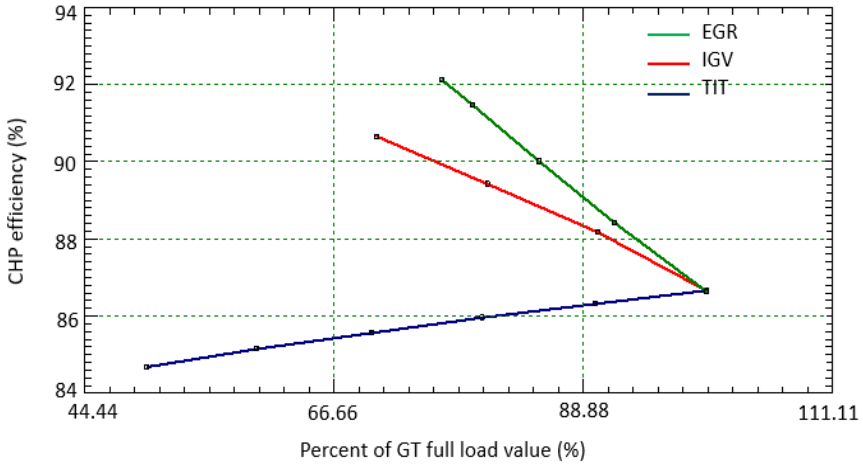

Figure A-6: GT load vs CHP efficiency for IGV, TIT and EGR control

Appendix B

Converting Power cycles to CHP

In chapter 4, only step 1 of the modelling approach discussed in section 4-2 is explained. In this section, step 2 is discussed in detail.

B-1 Step 2: Specifying mass flow rate and adding duct burner

Figure B-1 shows the simplistic model calculation routine.

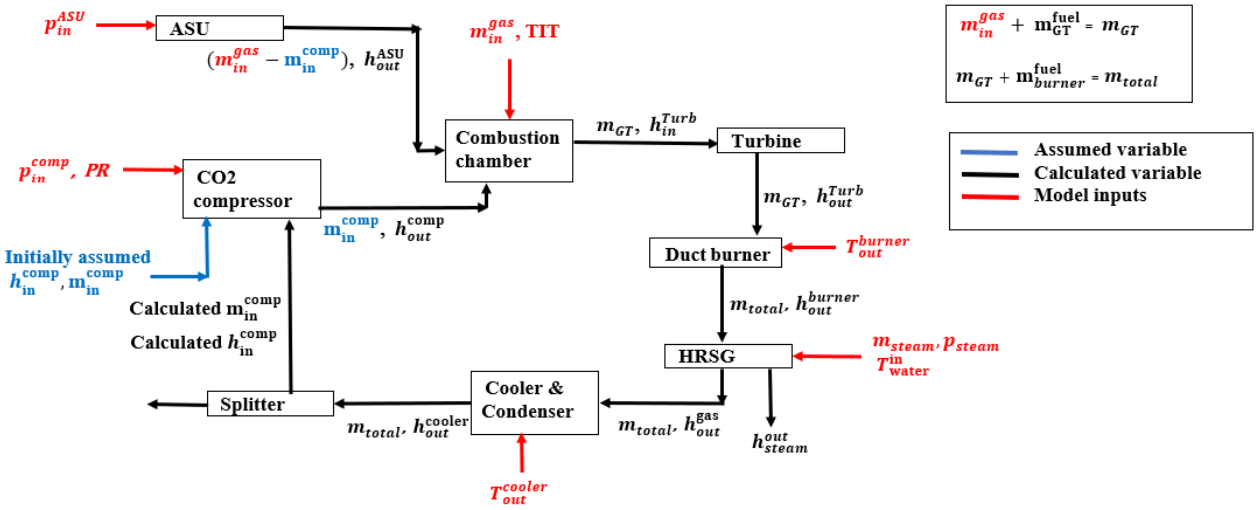

Figure B-1: Calculation routine for the CO_2 cycle model

In figure B-1, Variables in red show the inputs given to the respective component models. Variables in black are the outputs calculated from the inputs and component models. Variables in blue show the initially assumed variables, so called tear variables. Initially, no mass

flow through the compressor is assumed, so only fuel-O2 combustion takes place to give a 33% CO_2 and 66% H2O (equilibrium composition) flue gas mixture at the combustion chamber exhaust. Turbine model calculates the turbine exhaust conditions. In the cooler, the gas exit temperature set by the designer is such that all water is condensed. So for an initial model default value of the split ratio in the splitter, the calculated mass flow going through the compressor is mainly composed of CO_2. This process is repeated until a steady state is reached at a point where there is no difference between the mass flow and enthalpy values at compressor entry calculated in the previous and present iterations. In the figure B-1, for a particular duct burner outlet temperature given as input, and a certain total gas mass flow, the steam temperature from the HRSG is calculated for a fixed input steam mass flow rate. The duct burner outlet temperature is thus a control variable that the designer uses to get the desired steam conditions. The minimum duct burner temperature that meets the desired steam condition is required to avoid cooling losses in the condenser and maximize the CHP efficiency for that design.

In the model, m_{in}^{gas} is varied and the process steam conditions and demand is constant to obtain performance at different power to heat ratios.

B-2 PFD for Oxy-fuel cycles optimised for power

Figures B-2, B-3, B-4, B-5 and B-6 represent the process flow diagrams for the cases described in table 4-7.

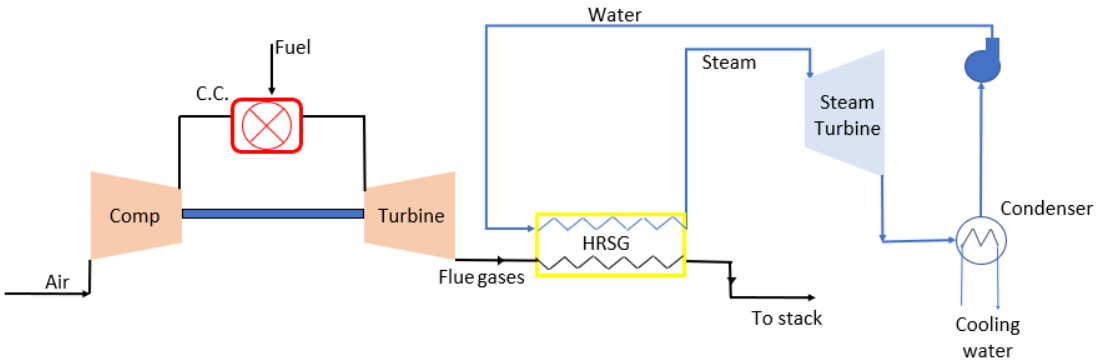

Figure B-2: Process flow diagram of air cycle with bottoming steam cycle (employing waste heat recovery for power generation.

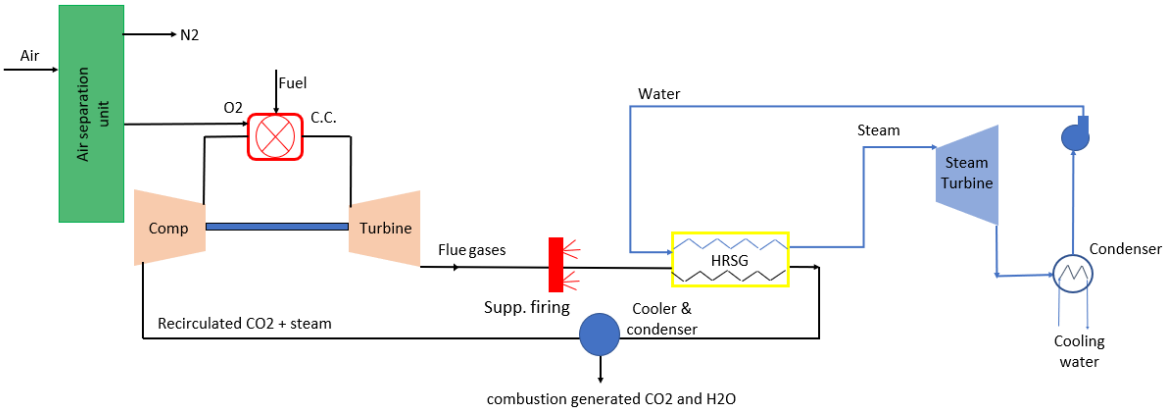

Figure B-3: Process flow diagram of CO_2 cycle with bottoming steam cycle (employing waste heat recovery for power generation.

The process flow diagram for the CO_2+ steam cycle with steam bottoming cycle is same as figure B-3, with only different operating parameters.

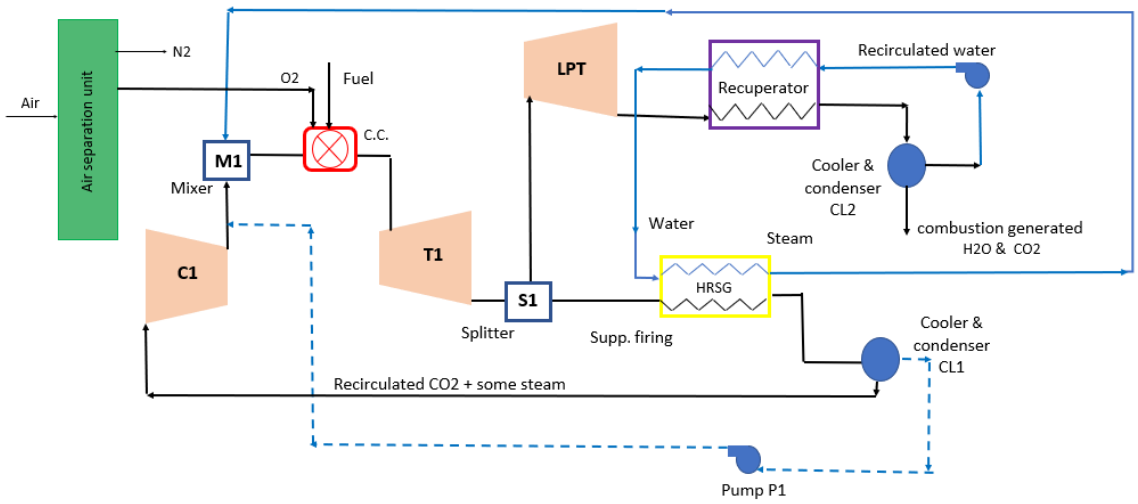

Figure B-4: Process flow diagram of split CO_2 steam cycle optimised for power.

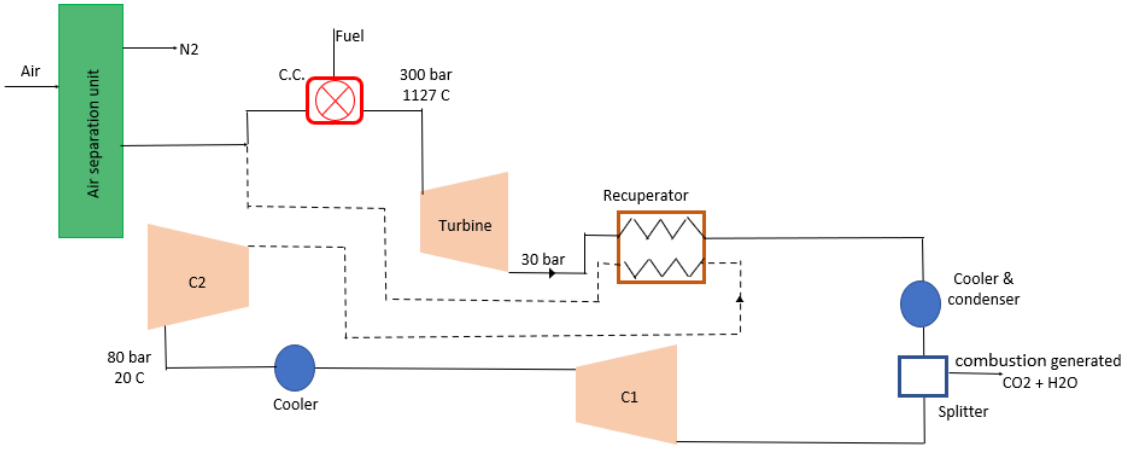

Figure B-5: Process flow diagram of s-CO_2 cycle optimised for power (Allam et al. (2014))

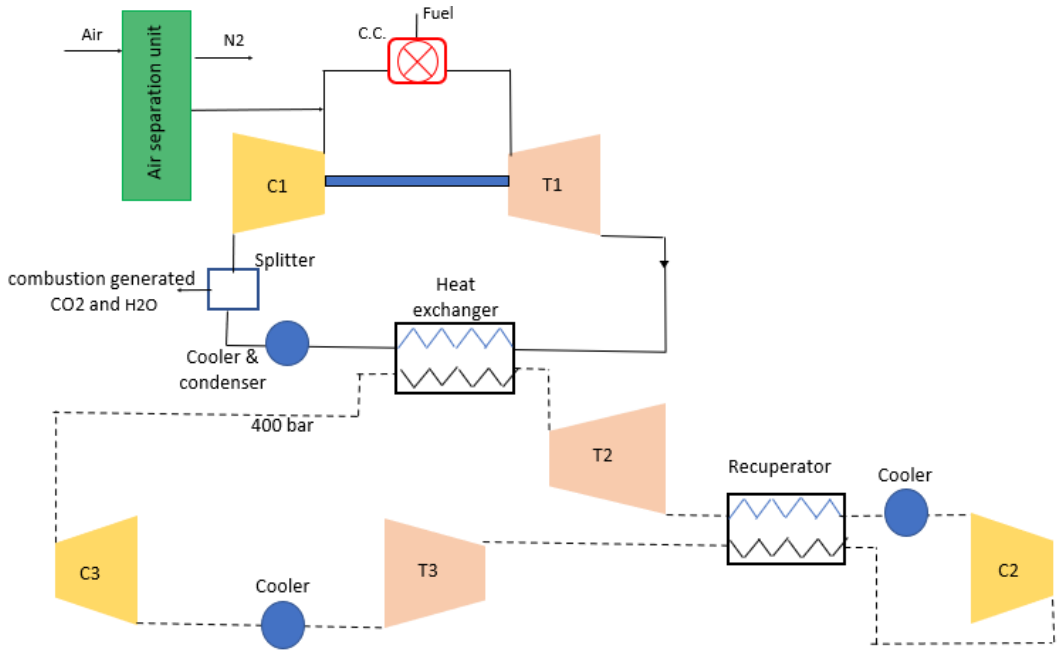

Figure B-6: Process flow diagram of CO_2 cycle with bottoming closed s-CO_2 cycle optimised for power

Appendix C

Effect of SMR operating parameters on fuel conversion

The figures C-1 and C-2 show the composition of the product species with respect to the operating parameters of an SMR.

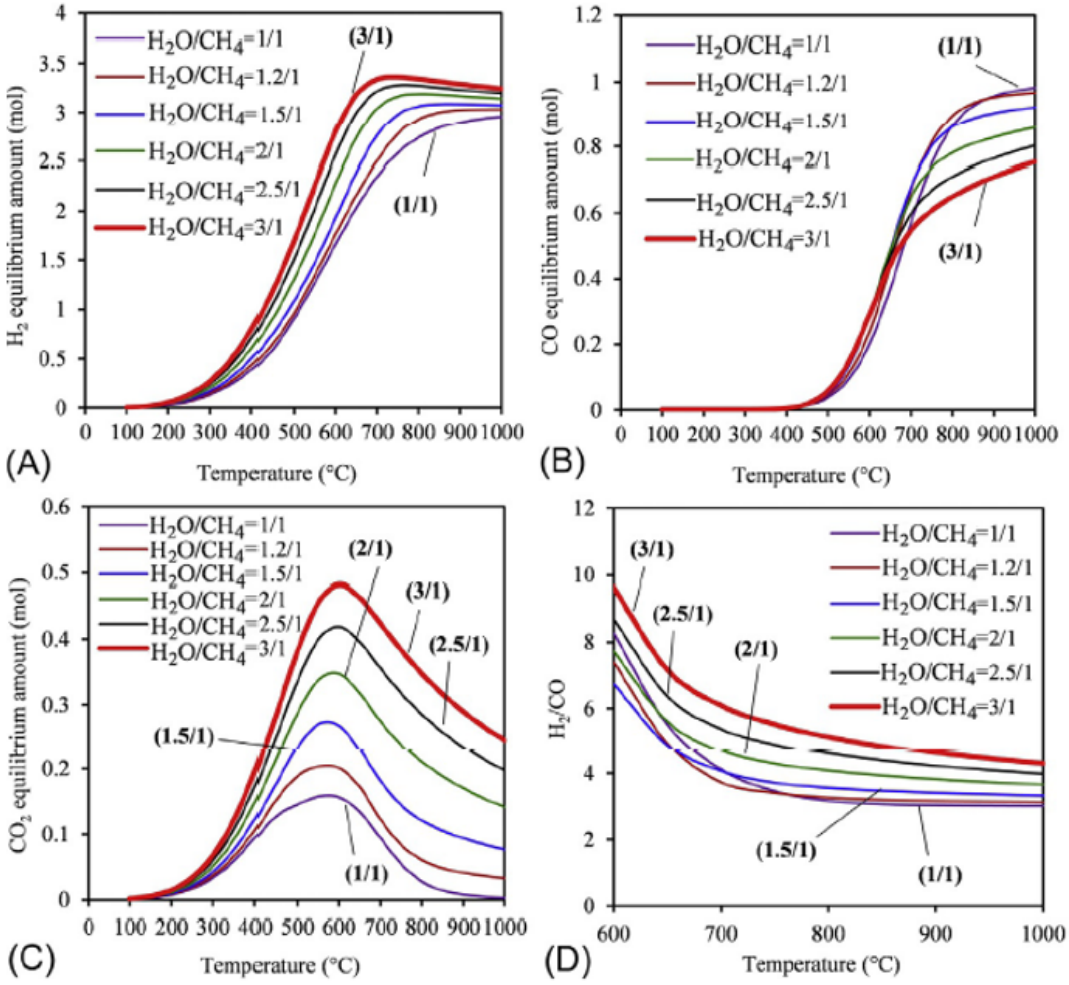

Figure C-1: Influence of steam to carbon ratio and the temperature on (A) H_2 amount, (B) CO amount, (C) CO_2 amount, and (D) molar ratio of H_2/CO at the thermodynamic equilibrium taken from Minh et al. (2018).

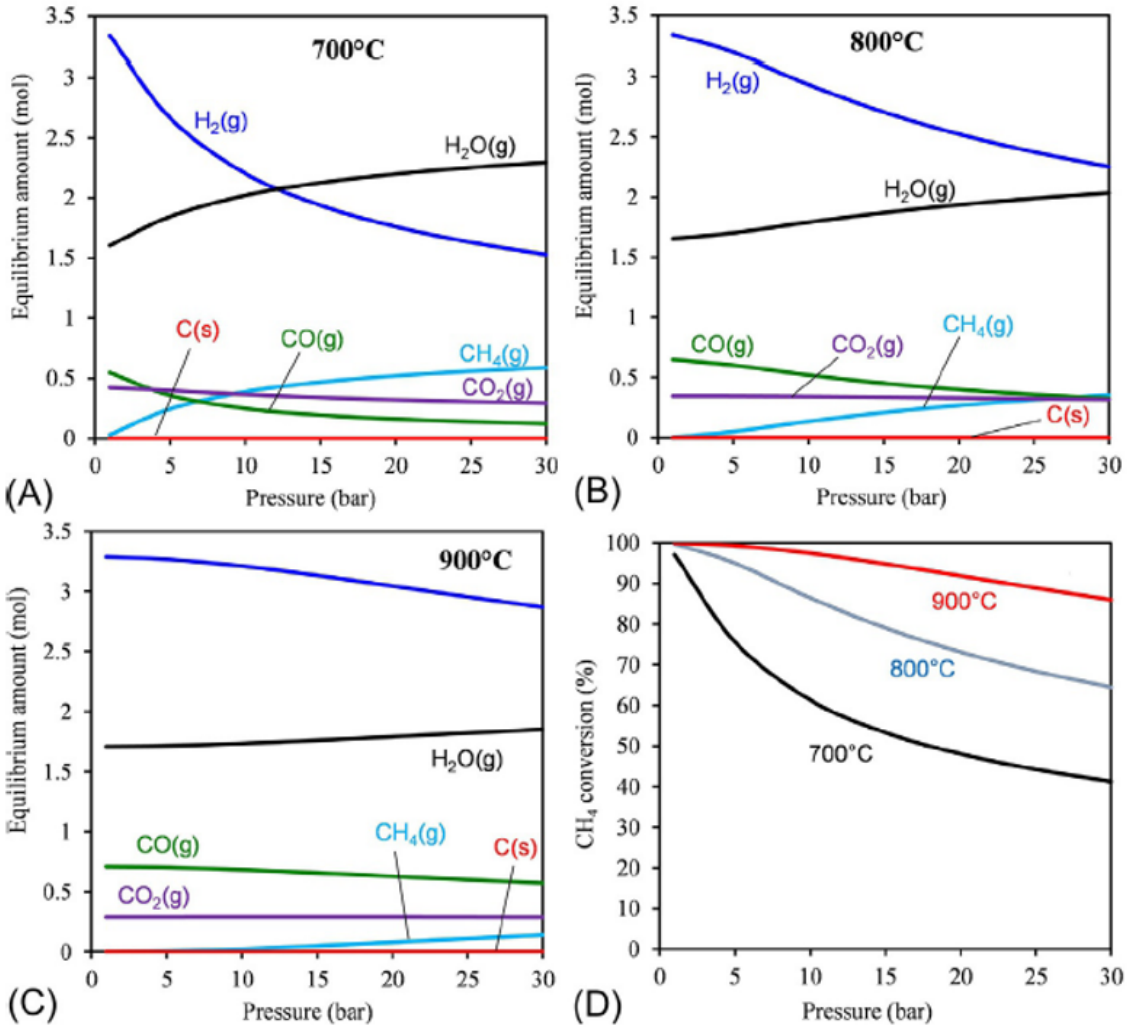

Figure C-2: Influence of the reaction pressure in steam methane reforming in the temperature range of 700–900°C for a mixture containing 1mol of methane and 3moles of steam: (A) 700°C, (B) 800°C, (C) 900°C, and (D) methane conversion at different temperatures taken from Minh et al. (2018).

Bibliography

M. R. Abu Zahra. Carbon dioxide capture from flue gas: development and evaluation of existing and novel process concepts. 2009.

R. Allam, J. Fetvedt, B. Forrest, and D. Freed. The oxy-fuel, supercritical co2 allam cycle: New cycle developments to produce even lower-cost electricity from fossil fuels without atmospheric emissions. In *Turbo Expo: Power for Land, Sea, and Air*, volume 45660, page V03BT36A016. American Society of Mechanical Engineers, 2014.

D. Almansoori, M. Abu Zahra, and T. Mezher. Towards zero co2 emissions fossil fuel power plants. *Available at SSRN 3819734*, 2021.

A. Basile, S. Liguori, and A. Iulianelli. 2 - membrane reactors for methane steam reforming (msr). In A. Basile, L. Di Paola, F. l. Hai, and V. Piemonte, editors, *Membrane Reactors for Energy Applications and Basic Chemical Production*, Woodhead Publishing Series in Energy, pages 31 – 59. Woodhead Publishing, 2015. ISBN 978-1-78242-223-5. doi: https://doi.org/10.1016/B978-1-78242-223-5.00002-9. URL http://www.sciencedirect.com/science/article/pii/B9781782422235000029.

O. Bolland and P. Mathieu. Comparison of two co2 removal options in combined cycle power plants. *Energy Conversion and Management*, 39(16-18):1653–1663, 1998.

Carbon-price. Link for price of co2 emitted. URL https://ember-climate.org/data/carbon-price-viewer/.

P. Chiesa, G. Lozza, and L. Mazzocchi. Using hydrogen as gas turbine fuel. *J. Eng. Gas Turbines Power*, 127(1):73–80, 2005.

CODE2 Project. Final cogeneration roadmap member state: The netherlands. URL http://www.code2-project.eu/wp-content/uploads/CODE2-CHP-Roadmap-Netherlands1.pdf.

S. L. Dixon and C. Hall. *Fluid mechanics and thermodynamics of turbomachinery*. Butterworth-Heinemann, 2013.

A. M. ElKady, A. Evulet, A. Brand, T. P. Ursin, and A. Lynghjem. Exhaust gas recirculation in dln f-class gas turbines for post-combustion co2 capture. In *Turbo Expo: Power for Land, Sea, and Air*, volume 43130, pages 847–854, 2008.

L. Espinal, D. L. Poster, W. Wong-Ng, A. J. Allen, and M. L. Green. Measurement, standards, and data needs for co2 capture materials: a critical review. *Environmental science & technology*, 47(21):11960–11975, 2013.

J. H. Horlock. *Axial flow compressors, fluid mechanics and thermodynamics*. Butterworths scientific publications, 1958.

Y. Hu and H. Ahn. Techno-economic analysis of a natural gas combined cycle power plant integrated with a ca-looping process for post-combustion capture. *Energy Procedia*, 105: 4555–4560, 2017.

IEA. Clean and efficient heat for industry, 2018. URL https://www.iea.org/commentaries/clean-and-efficient-heat-for-industry.

IEA. Co2 emissions from fuel combustion: Overview, iea, paris, 2020. URL https://www.iea.org/reports/co2-emissions-from-fuel-combustion-overview.

IEA. Net zero by 2050, iea, paris, 2021. URL https://www.iea.org/reports/net-zero-by-2050.

IEAGHG. Oxy-combustion turbine power plants, 2015. URL https://ieaghg.org/docs/General_Docs/Reports/2015-05.pdf.

IEAGHG. Techno-economic evaluation of smr based standalone hydrogen plant with ccs, 2017. URL https://ieaghg.org/exco_docs/2017-02.pdf.

Industrial Process Heating. Industrial process heating - technology assessment. URL https://www.energy.gov/sites/prod/files/2015/02/f19/QTR%20Ch8%20-%20Process%20Heating%20TA%20Feb-13-2015.pdf.

IRENA. A background paper to "renewable energy in manufacturing", 2015.

D. Jakobsen and V. Åtland. Concepts for large scale hydrogen production. Master's thesis, NTNU, 2016.

A. L. Kohl and R. Nielsen. *Gas purification*. Elsevier, 1997.

N.-S. Kwak, J. H. Lee, I. Y. Lee, K. R. Jang, and J.-G. Shim. A study of the co2 capture pilot plant by amine absorption. *Energy*, 47(1):41–46, 2012.

H. Li, G. Haugen, M. Ditaranto, D. Berstad, and K. Jordal. Impacts of exhaust gas recirculation (egr) on the natural gas combined cycle integrated with chemical absorption co2 capture technology. *Energy Procedia*, 4:1411–1418, 2011.

G. Lozza and P. Chiesa. Natural gas decarbonization to reduce co 2 emission from combined cycles—part ii: steam-methane reforming. *J. Eng. Gas Turbines Power*, 124(1):89–95, 2002.

R. H. Madona, M. Fawzib, K. I. Sarwanib, S. A. Osmanb, M. A. Razalib, and A. W. Mohammadc. Effect of steam to carbon ratio (s: C) on steam methane reforming's yield over coated nickel aluminide (ni. *Jurnal Kejuruteraan*, 32(4):657–662, 2020.

D. P. Minh, T. J. Siang, D.-V. N. Vo, T. S. Phan, C. Ridart, A. Nzihou, and D. Grouset. Hydrogen production from biogas reforming: An overview of steam reforming, dry reforming, dual reforming, and tri-reforming of methane. In *Hydrogen Supply Chains*, pages 111–166. Elsevier, 2018.

S. Naimoli and S. Ladislaw. Decarbonizing heavy industry. *Csis. October*, 2020.

Naturalgas-price. Link for spot market data- natural gas price. URL https://www.powernext.com/spot-market-data.

B. Page, G. Turan, and A. Zapantis. Global status of ccs 2020, 2020. URL https://www.globalccsinstitute.com/resources/global-status-report/.

M. Persico. Deep part load operation of combined cycles and combined heat and power plants. Master's thesis, Delft University of Technology, 2017.

A. B. Rao and E. S. Rubin. A technical, economic, and environmental assessment of amine-based co2 capture technology for power plant greenhouse gas control. *Environmental science & technology*, 36(20):4467–4475, 2002.

S. Rezvani, O. Bolland, F. Franco, Y. Huang, R. Span, J. Keyser, F. Sander, D. McIlveen-Wright, and N. Hewitt. Natural gas oxy-fuel cycles—part 3: Economic evaluation. *Energy Procedia*, 1(1):565–572, 2009.

P. Rokke and J. E. Hustad. Exhaust gas recirculation in gas turbines for reduction of co2 emissions; combustion testing with focus on stability and emissions. *International Journal of thermodynamics*, 8(4):167, 2005.

M. M. Sam Lamboo and S. Lensink. Concept advice co2 capture and storag, 2021. URL https://www.pbl.nl/sites/default/files/downloads/pbl-2021-conceptadvies-sde-plus-plus-2022-co2-afvang-en-opslag-ccs-4394.pdf.

W. Sanz, H. Jericha, F. Luckel, E. Go¨ ttlich, and F. Heitmeir. A further step towards a graz cycle power plant for co2 capture. In *Turbo Expo: Power for Land, Sea, and Air*, volume 47284, pages 181–190, 2005.

H. I. Saravanamuttoo, G. F. C. Rogers, and H. Cohen. *Gas turbine theory*. Pearson Education, 2001.

Solar Payback. Solar heat for industry, 2017. URL https://www.solar-payback.com/wp-content/uploads/2020/06/Solar-Heat-for-Industry-Solar-Payback-April-2017.pdf.

C. Soothill, M. Bialkowski, G. Guidati, and A. Zagorskiy. Carbon dioxide (co2) capture and storage for gas turbine systems. In *Modern Gas Turbine Systems*, pages 685–714. Elsevier, 2013.

R. Stanger, T. Wall, R. Spörl, M. Paneru, S. Grathwohl, M. Weidmann, G. Scheffknecht, D. McDonald, K. Myöhänen, J. Ritvanen, et al. Oxyfuel combustion for co2 capture in power plants. *International Journal of Greenhouse Gas Control*, 40:55–125, 2015.

J. Steimes, S. Klein, and M. Persico. Enabling efficient and low emissions deep part load operation of combined cycles and combined heat and power plants with external flue gas recirculation. In *Proceedings of GPPS Forum*, volume 18.

M. I. Stewart. Chapter nine - gas sweetening. In M. I. Stewart, editor, *Surface Production Operations (Third Edition)*, volume 2, pages 433 – 539. Gulf Professional Publishing, Boston, third edition edition, 2014. ISBN 978-0-12-382207-9. doi: https://doi.org/10.1016/B978-0-12-382207-9.00009-3. URL http://www.sciencedirect.com/science/article/pii/B9780123822079000093.

Thermoflow Inc. Thermoflex. URL https://www.thermoflow.com/products_generalpurpose.html.

G. P. Thiel and A. K. Stark. To decarbonize industry, we must decarbonize heat. *Joule*, 2021.

M. Wang, A. Lawal, P. Stephenson, J. Sidders, and C. Ramshaw. Post-combustion co2 capture with chemical absorption: a state-of-the-art review. *Chemical engineering research and design*, 89(9):1609–1624, 2011.